Department of Computer Science, Bioengineering,
Robotics and Systems Engineering

Probabilistic hydrological nowcasting on Mediterranean small catchments: from theoretical approaches to operational applications

by

Maria Laura Poletti

DIBRIS, Università di Genova
Via Opera Pia, 13 16145 Genova, Italy http://www.dibris.unige.it/

Università degli Studi di Genova

Dipartimento di Informatica, Bioingegneria,

Robotica ed Ingegneria dei Sistemi

Ph.D. Thesis in Computer Science and Systems Engineering

System Engineering Curriculum

Probabilistic hydrological nowcasting on Mediterranean small catchments: from theoretical approaches to operational applications

by

Maria Laura Poletti

May, 2019

Dottorato di Ricerca in Informatica ed Ingegneria dei Sistemi

Indirizzo Ingegneria dei Sistemi

Dipartimento di Informatica, Bioingegneria, Robotica ed Ingegneria dei Sistemi

Università degli Studi di Genova

DIBRIS, Univ. di Genova

Via Opera Pia, 13

I-16145 Genova, Italy

http://www.dibris.unige.it/

Ph.D. Thesis in Computer Science and Systems Engineering

Systems Engineering Curriculum

(S.S.D. ICAR/02)

Submitted by Maria Laura Poletti

DIBRIS, Univ. di Genova

Date of submission: *January 2019*

Title: *Probabilistic hydrological nowcasting on Mediterranean small catchments: from theoretical approaches to operational applications*

Advisors: *Luca Ferraris, Nicola Rebora, Francesco Silvestro*

Ext. Reviewers: *Marc Berenguer, Maria-Helena Ramos*

Summary

Summary 1
List of figures 2
Abstract 8
Chapter 1: Introduction 10
Chapter 2: Area of study 16
Chapter 3: State of the art 22
3.1 Nowcasting models 22
3.2 Numerical Weather Prediction System and data assimilation module 26
3.3 Blending technique 28
3.4 Hydrological models 30
3.5 Hydrological nowcasting chain 32
Chapter 4: New development of an integrated hydrological nowcasting chain 34
4.1 Input of the chain: radar rainfall data 34
4.2 The nowcasting algorithm: PhaSt 35
4.3 The meteorological model and the assimilation module 39
4.4 Application of the blending technique 42
4.5 The hydrological model: Continuum 44
4.6 Implementation of an integrated hydrological nowcasting chain 50
Chapter 5: Results and innovative aspects of the study 52
5.1 Implementation of the hydrological nowcasting chain 54
5.2 Modification of the nowcasting algorithm 55
5.3 Effects of the blending functions on hydrological forecast 65
5.3.2 Basin scale analysis 68
5.3.3 Distributed analysis 75
5.4 Intercomparison between two nowcasting methods 79
5.4.1 Deterministic comparison 81
5.4.2 Probabilistic comparison 88
5.5 Visualization of the results 94
Chapter 6: Conclusions 101
References 104
Appendix 1- Publications 118
Appendix 2- Participation to conferences and workshops 119

List of figures

Figure 1: Number of casualties in each documented flood event over the period 1940-2015 from in the Mediterranean area (Gaume et al. 2016)..... 10

Figure 2: Example of at soil effects of floods over Mediterranean area: a) event in the region of Cannes, October 2015; b) event in Catalunya, October 2016; c) event in Tuscany, September 2017. 11

Figure 3: Impacts of the event of 9-10-11 October 2018 across the Mediterranean area: a) flood in Mallorca; b) collapse of highway infrastructure in Sardinia due to the flood; c) flood and debris flow in the South France. 12

Figure 4: Location of Liguria Region in the north-west of Italy..... 16

Figure 5: Main events affecting Liguria region in the last decade: a) 4th October 2010 event, flooding of Genova Sestri Ponente; b) 25th October 2011 event, Val di Vara and Cinque Terre; c) 4th November 2011 event, Fereggiano and Bisagno going out of the banks flooding Genova city center; d) 9th October 2014 event, flooding of Bisagno..... 18

Figure 6: Location of the basin involved in the event of 9th October 2014: Bisagno, Scrivia and Sturla..... 19

Figure 7: Location of the basin mainly involved in the event of 11th November 2014, Entella 20

Figure 8: Location of the basins analyzed for the 15th November event..... 21

Figure 9: Settepani radar location in Liguria Region and structure of the radar..... 34

Figure 10: PhaSt forecast expressed in mm at 10 minutes for the run of 09-10-2014 at 19:00 37

Figure 11: Phast forecast expressed in mm at 1 hour for the run of 09-10-2014 at 19:00..... 38

Figure 12: NWP system: MOLOCH is nested on the limited area model BOLAM, that in turn is taking its initial and boundary conditions from the forecasts of ECMWF..... 39

Figure 13: Integration domain of MOLOCH NWP model: it covers northern and central Italy with a resolution of 0.02 degrees (2.2 km)..... 40

Figure 14: MOLOCH forecasts and data assimilation implementation:..... 41

Figure 15: Different blending function analyzed: on the left the weighting function related to the nowcasted rainfall field, on the right the complementary function, used to weight the NWPS forecast. The first weighting function (red line) is a step function while the other functions are increasingly smoother..... 43

Figure 16: Schematization of the hydrological modeling performed by Continuum taken by Silvestro et al., 2013..... 45

Figure 17: Domain of Continuum in Liguria Region: The discharge is calculated for every point of the domain, giving in output a distributed map..... 49

Figure 18: a) The hydrological nowcasting chain in its first version: the observed rainfall is the input until the now, then 2 hours of nowcasted rainfall field produced by PhaSt are added to the observations. Starting form a probabilistic input (20 rainfall scenarios for each time step) the result is an ensemble of forecasted discharge for the following 12 hours (example in b for 9th October 2014 event on Bisagno)..... 50

Figure 19: a) The hydrological nowcasting chain described in its elements: the main input is the observed radar rainfall. It is used up to the Now as it is, is evolved through the nowcasting method and it is used in the data assimilation process for the correction of the NWPS. The information regarding the total volume variation along the forecast time given by the meteorological model is used to modify the rainfall fields nowcasted. The rainfall fields produced in this framework are linearly combined through using the blending technique and then are the input of the hydrological model, that produces a probabilistic discharge forecast (example in b)..... 51

Figure 20: CRPS graphical representation (striped area): it is calculated as the difference between the cumulative density function of the forecasted discharge and the observed value represented by the step function..... 53

Figure 21: Forecasted hydrograph for 9th October 2014 at 19:40 UTC. The red lines are the different forecast of the hydrological model while the black line with asterisks is the reference hydrograph, built using the observed radar rainfall, taken as the discharge benchmark..... 54

Figure 22: Modification of the volume using the observed radar rainfall field: the trend extract from the observations is distributed along the first three time steps and then assumed constant..... 56

Figure 23: Modification of the volume using the information regarding the volume of the meteorological model as it is and the meteorological model corrected with DA: the trend is calculated per hour and then applied to the following two hours..... 57

Figure 24: Run of 19:20 (a) and 19:40 (b) UTC of 9th October 2014 for Bisagno Creek at Passerella Firpo section: the different envelope forecasted are related to different input in terms of nowcasted rainfall field: the first one uses the nowcasted rainfall field without volume variation, the second one the nowcasted

rainfall field with volume trend given by radar observed rainfall field, the third the nowcasted rainfall field with volume variation trend retrieved from the NWP model corrected with DA while the last one use the information of NWP model without DA correction 59

Figure 25: RCRPS for 9th October event (time window of the event between 13 UTC and 21 UTC): the boxplot groups all the values of the score distinct in the columns related to the various type of modification of the volume information expressed as a function of lead time..... 61

Figure 26: Run of 18:40 UTC of 10th November 2014 for Bisagno Creek at Passerella Firpo section: the different envelope forecasted are related to different input in terms of nowcasted rainfall field. Starting from the top the hydrological model is fed by the nowcasting PhaSt with the volume information not modified, then the volume modified with observations; in the last two the volume is modified with the NWP model corrected with DA and the NWP model as it is. 62

Figure 27: RCRPS for 10-11th November event: the values of the score, expressed as a function of lead time, are distinct in columns related to way of modifying the total volume on the domain. 63

Figure 28: Run of 9:00 UTC of 15 November 2014: the hydrographs represent the hydrological model fed by different versions of nowcasting PhaSt with the volume information not modified, modified with observations, modified according to the NWP model corrected with DA and the NWP model without DA... 64

Figure 29: RCRPS values for 15th November 2014 event: the four columns are related to the different versions of PhaSt with and without volume variation feeding the hydrological model. 65

Figure 30: Volume trend for rainfall field modification (example for 10-11-2014 at 12:00 UTC). The total volume on the domain considered is summed for each time step of the NWPS forecast with DA. The trend volume is applied as multiplicative factor to the first rainfall forecasted by the nowcasting technique..... 66

Figure 31: RCRPS for all the events: analysis of the discharge output related to the different four blending functions: the red column represents the results of applying the step function, the other three columns the effect of application of the other three growingly smoothing blending functions. The results are presented in form of boxplot distinguished in three drainage class area (15-20 kmq, 50-150 kmq and 150-500 kmq)..... 68

Figure 32: Example hydrographs for 9th October and 11th November event for Bisagno and Entella outlet sections. In both the figure the light blue envelope is the result of the forecast using 6 hours forecast of the nowcasting output without volume variation; the orange envelope results from the use of the nowcasting modified with the information regarding the volume; the red envelope takes in input the rainfall fields resulting from the linear combination obtained with the blending. 70

Figure 33: The hydrological nowcasting chain in its three configurations: : the first one in which is used only the nowcasted rainfall field without volume modification (a); the second one with the nowcasted rainfall

field modified with the trend retrieved by the NWP model (b); in the last one the nowcasted rainfall fields with volume modification are combined through blending with the fields forecasted by NWP model corrected with DA..... 71

Figure 34: Location of the basins considered in the analysis of the punctual sections: Bisagno for 9th October event; Graveglia for 10th November event; Polcevera for 15th November event..... 72

Figure 35: Scores calculated at river section (Passerella Firpo for Bisagno creek) for 9th October event (from 13:00 to 21:00 UTC of 9th October 2014). Nash Sutcliffe efficiency (a), Variance of the forecast (b), Reduced Continuous Probability Rank Score (c)..... 73

Figure 36: Scores calculated at river section Caminata for Graveglia catchment) for 11th November event (from 10:00 to 21:00 UTC of 10th November 2014). Nash Sutcliffe efficiency (a), Variance of the forecast (b), Reduced Continuous Probability Rank Score (c)..... 74

Figure 37: Scores calculated at river section (Rivarolo for Polcevera catchment) for 15th November event (from 02:00 to 11:00 UTC of 15th November 2014). Nash Sutcliffe efficiency (a), Variance of the forecast (b), Reduced Continuous Probability Rank Score (c)..... 75

Figure 38: 9 Oct. 2014 event: RCRPS for three distinct classes of area. Each column refers to a different configuration of the forecasting system, whose rainfall is provided by: nowcasting without volume variation (light blue), nowcasting with the volume variation (orange), blending using the step blending function (red), and blending using the best local blending function (blue) which in this case is the function f3..... 77

Figure 39: 11 Nov. 2014 event: RCRPS for three distinct classes of area. Each column refers to a different configuration of the forecasting system, whose rainfall is provided by: nowcasting without volume variation (light blue), nowcasting with the volume variation (orange), blending using the step blending function (red), and blending using the best local blending function (blue) which in this case is the function f2..... 77

Figure 40: 15 Nov. 2014 event: RCRPS for three distinct classes of area. Each column refers to a different configuration of the forecasting system, whose rainfall is provided by: nowcasting without volume variation (light blue), nowcasting with the volume variation (orange), blending using the step blending function (red), and blending using the best local blending function (blue) which in this case is the step function. 78

Figure 41: Cumulative rainfall map between 12 UTC of 9 October and 00 UTC of 10 October 2014 on the main basins involved in the event: Bisagno, Sturla and Scirvia..... 82

Figure 42: RMSE and BIAS calculated for rainfall aggregated at basin scale for Bisagno varying along the forecast time up to 2 hours lead time 82

Figure 43: RMSE and BIAS calculated for rainfall aggregated at basin scale for Scrivia varying along the forecast time up to 2 hours lead time *83*

Figure 44: RMSE and BIAS calculated for rainfall aggregated at basin scale for Sturla varying along the forecast time up to 2 hours lead time *83*

Figure 45: NS efficiency calculated for discharge forecasted through the different deterministic nowcasting (the Eulerian persistence, the two deterministic versions of PhaSt and SBMcast deterministic), the "perfect rainfall" and the "no rain" forecast in input to the hydrological model. For 9th October 2014 event the basins analyzed are Bisagno (a), Scrivia (b), Sturla (c)..... *84*

Figure 46: RMSE and BIAS calculated for rainfall aggregated at basin scale for Entella varying along the forecast time up to 2 hours lead time *85*

Figure 47: NS efficiency for Entella calculated for discharge forecasted through the different deterministic nowcasting (the Eulerian persistence, the two deterministic versions of PhaSt and SBMcast deterministic), the "perfect rainfall" and the "no rain" forecast in input to the hydrological model...... *86*

Figure 48: RMSE and BIAS calculated for rainfall aggregated at basin scale for Polcevera varying along the forecast time up to 2 hours lead time..... *87*

Figure 49: RMSE and BIAS calculated for rainfall aggregated at basin scale for Cerusa varying along the forecast time up to 2 hours lead time *87*

Figure 50: NS efficiency calculated for discharge forecasted through the different deterministic nowcasting (the Eulerian persistence, the two deterministic versions of PhaSt and SBMcast deterministic), the "perfect rainfall" and the "no rain" forecast in input to the hydrological model. For 15th November 2014 event the basins analyzed are Cerusa (a) and Polecevera (b) catchments...... *88*

Figure 51: Ensemble spread (solid line with circles) and RMSE (solid line with stars) calculated for the rainfall field nowcasted with PhaSt (a) and SBMcast (b). The third solid line represents the ratio between the ensemble spread and the RMSE *89*

Figure 52: Rank histogram calculated for forecasted discharge at lead time 10 minutes result of the probabilistic hydrological nowcasting chain fed with PhaSt and SBMcast..... *90*

Figure 53: Rank histogram calculated for forecasted discharge at lead time 30 minutes result of the probabilistic hydrological nowcasting chain fed with PhaSt and SBMcast..... *91*

Figure 54: Rank histogram calculated for forecasted discharge at lead time 1 hour result of the probabilistic hydrological nowcasting chain fed with PhaSt and SBMcast *91*

Figure 55: Rank histogram calculated for forecasted discharge at lead time 2 hours result of the probabilistic hydrological nowcasting chain fed with PhaSt and SBMcast *92*

Figure 56: Rank histogram calculated for forecasted discharge at lead time 4 hours result of the probabilistic hydrological nowcasting chain fed with PhaSt and SBMcast *93*

Figure 57: Comparison between observed rain field and PhaSt forecast for run at 23:00 of 1-08-2014 ..... *94*

Figure 58: Map of discharge forecasted at 19:40 of 9th October 2014: distinct into two series of maps, maximum and minimum discharge forecasted at 1, 2 and 3 hours of lead time. It is hard to determine which are the basins really involved in the event that are causing at soil effects because the value of the critical discharge is really sensitive to the characteristics of the basin such as the area and the *96*

Figure 59: Regression curve for Return Period - K_T values: starting from some known points of correspondence between K_T and T it is possible to build the curve interpolating them to obtain also the intermediate values of K_T *98*

Figure 60: Maps of the return period forecasted at 19:40 of 9th October 2014: in the upper part the maximum values of return period forecasted and in the lower part the minimum values. The maps are calculated following the regionalization method for 1, 2 and 3 hours of lead time. *99*

Abstract

The Mediterranean area in last century was affected by very intense rainfall events concentrated over small portion of the territory generating flash-floods and landslides. These events caused serious damages to urban areas and in the worst events led to human losses. The temporal scale of these events has been observed to be strictly linked to the size of the catchments involved. Considering the presence of a great number of catchments with small drainage area (order of some km^2) and related response time of few hours, a forecast at short lead time is essential for this kind of events. Nowcasting models, covering the time interval of the following two hours starting from the observation try to extend the predictability limits of the forecasting models in support of real-time flood alert system operations.

This research project points to the realization of an integrated hydrological nowcasting chain, coupling existing nowcasting techniques (PhaSt, a spectral-based nowcasting procedure) and hydrological model (Continuum, a continuous distributed hydrological model). A work of enhancement of the nowcasting technique has been firstly performed to extend the forecast horizon a modification of the algorithm has been inserted in order to take into account the mechanism of growth and decay of the precipitation structure. Then the blending with the meteorological models that could allow to integrate the prediction at short lead time of the nowcasting technique (0-2 hours) with the longer lead time of the meteorological models. A parallel work has been done in collaboration with the Centre of Applied Research in Hydrometeorology on the comparison of two probabilistic nowcasting technique and the effect of the propagation of the error of the rainfall forecast in the hydrological nowcasting chain.

The work focuses not only on the enhancement of the predictive ability of the single elements of the chain but is trying also to understand how each element can integrate in order to give a result that is reachable but also satisfying from an operational point of view and that can be used as a support in the decisional process for the warning system.

Chapter 1: Introduction

Liguria region, located in north-western Italy, has been recurrently affected in the last century by severe rainfall events that produced flash-floods and landslides (Acquaotta et al., 2018).

According to some recent studies (Gaume et al. 2009; Llassat et al. 2016; Gaume et al., 2016) the mostly damaging flash-floods occur more frequently in the Mediterranean area than in the rest of Europe and are causing losses both in economic terms and in terms of human lives (Figure 1). One of the main causes is the climate of the region: the geomorphological configuration of the area facing the Mediterranean Sea forces the formation of convergence in the low levels of the atmosphere and the raising warm wet masses of air that are carried to the coast produce convection. The second one is the high density of population in the coastal area, that lead to a change in the main land use due to the development of harbor, industrial, and residential areas.

The most severe floods occurring in the Mediterranean area can be ascribed to the development of strongly convective intense precipitation events (with intensities up to 180 mm/h in 5 minutes). These events are often associated to stationary mesoscale systems lasting several hours leading that produce rainfall amounts exceeding 200 mm in a few hours over a limited portion of area (typically less than 100 km^2).

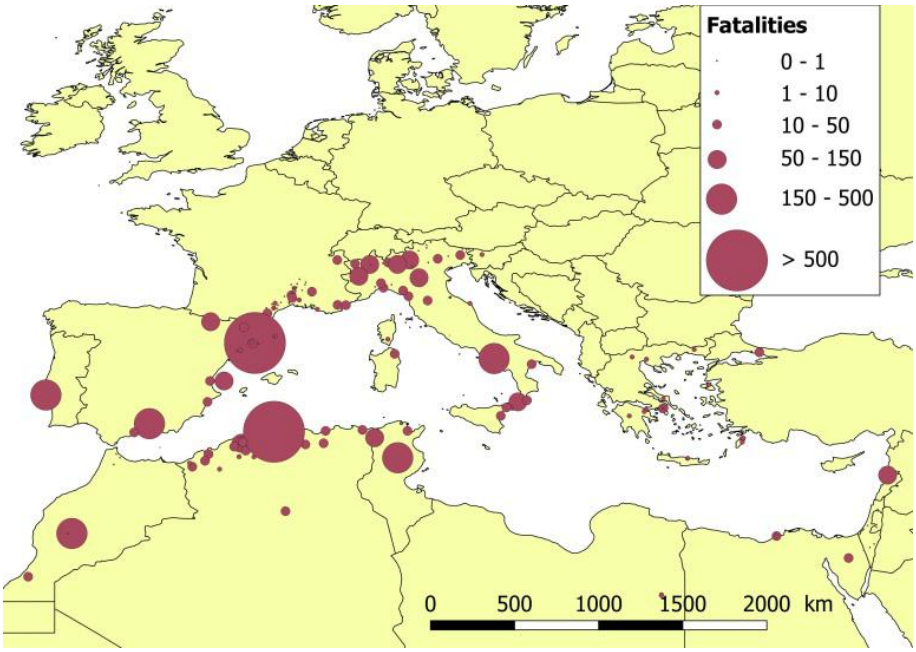

Figure 1: Number of casualties in each documented flood event over the period 1940-2015 from in the Mediterranean area (Gaume et al. 2016)

Only in the last few years there is plenty of examples of these kind of events. Between 8 and 9 September 2002, a major mesoscale convective system affected the Gard area in the Céven-nes–Vivarais region, France: 24 people were killed during this event and the economic damage is estimated at 1.2 billion euros (Delrieu et al., 2005, Huet et al., 2003). Still in the south of France, the 3rd October 2015, intense rainfalls led to major flash-floods in that caused 20 fatalities and a total cost of damage estimated at over 650 million Euros (Bourgin et al., 2017; Payrastre et al., 2016). The 12th October of the following year a flood event hit the county of Maresme in Catalunya, streets turned into rivers causing one death and damage to homes and some roads. Cars were swept along streets, in some cases as far as the sea (Cuevas et al., 2017).

In the night between September 9th and 10th 2017 a heavy precipitation event interested the coastal areas of Tuscany, Italy. Over 200 mm/2 hours of precipitation were recorded in the nearby of Livorno where flash-floods occurred the day after and caused 9 casualties (Cioni et al, 2018; Ricciardelli et el., 2018).

Figure 2: Example of at soil effects of floods over Mediterranean area: a) event in the region of Cannes, October 2015; b) event in Catalunya, October 2016; c) event in Tuscany, September 2017.

The last main event interested almost all the countries of the north-western Mediterranean area: during the days 9-10-11 October 2018 an event moving towards east hit progressively Spain, South France and Italy, causing damages and the death of many people (Figure 3). The town of Sant Llorenç des Cardassar (Mallorca, Spain) was severely struck and 12 people died because of the flood. On 10th October in Sainte-Maxime, France, two people died when their car was swept away by the flood. The same day in Sardinia a woman died in her car devastated by the flood, that cause the break of a highway passing over a river.

Figure 3: Impacts of the event of 9-10-11 October 2018 across the Mediterranean area: a) flood in Mallorca; b) collapse of highway infrastructure in Sardinia due to the flood; c) flood and debris flow in the South France.

These events caused severe damages in the coastal urbanized areas and sometimes caused human casualties in Liguria Region (Faccini et al., 2009; Faccini et al., 2012; Silvestro et al., 2012a; Davolio et al., 2015; Silvestro et al., 2016) but also in other area of the Mediterranean (Drobinski, 2014; Delrieu et al., 2005; Ducrocq et al., 2008). All these events were associated with well-organized, very intense and localized convective systems affecting the same area of few square kilometres for several hours (Parodi et al., 2012; Rebora et al., 2013; Fiori et al., 2014; Buzzi et al., 2014). In these cases the events are hardly predictable by the meteorological models due to their small spatial and temporal scales. Nowcasting models can help by predicting the evolution of the rainfall pattern at regional scale, starting from the last observed radar rainfall images (i.e. radar-based rainfall nowcasting) and by giving a short-term forecast (usually few hours).

Radar-based rainfall nowcasting can be achieved by extrapolating the future rainfall distribution from a sequence of radar images; the radar-based rainfall nowcast has shown better skill for short lead time forecasting. The basic techniques to produce quantitative rainfall forecasts (QPFs) from radar echoes are based on cross-correlation or individual radar echo-tracking (Collier, 1981). An evolution in the nowcasting procedure has been the development of nowcasting methods operating in the Fourier domain (Seed, 2003; Xu and Chandrasekar, 2005) to consider the fact that the predictability of precipitation depends on the spatial scale of the structures (Wilson et al. 1998; Germann and Zawadzki, 2002). Among the techniques that follows a probabilistic approach Metta et al. (2009) developed a stochastic spectral-based nowcasting technique that predict the future rainfall scenarios starting from the rainfall fields observed by radar end evolving them through a

Fourier decomposition, while Berenguer et al. (2011) presented a method based on the String of Beads model; Foresti et al. (2016) analyzed the performance of a nowcasting algorithm that accounts stochastically for the process of growth and decay of rainfall cells

The main limit of such nowcasting prediction is that its accuracy is quite high for very short lead times (20-120 minutes) but, since it is based on the extrapolation of the observed rainfall field, its accuracy rapidly decreases when lead time increases.

One of the reasons why the accuracy rapidly decreases with increasing lead times is that radar nowcasting techniques do not model (or model them stochastically) processes such as growth and decay of precipitation structures (Golding, 1998), that in longer lead times become important processes. So, for very short lead time of precipitation (0–3 h), radar nowcast performs best, whereas for longer lead times, forecasts based on Numerical Weather Prediction System (NWPS) are better (Kilambi and Zawadzki, 2005; Lin et al., 2005; Kober et al., 2012; Wang et al., 2015). On the other side NWPS allows rainfall predictions with not sufficient spatial and time detail (Davolio et al., 2015; Silvestro et al. 2016).

Therefore, after the very first hours (usually 0–3 h) of radar-based nowcasting, NWPS forecasts can be merged to generate a seamless 0-6 hour prediction with higher skill. This procedure requires an accurate QPF in the very short term from the meteorological model, at a high resolution of a few kilometers, since the tolerance for timing or location errors is very limited, especially in case of severe storms (Sun et al., 2014). In fact, a correct forecast allows a smooth transition from radar extrapolation to model prediction. To meet nowcasting requirements, NWP models have to be run at convection-permitting resolution (1-4 km, Weisman et al., 2008; Kain et al., 2006) starting from a better initial condition that also reduces the spin-up period. Therefore, several methodologies for rapid data assimilation have been developed in order to be suitable for nowcasting application. Rapid Update Cycle procedures have been widely used in operational framework (Wilson and Roberts, 2006; Benjamin et al., 2004) to provide a “warm start” and hence reduce the model spin-up. Also, radar reflectivity has been employed to improve the initial condition, e.g. exploiting the information on latent heating through the application of nudging technique (Sokol and Zacharov, 2012; Dow and Macpherson, 2013; Bick et al., 2016; Davolio et al., 2017a), eventually reducing the intensity/position error in rainfall prediction.

Hydrological forecast is useful in a hydrological nowcasting perspective but for limited lead times (Silvestro et al., 2015a) with applications also on urban hydrology (Thorndahl et al., 2017). Various works attempted also to improve hydrological forecasting by improving the rainfall forecast using

both observations and models. Rossa et al. (2010) assimilated radar data on NWPS to improve precipitation prediction; Davolio et al. (2017a) assimilated rainfall field derived from both radar and gauge observations (Sinclair and Pegram, 2005) in a NWPS and used the rainfall prediction in a probabilistic hydrometeorological forecast chain; Liechti et al. (2013) and Liechti and Zappa (2016) explored the impact on hydrological forecasting derived by different techniques of rainfall forecast based on both NWPS and radar data; Kyznarova et al., (2012, 2013) tried to use the INCA system (Haiden et al., 2011) precipitation products as input to an hydrological model evaluating the benefit in respect to use extrapolation techniques.

Within this framework, the present study attempts to use in a synergic way a nowcasting model, a high-resolution NWP model (MOLOCH) corrected by a data assimilation technique and rainfall observations. The rainfall estimation derived from both radar and gauge observations is used in a frequent (60 minutes) data assimilation framework on a NWPS; this should drive NWPS QPF to better reproduce observations in terms of spatial and time location (Davolio et al., 2017a). A probabilistic nowcasting model was improved in order to get as input the information derived from NWPS QPF. A blending technique based on previous studies (Kilambi and Zawadzki, 2005; Kober et al., 2012; Bowler et al., 2006, Nerini et al., 2018) is then used to smoothly combine nowcasting rainfall scenarios and NWPS QPF.

The use of the "nowcasted" rainfall field can effectively extend the lead time available for issuing flood and flash-flood forecasts by several hours depending on the accuracy of the precipitation forecasting technique. Sufficiently long lead time is required for flood early warning system to be useful for issue warnings in various forms, from taking flood mitigation measures, evacuating potentially affected residents and so on.

The possibility to predict with more accuracy the rainfall fields in input to the hydrological model can improve in a significant way the accuracy of the hydrological forecast applied on short lead times (Berenguer et al., 2005; Silvestro et al., 2012b).

The last module of the present nowcasting chain is represented by the distributed hydrological model Continuum (Silvestro et al., 2013; Silvestro et al., 2015b; Cenci et al., 2016) that is used to transform rainfall prediction in streamflow prediction in a frequent updated Flood Forecasting System (20 minutes). Using as input the forecast rainfall as described above, it provides a probabilistic output, with many predicted discharge scenarios, useful in real time management operations of emergency.

Although the elements of the chain are not innovative by themselves, some new elements are introduced within this study. Firstly, the blending was performed not only combining the rainfall fields forecasted by the nowcasting and the NWPS in their spatial distribution as in more standard approaches (Kilambi and Zawadzki, 2005); in fact the nowcasted rainfall field are modified along the forecast window according to the information related to the rainfall volume time variation derived by NWPS, this could be consider as a matter of fact, a sort of blending of the volume. Secondly the NWPS is rapidly updated with observations trough a data assimilation technique before its information content is used to trigger the nowcasting model; finally, the verifications are done on a hydrological perspective following both a point and distributed approach in order to enhance the sample of data.

The system is applied on three major flood events occurred on the Liguria Region located in north west of Italy; results are presented comparing streamflow forecast obtained using rainfall predictions from different configurations of the presented system, in order to evidence the benefit of using or not some modules of the presented system.

The thesis is organized as follows: the next Chapter will illustrate the area of application and the relevance of the study; in Chapter 3 can be found the state of the art of the research area related to the PhD work; Chapter 4 introduces the elements of the hydrological nowcasting chain; in Chapter 5 are presented the results of the study; Chapter 6 is aimed to summarize the work in the conclusions.

Chapter 2: Area of study

The area of application object of this study is Liguria Region, representative of the coastal environment in the Mediterranean area described in the Introduction. The problem of the sensitivity of the urban area to the floods is particularly significant in Liguria Region (Figure 4).

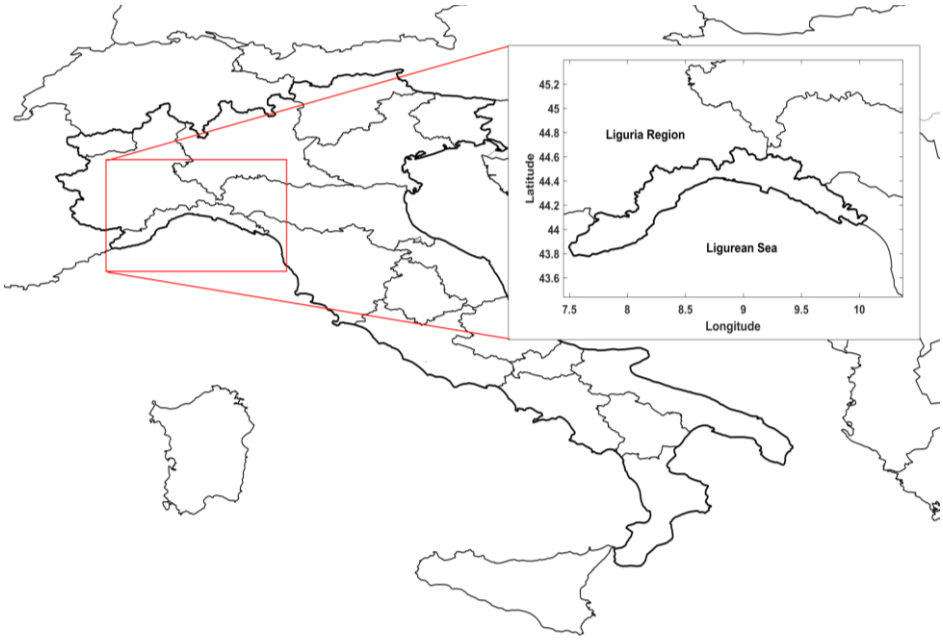

Figure 4: Location of Liguria Region in the north-west of Italy

Liguria is bordered by France (Provence-Alpes-Côte d'Azur) to the west, Piedmont to the north, and Emilia-Romagna and Tuscany to the east. It faces the Ligurean Sea and it is closed on the other side by the Alps and the Appenines mountains.

The region is mainly mountainous (65% of total), some mountains rise above 2000 m and, since is squeezed between mountains and sea, the narrow strip of land is characterized by high steep. Most of the urban areas developed along the coast in a process of land use change due to the development of harbour, industrial, and residential areas, which has strongly impacted geomorphologic processes (Brandolini, P., 2012; Faccini et al., 2015a).

Over the past and current century, recurring flash-flood events occurred (1953, 1970, 1992, 1993, 2011, 2014) and several landslides that have caused severe damage to urbanized areas on both the coastal-fluvial plains and surrounding slopes, sometimes involving human casualties. The analysis of the annual distribution of past events indicates that these phenomena have occurred with rising

frequency in the last seventy years. Only in the last decade many events hit the region, such as the flood event of 2010, 2011 and 2014, occurred in various part of the region (Figure 5).

The 4th October 2010 (Faccini et al., 2015a,b) heavy rainfall affected the western part of the city of Genoa (Sestri Ponente), with a total cumulative precipitation level of approximately 400 mm/6h. This rainfall amount caused the lower reach of the Chiaravagna catchment to flood and a large number of shallow landslides, debris flows in the upper part of the Molinassi catchment, both flowing in Genoa Sestri Ponente. The lower parts of these catchments, the urbanized fluvial-coastal plains, were almost completely flooded.

The 25th October of the following year, heavy rainfall affected the area between eastern Liguria and northern Tuscany (Cevasco et al., 2013). The event caused thousands of shallow landslides, erosive and depositional processes, floods, 13 casualties. Along the coast, the western sector of the Cinque Terre was affected by floods in Monterosso and Vernazza, severely damaging both from structural and economic point of view.

On the 4th of November of the same year the city of Genoa was rocked by severe flash-floods (Silvestro et al., 2012a, Rebora et al., 2013, Fiori et al., 2014). Nearly 500 mm of rain, a third of the average annual rainfall, fell in six hours. A flash-flood occurred in the Fereggiano catchment causing 6 casualties and millions of euros in damages.

The 9th of October 2014 a flash-flood took place in Genoa (Rebora et al., 2015; Silvestro et al., 2016).

These events caused severe damages in the coastal urbanized areas and sometimes caused human casualties in Liguria Region (Faccini et al., 2009; Faccini et al., 2012; Silvestro et al., 2012a; Davolio et al., 2015; Silvestro et al., 2016)

Figure 5: Main events affecting Liguria region in the last decade: a) 4th October 2010 event, flooding of Genova Sestri Ponente; b) 25th October 2011 event, Val di Vara and Cinque Terre; c) 4th November 2011 event, Fereggiano and Bisagno going out of the banks flooding Genova city center; d) 9th October 2014 event, flooding of Bisagno

During all these events rainfall was very localized, a large amount of precipitation fell in an area of few square kilometers with high intensities in few hours produced by well organized, very intense and localized mesoscale convective system (MCS) that remained stationary for a significant number of hours on the same area (Ferretti et al., 2013, Fiori et al. 2014, Rebora et al. 2013).

In addition to this a great number of catchments in Liguria has very limited spatial extension (less than 100 km^2) and, due to the geomorphologic configuration of the region, very steep slopes. Many of these basins, around 200, have a drained area even smaller than 15 km^2 (see Martina et al., 2018).

Considering these facts, it is clear that the corresponding hydrologic response timescale of these catchments is in the order of a few hours, threatening the urban areas, in which the time to take decision for emergency actions is consequently short. Hence a suitable forecast and early-warning of these kind of events is essential (Ferraris L., 2002).

For the PhD work three main cases have been analyzed occurring in Liguria Region during autumn of 2014. Hereafter a brief description of the events and of the main catchments involved and analyzed for the basin scale analysis.

One of the events analyzed is the already mentioned event of 9th October 2014: during this event a devastating flood affected the Bisagno Creek, located in the municipality of Genoa, causing the death of one person and hundreds of millions of euro in damage to public infrastructure, buildings and goods (Rebora et al., 2015; Silvestro et al., 2016). During the 8th and the morning of 9th of October a series of stationary storms affected the central and eastern parts of the Liguria Region. On the Bisagno Creek about 130 mm of rainfall was recorded at basin scale in 36 h, produced by three main events of 3–6 h duration. During the evening of 9th, after some hours of very light rain, there was a new, strong and intensified storm; approximately 4 h of very intense rainfall affected the central part of the catchment causing a very fast response of the basin.

This time, 130 mm of rainfall was recorded in 4 h as average amount at basin scale, but with local rainfall amounts within the basin (on areas of only a few square kilometers) of 250 mm. These very high rainfall intensities, even if for short durations, had a fundamental role in the runoff formation and led to a peak flow of about 1100–1200 m^3/s corresponding to a return period T of approximately 100–200 years.

This event affected mainly the Bisagno Creek and but also the basins Scrivia and Sturla, located nearby in the province of Genoa (Figure 6).

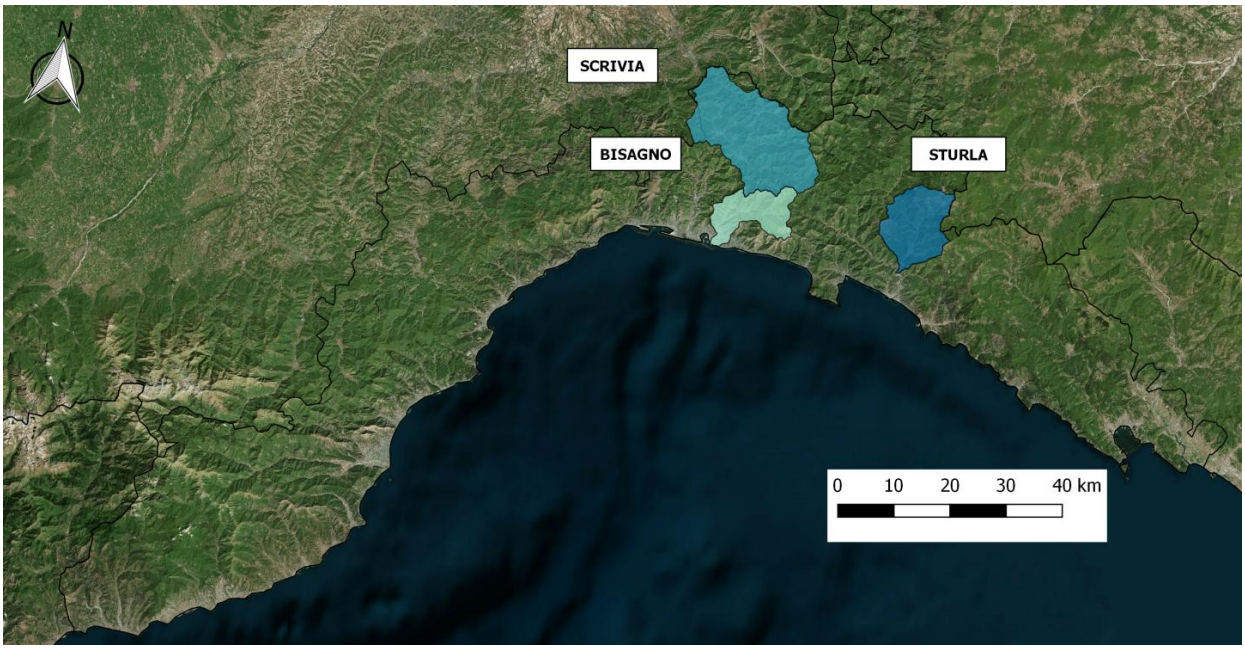

Figure 6: Location of the basin involved in the event of 9th October 2014: Bisagno, Scrivia and Sturla

During the second event event, that stroke the area of Chiavari and its inland Fontanabuona valley (Faccini et al., 2015c) between 10th and 11th of November 2014; many catchments of this area overflew causing damages and the loss of two human lives. Along the 10th November 24 hours of heavy rainfall interested Liguria region and in particular in the area of Entella catchment (Figure 7) were registered high amount of cumulative rainfall. In upper Graveglia Valley (eastern tributary of the Entella stream) and along the middle and lower Fontanabuona valley cumulative rainfall amounts of 170 mm/6 hours.

Figure 7: Location of the basin mainly involved in the event of 11th November 2014, Entella

The maximum rainfall rate was registered at the Panesi raingauge, inside Entella catchment, with 66 mm in 1 hour, 220mm in 6 hours. The main at ground effects were flash floods and landslides: the most important effects involved Entella catchment and its tributaries between 20:00 and 23:00 UTC causing the rising of Lavagna stream level at Carasco of 6 m and of Entella at Panesi of 7 m.

The last event occurred some days later on in the same month, during the first hours of the 15th of November. During this event rainfall intensities reached high values all over Liguria Region: maximum rainfall rates have been registered at Mignanego rain gauge, located along the course of Polcevera river, with 108 mm in 1 hour and 236 mm in 6 hours. In many rivers the creek level raised and many flooding were registered in Savona and Genoa provinces caused by small catchments. Within the municipality of Genoa many areas were flooded mainly because of the

flooding of Cerusa, Polcevera (see location in Figure 8) and its tributaries Riccò, Fegino e Rio Torbella.

Figure 8: Location of the basins analyzed for the 15th November event

The size of the catchments considered is really different: Cerusa has a drained area of 25 km^2 while Polcevera of almost 150 km^2. In both the basins occurred damages during this event flooding the urban area in which they are passing through.

Chapter 3: State of the art

The importance of a suitable hydrological nowcasting chain has been introduced in the previous section. Sufficiently long lead time is required for flood early warning system to be useful for issue timely warnings in various forms, from taking flood mitigation measures, evacuating potentially affected residents. In this chapter a literature review of all the elements composing the chain will be developed: the nowcasting models (3.1), the NWPS and the data assimilation module (3.2), the blending technique (3.3), the hydrological models (3.4), the hydrological nowcasting chain (3.5).

3.1 Nowcasting models

Rainfall forecasts can effectively extend the lead time available for issuing flood and flash-flood forecasts by several hours depending on the accuracy of the precipitation forecasting technique. To incorporate a short-term rainfall forecast into a hydrologic simulation, quantitative precipitation estimates (QPEs) from weather radars, satellites, and numerical weather models (Droegemeier et al. 2000) can be used to extrapolate rainfall fields and increase hydrologic predictability (Smith and Austin 2000; Berenguer et al. 2005). While quantitative precipitation estimation is a method that approximates the amount of precipitation that has fallen at a location or across a region, the Quantitative Precipitation Forecast (abbreviated QPF) is the expected amount of melted accumulated over a specified time period over a specified area.

Rainfall forecasting or quantitative precipitation forecasting (QPF) can be obtained through both medium range forecast (beyond 3 days), short-range forecast (usually a few days) and very short-term forecasting (in the order of hours) known as nowcasting.

Traditionally, QPFs can be achieved by extrapolating the future rainfall distribution from a sequence of radar images (i.e. radar-based rainfall nowcasting) or by solving numerically the equations of a NWP model.

It has been found that the radar-based rainfall nowcast has shown better skill for short lead time forecasting; this is expected as radar can capture very well the initial precipitation as they are based on the assimilation of the initial precipitation state as provided by the radar rainfall estimates (Smith and Austin, 2000; Lin et al., 2005; Berenguer et al., 2012). So, for very short lead time of precipitation (0–3 h), radar nowcast performs better, whereas for longer lead times, forecasts based on numerical models are better as they could provide signal of heavy rainfall.

One of the reasons why the accuracy rapidly decreases with increasing lead times is that radar nowcasting techniques do not model processes such as growth and decay of precipitation (Golding, 1998), that in longer lead times become crucial.

First attempts of deterministic radar-based rainfall nowcasts are represented by Eulerian or Lagrangian persistence. In the case of Eulerian persistence, the most recent radar rainfall observation is used as the nowcast. In Lagrangian persistence the motion field of the most recent observation is determined and then extrapolated into the future (examples of both techniques can be found in Germann and Zawadzki (2002, 2004)).

The first techniques for nowcasting thunderstorm location were developed in the 1960s and 1970s by extrapolating radar echoes. The basic techniques to produce quantitative rainfall forecasts from radar echoes are based on cross-correlation or individual radar echo-tracking (Collier, 1981). Austin and Bellon, (1974) implemented for the first time the cross-correlation pattern matching technique to forecast storms up to 3h ahead. An echo centroid tracking technique was implemented by Browning et al., (1982) for the extrapolation of frontal rainfall 6h ahead. The results showed that the loss of predictability was due to decay and development processes not modeled by these forecasting techniques.

In order to integrate the advantages of radar-based and NWP-based rainfall forecasting techniques, hybrid systems merging radar nowcasts and NWP forecasts started to be developed in the 1980s. The aim was to achieve more skillful forecasts than either radar nowcasting models or NWP models could provide (Golding, 1998).

Some nowcasting techniques like NIMROD (Golding, 1998) and GANDOLF (Pierce et al., 2000) try to combine radar data with satellite data and meteorological models, but the results are not always better than using radar information alone. NIMROD (Nowcasting and Initialization for Modelling Using Regional Observation Data System) was developed for tracking stratiform-type storms and has little potential with convective-type systems. NIMROD uses a combination of radar echoes and NWP wind fields.

GANDOLF (Generating Advanced Nowcasts for Deployment in Operational Land-surface flood Forecasts) is an automated system for generating short range (0–6h) forecasts of precipitation with high spatial (2 km) and temporal (15 min) resolutions which scheme combines cross-correlation and NWP based wind advection algorithms to forecast the motion of a discrete set of rain objects. GANDOLF was developed for tracking large-scale multi-cellular convective-type storms and

utilizes 3-D reflectivity data to identify convective storms. Once a storm has been identified it is then classified into different stages of development and when compared to the conceptual model for ideal storm evolution, the future development of the storm is estimated.

Several other nowcasting schemes have been introduced in the literature. Among these, the Thunderstorm Identification, Tracking, Analysis, and Nowcasting (TITAN) system (Dixon and Weiner, 1993) is a cell tracker that has the ability to grow and dissipate storm cells based on historical trends and it was specifically developed for convective-type storms. The thunderstorm Auto-nowcaster (ANC) system (Mueller et al., 2003) was developed to nowcast convective-type storms by using fuzzy logic. Radar reflectivity is extrapolated coupled with wind pattern data and the system can estimate initiation, growth and dissipation of storms (Wilson et al., 2004).

An important improvement in the nowcasting techniques has been done connecting the predictability of precipitation at short temporal scales with the spatial scale of the structures considered (Wilson et al. 1998; Germann and Zawadzki 2002). This has motivated the development of stochastic nowcasting methods operating in the Fourier domain, such as Spectral Prognosis (S-PROG; Seed 2003) or the method proposed by Xu and Chandrasekar (2005). In these techniques, the spectral representation allows for naturally considering the scale dependence of the statistical properties.

S-PROG is an advection-based nowcasting system that combines three components: the estimation of the field advection, decomposition of the field into Fourier components, and a model for the scale dependent Lagrangian evolution of the field. It exploits the observed rain fields using both spatial and dynamic scaling-dependent properties. The lifetime of a feature in the field is on the scale of the feature (large features evolve more slowly than small features), and that features at all scales between the outer and inner observed scales are present in the field. Fourier filters are used to decompose the rain field into its spectral components and the Lagrangian temporal evolution of each level in the cascade is modeled using an autoregressive model, which automatically causes the forecast field to become smooth as the structures at the various scales evolve through their lifetimes. The forecast field is then simply calculated as the sum of the advected Lagrangian forecasts for each Fourier component.

Another example of hybrid model is the Stochastic Probabilistic Precipitation Forecasting Scheme (STEPS), that merges an extrapolation nowcast with a downscaled NWP forecast (Bowler et al., 2006).

STEPS derives forecast data from two separate sources—radar-based rain analyses and NWP model forecasts. In order to merge these with uncertainty estimates, three cascades are maintained—an extrapolation forecast cascade, an NWP model forecast cascade and a noise cascade. Using estimates of the skill of the two forecast cascades permits the determination of the relative weights given to each cascade. The advection uncertainty is modeled by a random field of velocities which is correlated in space. The uncertainty in the field evolution is modeled using the S-PROG multiplicative cascade approach (Seed 2003).

The idea to express uncertainty by adding a stochastic component to the nowcasting forecast has been further explored within Germann et al. (2009), in which is presented REAL (Radar Ensemble generator designed for usage in the Alps using LU decomposition): the radar precipitation field is perturbed with correlated random noise, representing the residual space-time uncertainty in the radar estimates. Then in Berenguer et al. (2011) the SBMcast model, already presented in Berenguer et al. (2005) is adapted in its probabilistic version exploiting the String of Beads model (Pegram and Clothier, 2001) to generate ensembles of rainfall forecasts compatible with the observations (evolving from the most recent observations).

In this framework is located the probabilistic nowcasting technique PhaSt, introduced by Metta et al. (2009). PhaSt, which description will be deepened in section 4.1, is a spectral-based nonlinear stochastic nowcasting model based on the empirical nonlinear transformation of rainfall fields followed by their stochastic evolution in spectral space.

In the last years development has been done in this field under different perspectives. One of these is the use of machine learning to recognize certain pattern of precipitation. Panziera et al., (2011) developed a tool, NORA (Nowcasting of Orographic Rainfall by means of Analogues), for short-term forecasting of precipitation exploiting the orographic forcing and the increasing volumes of radar data archives using the method of analogues. Advances in this field have been done also in Foresti et al. (2018), in which a 10 years archive of composite radar images is exploited to perform a statistical analysis of precipitation growth and decay highlighting the mesoscale flow conditions and geographical locations most prone to orographic precipitation enhancement in mountainous regions.

Another aspect under which the studies upon nowcasting are moving forward is the connection of the nowcasting output to the forecast of the NWP model; this technique, called blending, will be further analyzed in section 3.3. Within this framework a further step is done: the NWP model used

is corrected with data assimilation of radar data, to obtain a forecast, more reliable, updated with observations. This element of the chain will be described in the following section (3.2)

3.2 Numerical Weather Prediction System and data assimilation module

In the last decades many advancements led to a substantial improvement of the Numerical Weather Prediction Systems (NWPSs) forecast skill (Buizza et al. 1999). The increasing resolution of them recently allowed their use in a operational framework at small spatial scale (2 km or less). Despite of that the Quantitative Precipitation Forecasts are still affected by errors that are really relevant at small spatial and temporal scales such as those characterizing the events mentioned before characterized by intense and persistent rainfall structures lasting several hours leading and producing high rainfall amounts falling over a limited portion of area in (Siccardi et al.,2005).

Besides that, those events are often associated with phenomena, as deep convection, that presents a chaotic behavior and a consequently low predictability. Hence, errors in the initial and boundary conditions can rapidly worsen the accuracy of the QPFs. To deal with this problem recently several studies focused in the assimilation of observations, in particular rainfall data, into the NWPS (Sun 2005, Dixon et al. 2009; Dow and Macpherson 2013).

The main purpose of Data Assimilation (DA) is the merging of measurements and model predictions under the assumption that both supply useful information on the system state. In recent years several DA techniques have been developed, differing in numerical cost, optimality and suitability for real-time applications.

The main DA techniques can be distinct in two approaches: the sequential and the variational approach. The most basic technique, part of the family of the sequential approach, is the Direct Insertion (DI), that is adopting a simple replacement of forecast predictions with observations, whenever they are available, within the model simulations. In the same family but with rising complexity, an improved version of this scheme is the Optimal Interpolation (OI) technique. Whenever observations are available and assimilated, model predictions are adjusted according to an a priori error structure of both observations and model estimates, which are supposed to be constant throughout the simulation.

Among these sequential techniques is located the Nudging method (or Newtonian relaxation) (Stauffer and Seaman, 1990), that will be further described in section 4.3. The nudging method allows to take into account the observational uncertainty, which is a priori defined. According to this DA technique, a correction term is added to the prognostic model equations with the aim of gradually relaxing the predictions towards observations

At a higher level of complexity among the sequential DA methods, the Kalman filter (Kalman, 1960; Evensen, 2003) and several techniques based on Kalman filtering. It enables to evaluate the optimal weighting between modelled and observed states, according to their degrees of uncertainty. The main feature distinguishing this approach from more static ones is the dynamic updating of the forecast error covariance during the simulation.

As an alternative to sequential assimilation, the variational (VAR) methods can be efficiently used in complex modelling system (Ercolani and Castelli, 2017). Instead of using only the observations available at each assimilation time step, the VAR methods simultaneously process all the observations in the assimilation window to estimate the system state and obtain the best solution to the analysis problem (Holm, 2003). The variational data-assimilation technique achieves this through the iterative minimization of a prescribed cost function (Ide et al., 1997).

The objective function is defined in terms of a trade-off between the amount of noise introduced into the model and the distance between simulated and observed variables (Lee et al., 2012). The assimilation problem is therefore redefined as an iterative process aiming at minimizing the gap between observed fields and model states.

Among the variational techniques the three-dimensional (i.e. space dimensions) VAR DA (3DVAR) uses one-time observations to statistically produce initial conditions through forecast fields and observational data. The four-dimensional (i.e. space and time dimensions) VAR DA (4DVAR) differs from the 3DVAR for including the dynamic evolution of the model in the assimilation (Holm, 2003).

The assimilation of rainfall data is not of easy implementation since this variable is not directly forecasted by a NWP model but is the result of dynamical and microphysical atmosphere processes.

In Xiao and Sun (2007) high-resolution (2 km) radar data assimilation into the NWP model proved to better represent the convective systems in the model initial conditions. Other studies applied data

assimilation on rainfall observations converted from the radar reflectivity data into the NWP model (Stephan et al., 2008).

Among the developed technique at ECMWF, a 4DVAR analysis system has been used operationally since November 1997 (Rabier et al. 1992; Mahfouf and Rabier 2000; Klinker et al. 2000). Remaining in an operational framework Macpherson (2001) introduced the assimilation of radar-derived rainfall data into the UK Met Office.

Even though DA is a suitable technique to enhance the NWPS forecasts, in the first time steps short term forecasting is till performing better: for this reason the blending technique can be the solution to combine different rainfall input into a unique rainfall field that try to take the best from every forecasting method. The literature review related to this research area is reported in the next section (3.3).

3.3 Blending technique

As said in section 3.1, nowcasting models have shown to have a predictability limit after some hours of forecast. This behavior is mainly due to the fact that in the nowcasting model the evolution of the precipitation systems is only related to the motion of the existing precipitation structures. The processes of growth and decay of the precipitation systems are not considered while their importance increases with increasing lead time (Germann et al., 2006). The blending technique tries to overcome this limit aiming to connect the nowcasting output with the NWPS forecast.

Blending has been previously analyzed in some studies with the purpose of improving the rainfall forecast smoothly mixing nowcasting rainfall scenarios and NWPS QPF. First attempts have been made by Golding (1998) and by Bowler et al. (2006). Most of the published methods for combining nowcasts and forecasts use a weighted sum of the two fields. The weighting functions are defined by the skill of the predictions derived from suitable quality measures.

In Kilambi and Zawadzky (2005), a combination of nowcasts obtained with MAPLE (McGill Algorithm for Precipitation nowcasting by Lagrangian Extrapolation, Turner et al., 2004) and precipitation forecasts from NWP models WRF and GEM (Cote et al.,1998 and Carpenter et al., 2004) is performed after an evaluation of their relative skills. The weight scheme is based upon the climatological, or long term average, value of Critical Success Index (CSI, see Equation 1) of each individual component of the ensemble as a function of lead time.

$$weight = \frac{1}{1-(CSI)^{2.5}} - 1 \qquad Eq.1$$

In Kober et al. (2012) probabilistic nowcasts are created by combining the output of the radar tracker Radar TRAcking and Monitoring (Rad-TRAM, Kober and Tafferner, 2009) with the forecasts of COSMO-DE-EPS (DWD development of the COSMO-DE model, Baldauf et al., 2011). The combination of the forecasted rainfall fields is performed through a weighting function derived from an index, the Conditional Square Root of Ranked (CSRR) probability score, representing the skill of the nowcasting technique. The weighting function for Rad-TRAM, is defined in Equation 2, depending on the CSRR expressed in function of the lead time τ:

$$w_r(\tau) = 2.11 - \frac{1}{1-CSRR(\tau)^{2.8}} \qquad Eq.2$$

The weight w_c for the COSMO-DE-EPS based forecasts is described in Equation 3:

$$w_c(\tau) = 1 - w_r(\tau) \qquad Eq.3$$

The resulting blended rainfall field is then a linear combination of the weighted rainfall fields .

In Atencia et al. (2010) two blending techniques are compared aiming at obtaining from three methodologies [advection of the radar reflectivity field (ADV), Identification, tracking and forecasting of convective structures (CST) and NWP] a single and optimized QPF at each lead time. The first one is based on previous methodologies as the ones described above, but different indexes to compute the weights are tested (CSI, POD, FAR, bias etc). To summarize the different performances of the indexes, a standard index is defined converting every index into an dimensionless index that varies between zero for the perfect forecast and infinity for totally mismatching forecasts. Known the standard index for the NWP model (ν_m) and the standard index related to the advection forecast (ν_a), the weight for the NWP model is calculated as follows:

$$W_m = \frac{\nu_a}{\nu_a + \nu_m} \qquad Eq.4$$

While the weight for the advection forecast is described in Equation 5:

$$W_a = 1 - W_m \qquad Eq.5$$

Such as for the other blending techniques, the resulting field is a linear combination of the weighted rainfall fields.

A different approach is represented in Atencia et al. (2010) by the second blending technique, called spatial blending, that introduces spatial dependence of weights as distance function to rainfall structures. To avoid loss of information about the new rainfall areas the advection and evolution term and the source term are separated; the forecast area is divided in a region where precipitation is recorded, a second area called weight variation area (where the advection is forecasting precipitation and 20 km around the first and the second area) and, finally, a third region where only the source term is taken into account. In the first two area the weight computed as in the classical blending. The third area is not weighted, but only corrected by an intensity bias index, obtained comparing previous model forecasting with the final observed rainfall. This technique was proven to improve mainly at the beginning of the forecast because of maintaining the new precipitation areas coming from the model.

As in this PhD work the focus is not only on the blending technique, the technique used, referring to the research area of the classical blending, will be the one described in Section 4.4.

All the elements defined up to this point represent only the input of the hydrological model: the framework in which the hydrological model used is located is hereafter illustrated (Section 3.4).

3.4 Hydrological models

The suitable choice of hydrologic model depends on the forecast lead time, catchment size, and the characteristics of runoff (Arduino et al. 2005).

In the wide range of hydrological models a distinction has to be done according to representation of the spatial dimension: the model may be lumped, semi-distributed and distributed. A lumped model views a watershed as a system that produces outputs (hydrographs) without detailed spatial variability of the physical processes that produce that response. They use mean values of the basin features as well spatially-averaged values of inputs/outputs. The use of mean parameters leads to average the represented process; this can lead to significant errors due to the non-linearity of the hydrological processes.

In semi-distributed models the sub-basins are represented as irregularly shaped but hydrologically homogeneous: runoff is aggregated to the catchment outlet using routing methods. Conversely, distributed models consider the spatial variability of processes, inputs and outputs. Usually the basin area is divided in different sub-units on which the equations for the different processes are solved so that flood information across the catchment can be more easily derived. Because of the distributed nature of hydrological properties like soil type, slope and land-use, they are expected to accurately represent the watershed processes.

In distributed models, basin runoff response can vary within the watershed according to the temporal and spatial variability in rainfall, surface properties, and antecedent wetness (Ivanov et al. 2004a, b). Their detailed and complete description of the hydrological cycle characterize these models with abundant number of parameters, that need the knowledge of many information regarding the modeled catchments.

Physics-based distributed hydrologic models are more likely to represent the cause–effect relationships leading to changing runoff behavior (Arduino et al. 2005). These models can offer distinct advantages over conceptual, lumped models and are used widely for flood forecasting (e.g., Garrote and Bras 1995; Reed et al. 2004; Ivanov et al. 2004b).

Another distinction can be done according to representation of the temporal dimension: it is possible to distinct event based model and continuous models.

An event-based model represents a single discharge event with a duration in a range from a few hours to some days. Initial conditions (especially moisture) should be a priori determined and introduced as input (Berthet et al., 2009). Output accuracy is strongly influenced by initial conditions reliability. Usually some processes are neglected (evapotranspiration, water table recharge…). A continuous model resolves the hydrological processes on a longer period of time. It considers all the processes involved in the hydrologic cycle, the influence of initial conditions rapidly decreases with time.

In this thesis we use a distributed hydrological model that will be described in section 4.5. The connection of all the elements led to the implementation of a hydrological nowcasting chain, referring to the research area hereafter presented (section 3.5).

3.5 Hydrological nowcasting chain

The use of the hydrological nowcasting chain helps technicians to evaluate the possible scenarios of discharge that will be occurring (Siccardi et al., 2005; Pappenberger et al., 2013). For small and very small basins with short response times prone to flash-flooding radar rainfall estimates have proven to be extremely valuable because of their high spatial and temporal resolution which allows for near real-time tracking of storms (Berenguer et al., 2011).

A number of studies (Giannoni et al., 2003; Berenguer et al., 2005; Vivoni et al., 2006 and 2007; Germann et al., 2009, Gourley et al., 2010) have shown the benefit of coupling radar rainfall measurements with distributed rainfall–runoff models to improve the simulation of the response of small- to medium-sized catchments.

In Berenguer et al. (2005), a modified version of S-PROG is applied in the Mediterranean Region and the performances of the flood nowcasting chain, result of the connection between S-PROG and the distributed rainfall-runoff model DiCHiTop (Corral et al., 2001), are evaluated. Results show better performances of the chain fed by the nowcasting technique with respect to the simpler Eulerian and Lagrangian persistence with an increase in terms of gained lead time in the forecast.

In Foresti et al. (2016) it is possible to find that many studies already analyzed the added value of the deterministic nowcasting systems in catchments hydrology but is more difficult to find the same for probabilistic hydrological nowcasting chain. Deterministic forecasts have the advantage that they are usually easier to produce and verify by forecasters, and interpret by the wider community. On the other hand probabilistic forecasts allow the forecaster to provide information on the certainty/uncertainty associated with the occurrence of a particular event. By the side of the end user probabilistic forecasts inform the user of the uncertainty and provide information necessary for making rational decisions, enabling the user to take risk explicitly into account (Krzysztofowicz, 2001; Ramos et al., 2013).

However, in the last years, radar-based ensemble nowcasting systems are increasingly used as inputs for flood and sewer system modeling (Silvestro et al., 2012b; Silvestro et al.,2015a; Codo & Rico-Ramirez, 2018)

In Silvestro et al. (2012b and 2015a) the nowcasting technique used in this work, PhaSt (Metta et al., 2009), has been used as part of a probabilistic nowcasting chain with a linear, semi-distributed rainfall-runoff model (DRiFt, Giannoni et al., 2000) for small and medium size basins with drainage

area of order of magnitude greater than 10^1 km^2 in specific case studies. In this work, PhaSt is used coupled with Continuum (Silvestro et al., 2013, 2015b) for creating a flood nowcasting chain (description in Chapter 4).

In Europe, since 2009, the operational European Flood Awareness System (EFAS) produces flash flood warnings based on the European Precipitation Index (EPIC), calculated using the cumulated rainfall forecasted by COSMO-LEPS for different durations compared with climatologic values (Thielen et al., 2009; Pappenberger et al., 2011).

The AIGA system (Javelle et al., 2016), operationally running in France, compares discharges generated by a simple conceptual hourly hydrologic model run based on radar rainfall estimations, to reference flood quantiles of different return periods, at any point along the river network. The system hence gives in real time an information on the severity of ongoing events using the range of the return period estimated.

According to Cuo et al. (2011) in literature it is possible to find many examples of using NWP model–based ensembles and using radar ensembles, but none use both in combination with forecasting streamflow. This is the attempt of the current work, the definition and the testing of an integrated hydrological nowcasting chain that takes in input the best combination of QPF and produces a probabilistic forecast of discharge. The elements of this chain will be analyzed in the next Chapter (4).

Chapter 4: New development of an integrated hydrological nowcasting chain

In this chapter all the elements that compose the hydrological nowcasting chain developed along the PhD will be described. Starting from the main input of the chain, the rainfall observed through the radar (4.1), the nowcasting technique, PhaSt (4.2), the meteorological model and the data assimilation scheme used (4.3), the blending technique and the blending functions examined (4.4), the hydrological model Continuum (4.5), the whole hydrological nowcasting chain (4.6)

4.1 Input of the chain: radar rainfall data

The main input of the hydrological forecasting chain is the observed rainfall. This observed rainfall field comes from the Doppler polarimetric C-band radar, located on Mount Settepani (Figure 9) at an altitude of 1386 m, that works operationally with 10 min scan time and 1x1 km^2 spatial resolution. The rainfall field is estimated through the algorithm described in Silvestro et al. (2009) and is currently used by the Meteorological Weather Services in the Italian regions of Piedmont and Liguria and by the Italian Civil Protection Department. The observed rainfall field is also the input of the nowcasting model and it is used in the assimilation scheme: both the processes will be explained in the following chapter.

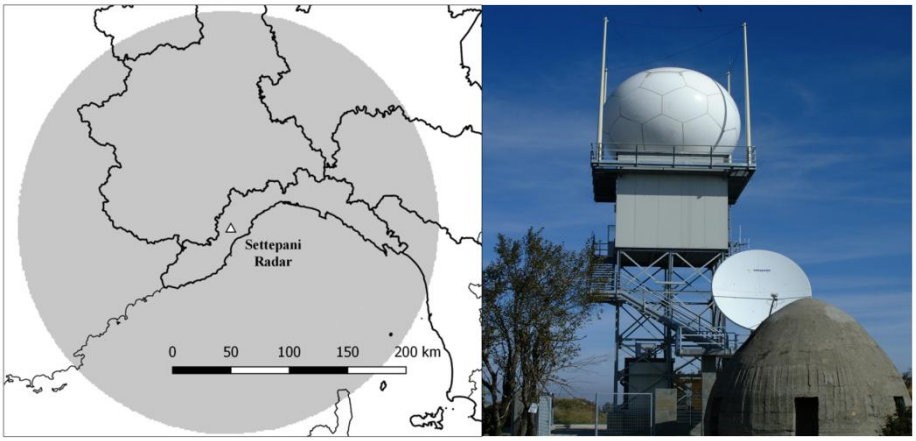

Figure 9: Settepani radar location in Liguria Region and structure of the radar

4.2 The nowcasting algorithm: PhaSt

PhaSt (Metta et al., 2009) is a spectral-based nowcasting procedure based on the empirical nonlinear transformation of precipitation fields provided by radar measurements and on the stochastic evolution of the transformed fields in spectral space. This procedure is able to provide an ensemble, probabilistic nowcasting of precipitation fields up to a lead time of two hours.

In this approach, the initial one-point distribution and power spectrum of the precipitation field are kept constant, and a stochastic Ornstein–Uhlenbeck process (Uhlenbeck and Ornstein, 1930) is used for the time evolution of the Fourier phases of the Gaussianized precipitation field. The method automatically includes large-scale advection of precipitation structures, and it reproduces the nonlinear and intermittent nature of rain fields. In addition, the use of spectral space instead of physical space assures that the spatial correlations of precipitation fields are preserved.

The model requires two initial precipitation fields, to be used as initial conditions. It takes an empirical nonlinear transformation of the two precipitation fields used as initial conditions, $p(x, y, t = 0)$ and $p(x, y, t = -\Delta t)$, generates two Gaussian fields, $g(x, y, 0)$ and $g(x,y, -\Delta t)$. The Fourier transform of the Gaussianized fields are taken and their Fourier spectra, $\hat{g}(k_x,k_y, 0)$ and $\hat{g}(k_x, k_y, -\Delta t)$, is obtained. From these for each wavenumber (k_x,k_y) the Fourier phase, ϕ, and an estimate of the Fourier angular frequency are calculated. Fourier phases are then evolved in time by a stochastic process while Fourier amplitudes are kept fixed. There are several stochastic models that can be used to evolve the Fourier phases.

To allow for the presence of time correlations in the angular frequencies a Langevin-type model is used: the temporal evolution of the Fourier phase $\phi(k_x, k_y)$ at a given wavenumber (k_x, k_y) is written in terms of a linear Ornstein–Uhlenbeck stochastic process for the angular frequency. The Ornstein–Uhlenbeck process generates angular frequencies that have a Gaussian distribution with zero mean and variance σ^2 and an exponentially decaying temporal autocorrelation.

The spectrum with the evolved Fourier phases is inverted to generate a nowcasted Gaussian field at the time t of interest, $g(x, y, t)$. This evolved field has the same power spectrum as the initial Gaussianized field, $g(x, y, 0)$. Different realizations of the stochastic process allow for generating different evolutions of the precipitation field and for creating an ensemble of precipitation nowcasts.

Then an inverse nonlinear transformation to pass from the evolved Gaussian field $g(x, y, t)$ to the nowcasted precipitation field is performed.

The use of a stochastic process for the evolution of Fourier phases allows for generating many realizations, to be used as members of an ensemble of precipitation nowcasts. All ensemble members are characterized by the same amplitude distribution and very similar power spectra. However, the phase evolution (i.e., the positioning of rainfall structures) evolves differently in the different realizations, providing an estimate of the probability of occurrence of precipitation at a given point in space and a given moment in time.

One of the first steps of this PhD work has been a study on the nowcasting model PhaSt: starting from the formulation as it was operational at CFMI-PC of Liguria Region, a deep analysis on the model characteristics has been performed, calibrating some of the parameters in input.

In the previous version of the model there were some issues in the forecast: the fields forecasted where really similar between each other but the correlation with the initial radar rainfall field is decreasing too much along the forecast time originating forecast very different in comparison with the observed rainfall field. To cope with these problems the equations that characterize the nowcasting model have been rewritten as follows:

$$\begin{cases} k_s = \left(k_x^2 + k_y^2\right)^{\frac{1}{pwr}} \\ d\Phi_{k_s} = \omega_{k_s} dt \\ d\omega_{k_s} = -\left(\omega_{k_s} - \omega'\right)\frac{dt}{T} + \sqrt{\frac{2\sigma^2}{T}}\sqrt{1 - \frac{dt}{2T}}\, k_s dW \qquad (Ornstein - Ulhenbeck\ process) \end{cases} \qquad Eq.6$$

Where:

- k_s is the spectral phase, dependent on the wavenumbers k_x and k_y: k_s was set to one in the original equations. Through this relation is possible to give more weight to the small scales and less weight to the bigger ones;
- T is the decorrelation-time, after which the rainfall field is assumed to stop
- σ^2 is the variance of the Gaussian noise used to take into account the uncertainty of the nowcasting process;
- dW a is a random increment drawn from a normal distribution with zero mean and second-order moment (W is a Wiener process).

Different attempts have been performed to test the behavior of the nowcasting technique and assess the representativeness of the produced rainfall fields. Parameters as the power at which the sum of the wavenumbers is elevated, the variance of the process and the tendency velocity of the rainfall

field have been calibrated. The power of the wavenumbers changed in order to give more importance to the change in the rainfall structure at small scale than in the larger scale.

The representation of the noise of the forecasted rainfall filed has been distinguished into two components, one related to a noise constant in time and the other one to a noise changing in time and space in order to have forecasted rainfall fields different between each other along the dimension related to the ensembles but coherent with the initial observed rainfall field.

This recalibration allowed to set the variability of the different scenarios to a suitable range: as it can be seen in Figure 10 after 10 minutes the forecast is almost identical for all the scenarios. This is representative of the reality: the movement of the precipitation structures should be minimal and there should not be many differences between the ensembles as at the beginning of the forecast the uncertainty is low.

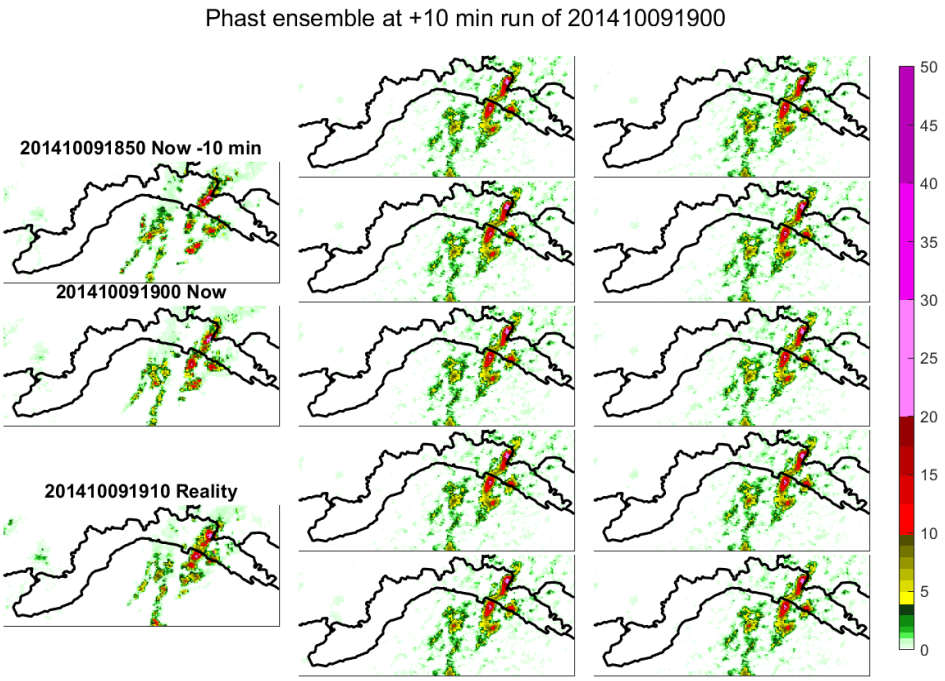

Figure 10: PhaSt forecast expressed in mm at 10 minutes for the run of 09-10-2014 at 19:00

After 1 hour (Figure 11) the differences between the 10 forecasted rainfall field are in this version appreciable while after two hours from the start of the run the forecast become less reliable and every forecast is very different from the others.

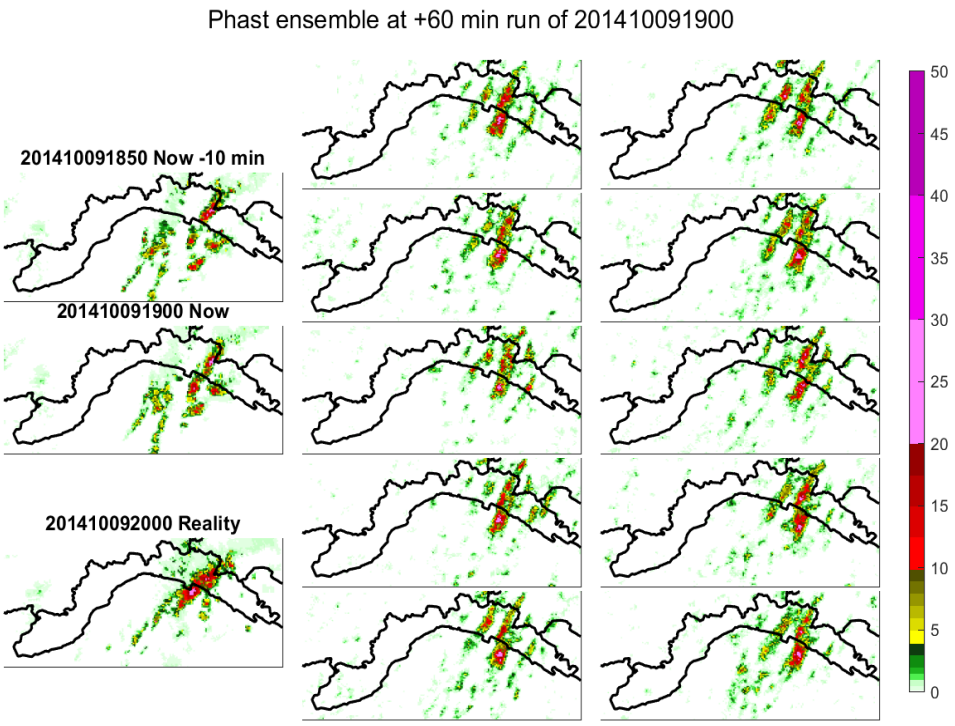

Figure 11: Phast forecast expressed in mm at 1 hour for the run of 09-10-2014 at 19:00

For this first step of the study the number of members that was used operationally at CFMI-PC of Liguria Region (10) has been maintained. For the next developments the number of ensemble has been raised to 20: for the spatial scale in which the model is applied this number can be considered sufficiently representative of the variability of the rainfall structures. Further increasing of the number of ensemble is not recommendable considering the computational time of the hydrological nowcasting chain as a whole. Since the rainfall input is updated every 10 minutes it would be really demanding to run also the hydrological model with the same frequency and high number of ensembles.

4.3 The meteorological model and the assimilation module

In the second part of the study the hydrological nowcasting chain is enriched with a new input: The model used has been developed and updated by the institute of research ISAC-CNR of Bologna. The operational chain includes the non-hydrostatic model MOLOCH, nested on the BOLAM model (Figure 12).

BOLAM is a limited-area hydrostatic model (Buzzi et al., 2004) based on primitive equations with a convective parameterization derived from Kain (2004) operating over a limited area of the globe (Europe).

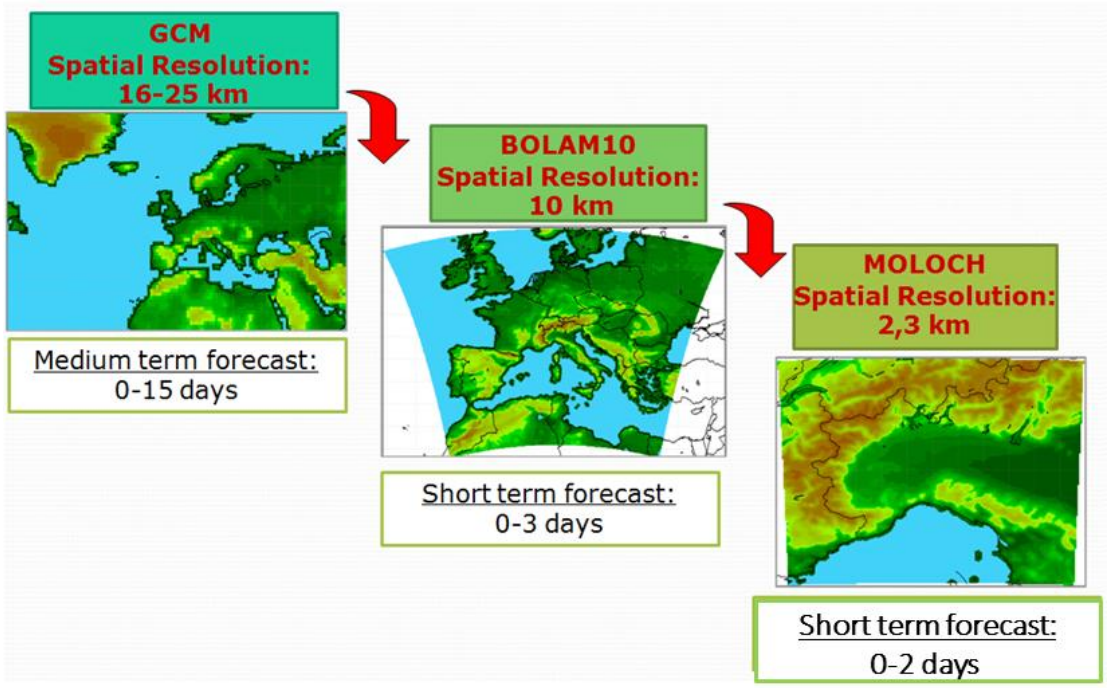

Figure 12: NWP system: MOLOCH is nested on the limited area model BOLAM, that in turn is taking its initial and boundary conditions from the forecasts of ECMWF

The initial and boundary conditions of BOLAM are supplied by four analysis per day (at 00, 06, 12, 18 UTC) and by the forecast of the ECMWF (European Centre for Medium-Range Weather Forecasts) global model at 0.125°; this allows to have updated run every 6 hours. The integration domain of BOLAM covers most of Europe with a total of 362x322 grid points on 45 levels and at present it runs on a horizontal grid size of 0.075 degrees (8.3 km) in rotated geographical coordinates. BOLAM runs are initialized at 00, 06, 12, 18 UTC of each day.

MOLOCH was more recently developed (details in Malguzzi et al., 2006; Buzzi et al., 2014; Davolio et al., 2017b) in order to perform forecasts with higher spatial detail, allowing an explicit representation of convective phenomena.

MOLOCH is nested in a 3-hour forecast of BOLAM to avoid a direct downscaling form the global analysis to the high-resolution grid and runs for 21 hours. BOLAM and MOLOCH differ mainly in the dynamical core, including the fact that MOLOCH resolves explicitly deep convection, while the following parameterization schemes are common in the two models: atmospheric radiation, atmospheric boundary layer and surface layer, soil processes and, to a large extent, microphysical processes.

The prognostic variables are the wind components u and v, the absolute temperature, the surface pressure, the specific humidity and the turbulent kinetic energy. The water cycle for stratiform precipitation is described by means of five additional prognostic variables: cloud ice, cloud water, rain, snow and graupel.

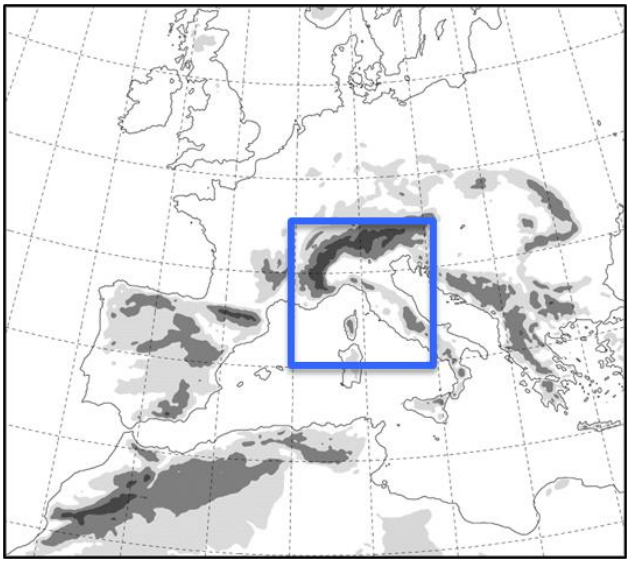

Figure 13: Integration domain of MOLOCH NWP model: it covers northern and central Italy with a resolution of 0.02 degrees (2.2 km)

The integration domain (Figure 13) covers north and central Italy. MOLOCH integrates the non-hydrostatic, fully compressible equations for the atmosphere, on a latitude-longitude rotated Arakawa C-grid, with a grid spacing resolution of 0.02 degrees, equivalent to about 2.2 km, and on 60 vertical levels (hybrid terrain-following coordinates).

The assimilation method, whose implementation in MOLOCH is shown in Figure 14, is based on nudging. The nudging technique represents a simple and empirical approach that has been proven to

significantly improve QPFs, although with an impact limited to the first lead hours of model forecasts (Leuenberger and Rossa 2007; Stephan et al. 2008; Sokol 2009; Sokol and Zacharov 2012; Craig et al. 2012; Dow and Macpherson 2013; Bick et al. 2016). It is also very simple and computationally cheap and therefore suitable to be exploited in very short range hydrometeorological forecasting systems (Rossa et al. 2010).

This scheme was applied to large-scale precipitation systems and to a model with parameterized convection and demonstrated to be able to improve the QPF for several heavy precipitation events (Buzzi and Davolio 2007).

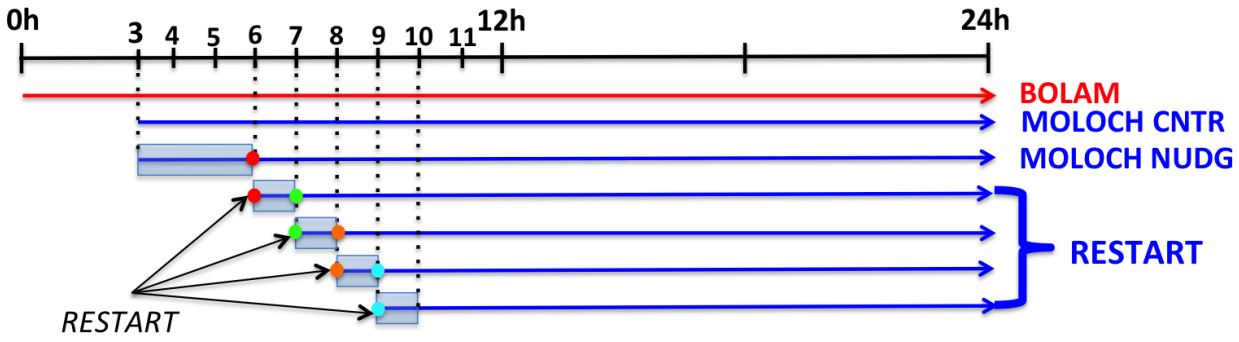

Figure 14: MOLOCH forecasts and data assimilation implementation:

During the assimilation window, model specific humidity profiles at each grid point are progressively modified depending on the comparison between observed and forecast rainfall. To attain this aim, hourly precipitation estimates provided by Settepani radar are used as observations. The assimilation scheme is explained in detail in Davolio et al. (2017a). The set up conceived for the present application takes into account the time requirements for an operational implementation. Considering the timing for global data availability and radar estimates delivery and processing, the first assimilation windows covers the first 6 hours of forecast. At the end of this period, the model state is stored, and a free forecast is run to cover the following hours. In this way, once a new hourly rainfall observation is available, an additional 1-h assimilation is performed, re-starting the model from the stored condition. This procedure can proceed for several hours, at least until the following global analysis is available, and allows for updating and improving forecasts, as a consequence of a longer assimilation period.

The information retrieved from the NWP model corrected with DA is used within the hydrological nowcasting chain in two main forms: firstly a work has been done using the information regarding

the volume variation along the forecast horizon (see section 5.2). Secondly, the rainfall field forecasted by the NWP model corrected with DA is used as it is in input to the hydrological model: in this case the fields forecasted are merged with the nowcasted rainfall field to obtain a seamless rainfall input of 6 hours to the hydrological model. The results of this work will be explained in section 5.3.

4.4 Application of the blending technique

As said in section 3.1 the main limit of the nowcasting methods is that usually they do not include processes such as growth and decay of precipitation (Golding, 1998), that in longer lead times have increasing importance. On the other hand, these physical processes are represented in the NWPS so that it is worth to connect the two output of the nowcasting and the meteorological model in a resulting rainfall forecast the most accurate as possible. To combine the rainfall forecasted fields, in this work a blending function has been written in order to balance the forecast reliability of the two models

Recalling at what has been introduced in section 3.3, many of the previous methodologies to estimate the blending function start from the statistical indexes calculated on the forecasted rainfall field for the two models. These indexes allow to calculate the weight to give to the different rainfall fields forecasted. This strategy cannot be applied in this case due to the scarcity of rainfall events considered: having only three case studies it is not possible to have representative scores for the two methodologies. Only few events have been studied because of computational costs: long series of high resolution NWP models are usually not run in hindcast mode for a large number of flood events. In this work, looking at the blending functions already presented in literature and according to the arguments presented before about the representativeness of the models of the physical processes after the first hours of forecast a first guess of the possible blending functions to use has been performed and reported in Figure 15.

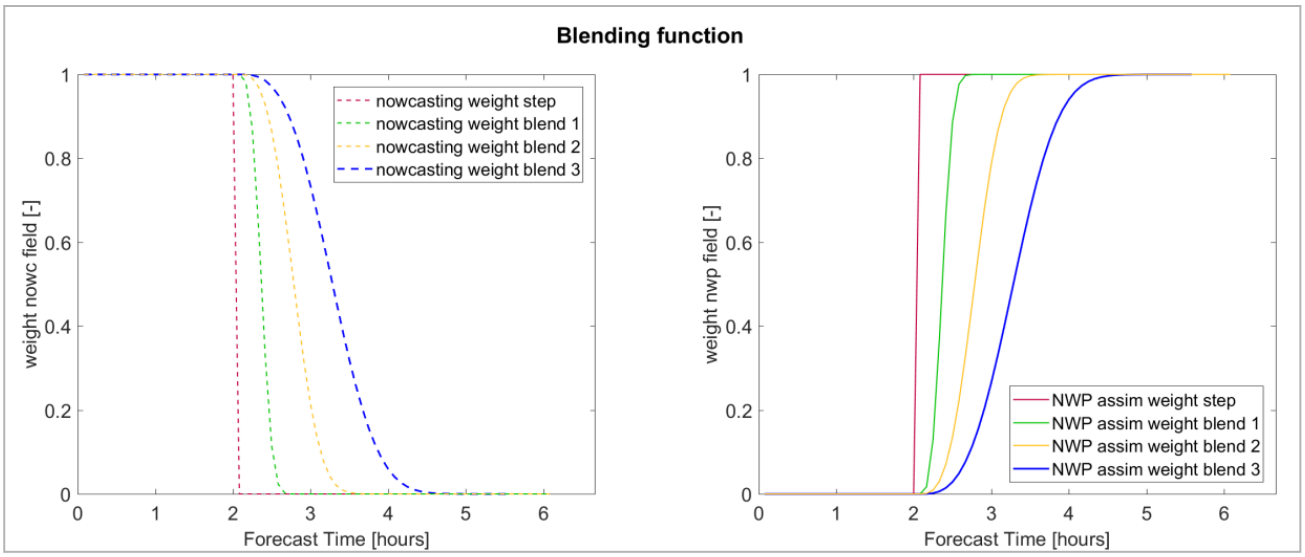

Figure 15: Different blending function analyzed: on the left the weighting function related to the nowcasted rainfall field, on the right the complementary function, used to weight the NWPS forecast. The first weighting function (red line) is a step function while the other functions are increasingly smoother.

The first thing to notice is that the weights of the NWPS forecasted rainfall fields are calculated as the symmetric function with respect to the half of the y axis in this way:

$$Weight_{NWPS} = 1 - Weight_{NOWC} \qquad Eq.7$$

Then, looking at the four different blending functions: the first function, that will be called below "step function", is gives all the weight for the first two hours to the nowcasted rainfall field and then, up to the end of the forecast, all the weight to the NWPS forecast as a switch on/off between the two models. The other three functions are then a progressive smoothing of this step function, trying to produce an intermediate forecasted rainfall field between the nowcasted and the forecasted that is a representative linear combination of them.

At a first glance could seem that all blending functions give too much weight in the first time steps to the nowcasting model. This trend is due to the fact that, beside the weighting function that (more or less) smoothly combine the forecasted field starting from the two hours of forecast, a first blending is performed through the modification of the rainfall volume, information derived from the NWPS forecast corrected hourly with data assimilation, in the nowcasted rainfall field. Moreover, we expect that forecast derived by extrapolation from observation can capture the spatial-temporal pattern better than NWPS along the first two hours of forecast (Metta et al., 2009; Collier, 1981; Seed, 2003; Xu and Chandrasekar, 2005; Berenguer et al., 2011). In this way more weight is given to the information of the nowcasting model regarding the positioning of the rainfall structures and a first correction of the forecast is done through the modification of the volume. Then, going ahead

with the forecast time, less weight is given to the nowcasted rainfall field in favor of the NWPS forecast, that gains more importance with time up to almost 5 hours ahead, time in which the rainfall field coincide with the one forecasted by the meteorological model. In fact at this time step, in spite of the modification of the volume of the nowcasted rainfall field, the absence of dynamic modeling in the nowcasting would affect too much the quality of the forecast in terms of spatio-temporal evolution of the rainfall fields.

Hence the rainfall blended field at a certain forecast time T results then from the linear combination of the field nowcasted and the field forecasted by the meteorological models assimilated as follows:

$$Rainfall\ field_{blended}(T) = (weight_{NOWC}(T) * rain_{NOWC}(T)) + (weight_{NWPS}(T) * rain_{NWPS}(T)) \qquad Eq.8$$

Since the forecast of the NWPS is deterministic the rainfall field that will be combined with the probabilistic forecast of the nowcasting is always the same field for the 20 forecasted rainfall field. Hence initially, as long as the weight of the nowcasted field is higher than the other weight the rainfall blended fields will be different between each other according to the spread of the nowcasting. When the weight of the nowcast is approaching to zero all the forecasted rainfall fields are more similar one to each other and similar to the deterministic forecast of the NWPS.

The resulting rainfall fields for six hours of forecast are the input of the hydrological model, whose detailed description is the topic of the next section (4.5).

4.5 The hydrological model: Continuum

C-DRiFt (Continuous Discharge River Forecast), named Continuum (Silvestro et al., 2013, 2015b) hereafter, is an evolution of DRiFt model. DRiFt (Discharge River Forecast) is a semi-distributed hydrological model (Giannoni et al., 2000) that simulates the discharge process within a basin. It takes into account the spatial variation of inputs such as meteorological input, morphologic, geological and anthropic characteristics of the basin, but it is lumped in parameters, and the discharge can be obtained in a given location wherever in the catchment. For these reasons, DRiFt is in the class of calibrated-parameters, semi-distributed models.

Continuum is a continuous distributed hydrological model and all the main hydrological phenomena are modeled in a distributed way. It strongly relies on a morphological approach, based on a novel way for the drainage network components identification (Giannoni et al., 2005).

The basin is represented using a regular square mesh, based on Digital Elevation Model (DEM), the flow directions are identified on the basis of the directions of maximum slope derived from the DEM (O'Callaghan and Mark, 1984). The drainage network distinguishes between hillslope and channeled flow (Giannoni et al., 2000).

As input, together with the interpolated meteorological data from ground sensors (rainfall, air temperature, wind velocity, short-wave solar radiation, relative humidity) and LAI (Leaf Area Index) matrices from satellite products (optional), Continuum only needs DEM and Soil Conservation Service Curve Number (SCS-CN) values (Mishra and Singh, 2013)

The model (schematized in Figure 16) solves explicitly both the continuity equation and the energy balance in a distributed fashion, using well known simplifications.

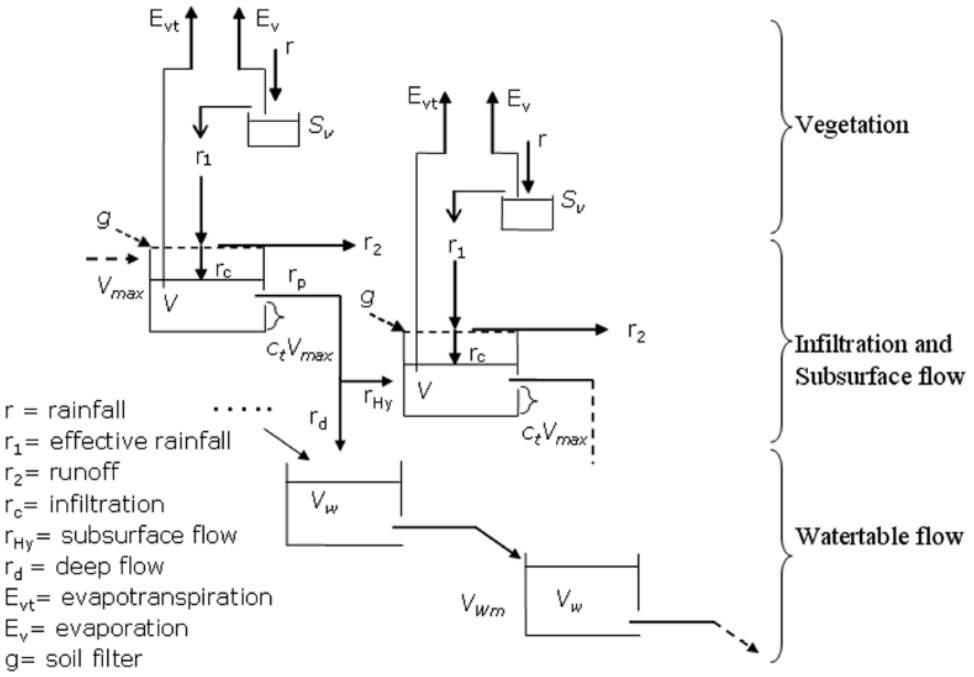

Figure 16: Schematization of the hydrological modeling performed by Continuum taken by Silvestro et al., 2013

Infiltration and subsurface flows are described using a semi-empirical, but quite detailed, methodology based on a modification of the Horton algorithm (Gabellani et al., 2008), the dynamic of soil moisture is schematized through the following mass balance equation computed for the root zone:

$$\frac{\Delta V}{\Delta t} = g(t) - r_p(t) \qquad \textit{Eq.9}$$

where $\frac{\Delta V}{\Delta t}$ [L t^{-1}] is the time evolution of volumetric soil moisture per unit area, $g(t)$ is the infiltration rate [L t^{-1}] and $r_p(t)$ [L t^{-1}] is the percolation rate that is, in turn, subdivided in two components according to the values of the terrain slope: subsurface flow that goes to increase the V in the downslope cells, and deep flow that goes to feed the deep layer containing the water table level.

Water table flow has been also schematized and it can influence the soil moisture level by inhibiting the deep percolation when the water table reaches the surface.

The infiltration rate is based on a modification of Horton algorithm (Diskin & Nazimov, 1995; Gabellani et al., 2008) that manages the inflow into the root zone with capacity V_{max} as:

$$g(t) = f_0 + (f_1 - f_0)\frac{V(t)}{V_{max}} \qquad \textit{Eq.10}$$

where f_0 [Lt^{-1}] is the maximum infiltration rate for completely dry soil and f_1 [Lt^{-1}] is the asymptotic minimum infiltration rate for saturated soils that is found as:

$$f_1 = f_0 * c_f \qquad \textit{Eq.11}$$

where c_f is a calibration parameter assumed constant for the whole basin as well as the other parameter c_t [0÷1] that describes the field capacity of the soil (i.e. the water content that can be held by capillarity against the force of gravity) needed to calculate the percolation $r_p(t)$:

$$r_p(t) = f_1 * \frac{V(t) - c_t * V_{max}}{V_{max} * (1 - c_t)} \qquad \textit{Eq.12}$$

When the precipitation rate, depleted by vegetation interception, is higher than $g(t)$ then surface runoff is generated and infiltration rate depends on the level of soil moisture (for $V(t)$ higher than

$V(t)$ at field capacity (V_{fc}=$V_{max} * c_t$) the percolation begins otherwise V is directly increased by $g(t)$). Conversely, precipitation rate lower than $g(t)$ will infiltrate directly into the root zone, provided that $V(t)$ is not at saturation. Actually, the rooting depth is not defined but it can be assumed equals to V_{max}. $V(t)$ is updated at each time step solving numerically the convolution method that integrates the overland, subsurface and deep flows between the selected cell and the adjacent ones.

The V_{max} and f_0 are distributed parameters derived from the value of Curve Number (Risse et al., 1995) in each cell of the domain while c_t and c_f need a previous calibration process and they are generally kept constant for the whole basin. This semiempirical but quite detailed methodology for modeling infiltration and subsurface flow, even in condition of intermittent and low-intensity rainfall, allows Continuum to accurately predicts the unsaturated zone processes which represent an essential factor to determine the actual contribution of individual storms. It allows to quantify the partitioning of precipitation water into infiltration and runoff and regulate the flow and the recharge of deep water. In this way a dynamic description of the soil moisture state is possible for each pixel in which the basin is discretized (Giannoni et al., 2000, 2005; Gabellani, 2008).

For what regards the vegetation interaction, the maximum vegetation interception S_v is a function of LAI by the relationship (Kozak, Ahuja, Green, & Ma, 2007):

$$S_v = 0.95 + 0.5 * LAI - 0.06 * LAI^2 \qquad Eq.13$$

Where S_v is seen as the storage of a "vegetation reservoir" or the maximum volume of precipitation that can be retained by vegetation cover and it changes both spatially and temporally according to the LAI values.

For the energy balance the model uses the widely used approximation called force-restore approach (Dickinson, 1988) has been applied because is a tradeoff between precision and parsimonious parameterization. This approach subdivided the soil layer into two levels: an upper thin layer where temperature is approximated as uniform (LST) and a deeper layer also with uniform but different temperature (T_{deep}). The net result is that flux from the deep soil layer tends to restore the top layer, opposing any radiative forcing from the atmosphere (Montaldo and Albertson, 2001). The force restore method supposes that the time evolution of LST, at the surface interface, responds to variations in surface boundary forcing G occurring at a principal diurnal frequency, so the following assumptions are needed: G(t) has a strong single-frequency behavior in time; the soil thermal properties are nearly constant with depth.

Based on these assumptions, the force restore equation is derived and used to solve the energy balance at the surface:

$$\frac{dLST}{dt} = 2\sqrt{\pi\omega}\left(\frac{R_n - H - \lambda ET}{\varphi}\right) - 2\pi\omega\left(LST - T_{deep}\right) \qquad Eq.14$$

where ϕ [$EL^{-2}\ T^{-1}\ t^{(1/2)}$] is the effective thermal inertia, ω [t^{-1}] is the diurnal frequency, and T_{deep} [T] is the restoring 'deep' ground temperature, which it represents the temperature below the depth of diurnal heat wave. T_{deep} is evaluated by filtering data for air temperature at ground level (Caparrini et al., 2003; Caparrini et al., 2004). For each time step (Δt=1 hour), the model uses a fourth-order Runge-Kutta method to iteratively solve the equation with good accuracy. The soil moisture greatly influences the LST because, beyond directly changing the beta function values, it is positively related with the thermal inertia. The effective thermal inertia is given by:

$$\varphi = \sqrt{K_{soil} * C_{soil}} \qquad Eq.15$$

where K_{soil} [$E\ t^{-1}\ L^{-1}T^{-1}$] is the thermal conductivity and C_{soil} [$E\ L^{-3}T^{-1}$] is the soil heat capacity which increases substantially passing from dry to completely wet conditions (Monteith and Unsworth, 2013). The following expression is used in Continuum to determine C_{soil} :

$$C_{soil} = (1-n) * \rho_{soil} * c_{psoil} + n * s * \rho_w * c_{pw} \qquad Eq.16$$

where n is the soil porosity [%], ρ_{soil} [$M\ L^{-3}$] is the soil density, c_{psoil} [$E\ M^{-1}\ T^{-1}$] is the soil specific heat, the ρ_w [ML^{-3}] is the water density, c_{pw}[$E\ M^{-1}\ T^{-1}$] is the water specific heat, and s [0÷1] is the degree of saturation expressed as: $s = \frac{V}{V_{max}}$

Evapotranspiration is the link between the water balance and energy balance: the flux exchanged vertically between the surface and the air at a given elevation z_m, it can be simplified by the bulk formulation (Dingman, 2002):

$$ET = K_{atm} * C_{sur} * [e_s - e_a(z_m)] = K_{atm} * C_{sur} * D \qquad Eq.17$$

Where $K_{atm} = \frac{0.622*\rho_a}{P_{atm}*\rho_w}$, ET [$Lt^{-1}$] is evaporation rate, e_a [FL^{-2}] is the air vapor pressure, e_s [FL^{-2}] is the surface vapor pressure at saturation computed for LST derived at each time step, and their differences is usually called vapor pressure deficit D. z_m is the z-level at which e_a and wind speed are obtained and C_{sur} [Lt^{-1}] is the surface conductance. K_{atm} [L^2F] is an atmospheric constant

determined by the air density ρ_a [ML^{-3}], the water density ρ_w [ML^{-3}], the atmospheric pressure P_{atm} [FL^{-2}] and 0.622 is a multiplicative factor that derives from the different molecular weight between air and water vapor.

The hydrological model described represents the final element of the hydrological nowcasting chain: the output, since the model is distributed, are maps in which, for every point of the domain (the points of the river network in Liguria region domain, as represented in Figure 17), the discharge is calculated.

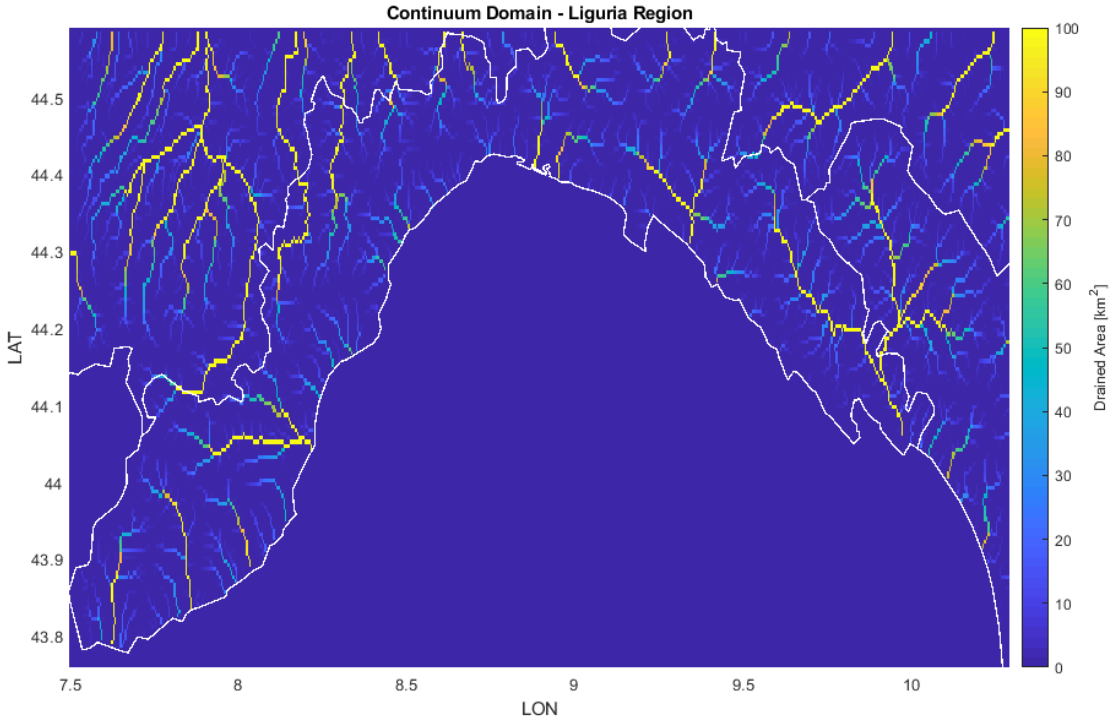

Figure 17: Domain of Continuum in Liguria Region: The discharge is calculated for every point of the domain, giving in output a distributed map.

This distributed feature of the hydrological model allows to analyze more sections to evaluate the performances of the chain.

4.6 Implementation of an integrated hydrological nowcasting chain

The first step has been the simple connection of the starting elements of the chain: the observed radar rainfall input up to the now and two hours of rainfall fields forecasted by nowcasting used as input for the hydrological model Continuum (Figure 18). This will be seen in the results in Section 5.1.

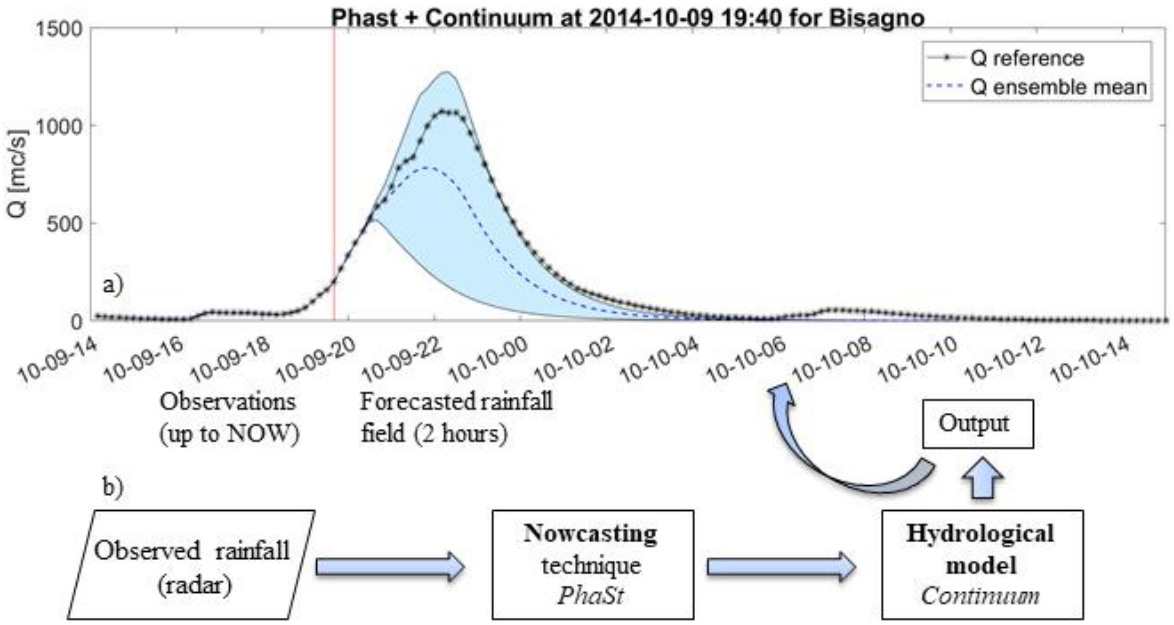

Figure 18: a) The hydrological nowcasting chain in its first version: the observed rainfall is the input until the now, then 2 hours of nowcasted rainfall field produced by PhaSt are added to the observations. Starting form a probabilistic input (20 rainfall scenarios for each time step) the result is an ensemble of forecasted discharge for the following 12 hours (example in b for 9th October 2014 event on Bisagno)

A second step has been the modification of the hydrological nowcasting chain varying the input provided by the nowcasting: a change in the algorithm made possible to take into account the variation of the total volume of rain along the forecast horizon. Some attempts have been done to find the best source of information from which retrieve the volume trend to apply for obtaining the best results from the hydrological point of view. The results regarding this part will be detailed in Section 5.2.

The complete forecasting chain (schematization reported in Figure 19) is the result of an attempt of integrating the algorithms available up to now, presented in a unique tool for the hydrological forecasting for real time applications. It uses the observed rainfall fields to build the rainfall scenarios in the recent past, then for the first two hours of forecast the rainfall fields are forecasted by the nowcasting model with the assumption of the modification of the precipitation volume, finally from the second hour the rainfall field is a linear combination of the nowcasted field and the rainfall field from the NWPS according to the blending function described in Section 4.4; in the meanwhile the NWPS is hourly corrected with observation in order to furnish to the nowcasting technique updated information regarding the precipitation volume trend. The hydrological model takes in input the rainfall scenarios and produces the forecast in terms of streamflow. The output of the chain is an ensemble of possible discharge scenarios (20 ensemble) for the following 12 hours.

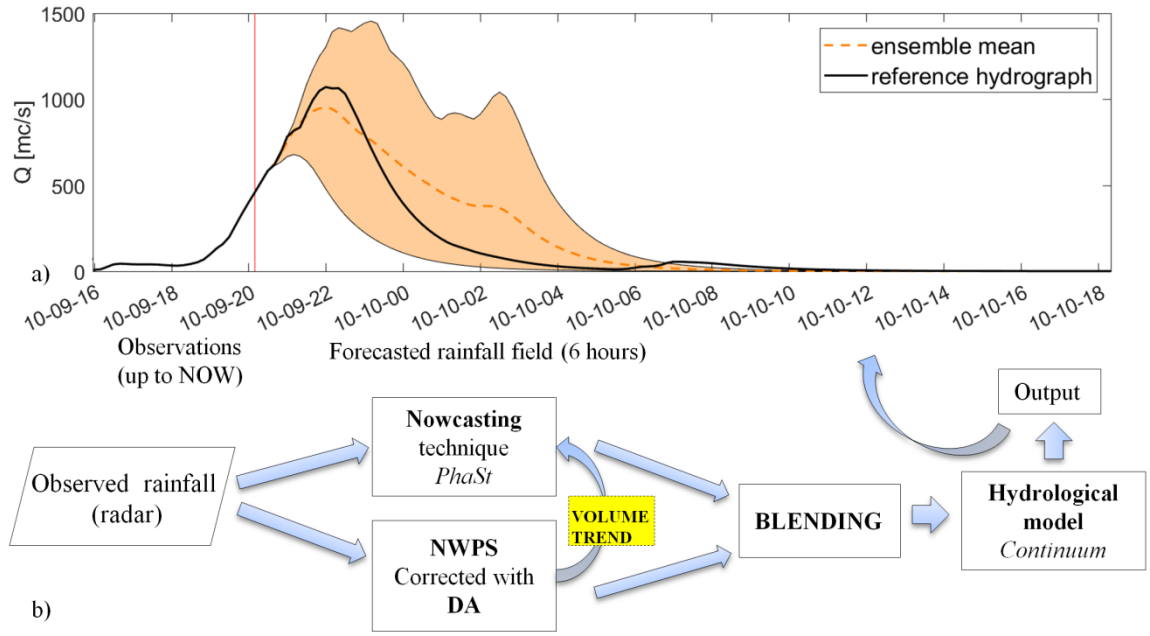

Figure 19: a) The hydrological nowcasting chain described in its elements: the main input is the observed radar rainfall. It is used up to the Now as it is, is evolved through the nowcasting method and it is used in the data assimilation process for the correction of the NWPS. The information regarding the total volume variation along the forecast time given by the meteorological model is used to modify the rainfall fields nowcasted. The rainfall fields produced in this framework are linearly combined through using the blending technique and then are the input of the hydrological model, that produces a probabilistic discharge forecast (example in b).

In the following Chapter (5) the new elements that have been analyzed and the results obtained along this PhD study will be illustrated.

Chapter 5: Results and innovative aspects of the study

A first thing to say is that all the analyses on the results form an hydrological point of view have been performed on three case studies related to three major events that stroke Liguria Region during autumn 2014.

Even though these three events could seem a small sample on which conduct a study it is with worth to say that the output of the distributed hydrological model allows to compute the score on a great number of points inside the domain. This permits to have representative results even considering few events.

The results have been analyzed in a probabilistic framework using different indexes to take into account the performances of the hydrological forecast in terms of reproduction of the flow but also in terms of anticipation time gained with the use of the rainfall forecasted. To evaluate the performances of the hydrological forecast in the control sections three scores have been used: the Nash Suttcliffe (NS) coefficient, the Variance of the discharge (Var) and the Continuous Rank Probability Score.

The Nash Sutcliffe (NS, Nash and Sutcliffe, 1970) coefficient was chosen since is one of the widely used measure to evaluate models performances in hydrology, especially for streamflow reproduction:

$$NS = 1 - \frac{\sum_{t=1}^{T}(Q_m(t) - Q_{obs}(t))^2}{\sum_{t=1}^{T}(Q_{obs} - \overline{Q_{obs}})^2} \qquad Eq.18$$

Where $Q_m(t)$ e $Q_{obs}(t)$ are the modeled and observed streamflow at time t. Nash–Sutcliffe efficiency ranges from $-\infty$ to 1. Values of NS equal to 1 indicate a perfect match of modeled discharge to the observed data, while NS=0 means that the model forecasts are as accurate as the mean of the observed data. Negative values of NS occurs when the observed mean is a better predictor than the model. So closer the NS is to 1, the more accurate the model is. Using a probabilistic forecast the index is calculated for each of the 20 realizations and then a mean value is taken.

To relate this index to the spread of the ensemble of discharge forecast the variance is also calculated.

$$Var(X) = E[(X - \mu)^2] \qquad Eq.19$$

Where X is the forecasted discharge and μ is the mean of the forecast. There is not a optimal value of this index but it is used to measure the variability of the forecasts in respect to the average value.

The Reduced Continuous Rank Probability Score (Trinh et al., 2013) is used, calculated as the CRPS (Brown, 1974; Matheson and Winkler, 1976; Unger, 1985; Stanki et al., 1989; Hersbach, H., 2000), reduced with the standard deviation of the observed discharge over the analyzed time period (hereafter σ^2).

$$RCRPS(F,x) = \frac{1}{\sigma^2}\int_{-\infty}^{\infty}(F(y) - \mathbb{1}(y-x))^2 dy \qquad Eq.20$$

Where *F(y)* is the forecast probability CDF for the forecast and $\mathbb{1}$ is the step function of the observed value. Values of this score (adimensional) equals to zero means a perfect forecast: observation and forecast coincide. Increasing values corresponds to a bigger distance between observations and forecast.

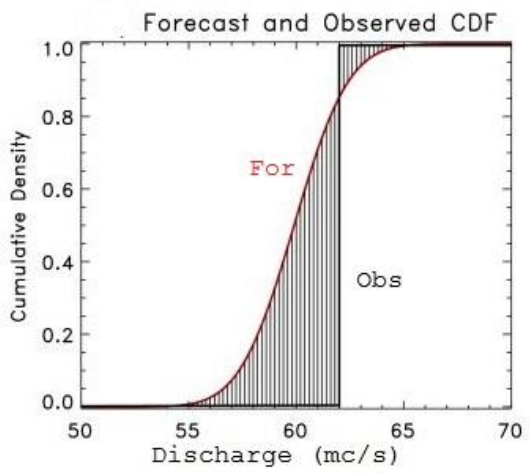

Figure 20: CRPS graphical representation (striped area): it is calculated as the difference between the cumulative density function of the forecasted discharge and the observed value represented by the step function

NS and Var(X) have been applied on the mean of the streamflow ensemble following a deterministic approach in the comparison, while the RCRPS is used to evaluate results in a probabilistic perspective (Trinh et al., 2013; Davolio et al., 2017a). The calculated values of all the scores are expressed as function of lead time; to cope with the large number of values of the RCRPS its visualization has been done using boxplot, as it will be shown in the following sections.

5.1 Implementation of the hydrological nowcasting chain

The first result of this work has been the realization of the hydrological nowcasting chain (Figure 18) connecting different pieces already in use in operational forecasting in a unique tool. The main input of the chain, the observed rainfall, has been connected with the rainfall forecast performed through the nowcasting. In this way the rainfall input is extended to 2 hours ahead.

Since the nowcasted rainfall field is the product of a probabilistic forecast, the result is made by an ensemble of rainfall scenarios (20 in this study). The differences are growing with the forecast time to take into account the forecast uncertainty that increases going on with the lead time.

Hence the hydrological model fed by the rainfall scenarios gives an output that is probabilistic: there is not only a forecast of discharge but an ensemble of forecast. In Figure 21 is possible to see an example of output of the chain with 20 possible forecasted hydrographs for the run on 9th October at 19:40 UTC at Bisagno river section Passerella Firpo (almost at the outlet of the basin).

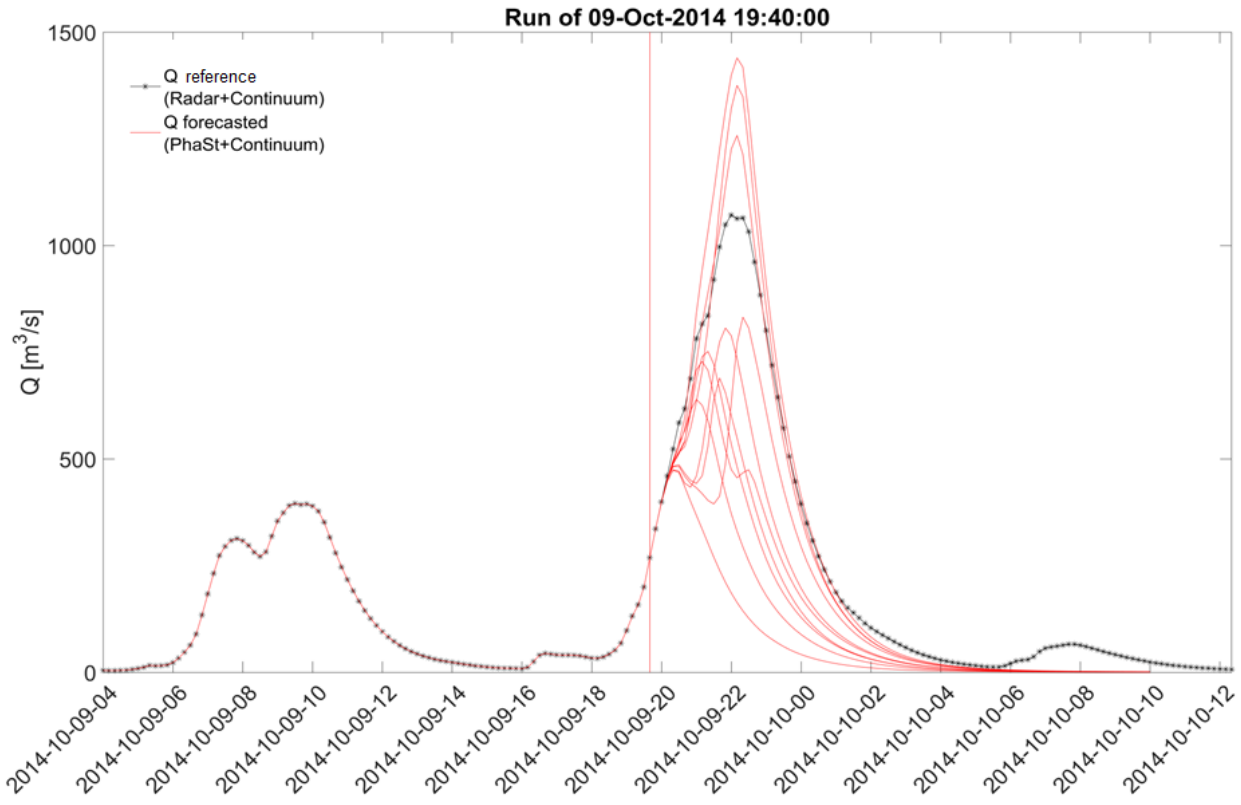

Figure 21: Forecasted hydrograph for 9th October 2014 at 19:40 UTC. The red lines are the different forecast of the hydrological model while the black line with asterisks is the reference hydrograph, built using the observed radar rainfall, taken as the discharge benchmark

The evaluation of the performances of the chain has been done comparing the results in terms of the output of the chain, namely the forecasted discharge. This comparison has been performed using as observed discharge the simulated discharge obtained using the radar rainfall observed as input to the distributed hydrological model; the resulting hydrograph will be hereafter defined as "reference hydrograph" (Borga, 2002; Vieux and Bedient, 2004, Berenguer et al., 2005). This approach does not consider errors in the hydrological model, however already calibrated, since it is aimed at evaluating possible improvements in rainfall forecast.

5.2 Modification of the nowcasting algorithm

After the first modifications in the nowcasting algorithm explained in section 4.2, a second step has been the attempt of considering the variation of the total precipitation volume on the radar domain along the forecast horizon (of 2 hours). This should extend the validity of the forecast trying to take into account the processes such as growth and decay of the precipitation structures that have increasing importance with increasing lead times (see section 3.1). To do this a first initiative has been the relaxation of a constraint of the original version of PhaSt. This constraint regards the spectral amplitude of the rainfall field that is kept constant along the forecast horizon, that mean fixing, in the real space, the total volume on the forecasted rainfall fields equal to the one of the last observed radar image. This hypothesis of constant volume along the forecast horizon has been relaxed. The modification of the volume on the domain is then performed according to the information retrieved in three different way:

1) The volume is modified according to a trend estimated by the last available observations: the two most recent radar observed rainfall field are used to calculate the trend of growth or decay of the volume of rainfall on the radar domain.

$$Vol_{Trend} = \frac{Vol_{NOW} - Vol_{NOW-1}}{Vol_{NOW-1}} \qquad Eq.21$$

   Then the trend in this way calculated is applied to the first three time steps (up to 30 minutes ahead) and then is kept constant for the rest of the time. The trend is applied only at the beginning of the forecast since the calculated trend, as it is based on observations, cannot be reliable for longer lead times.

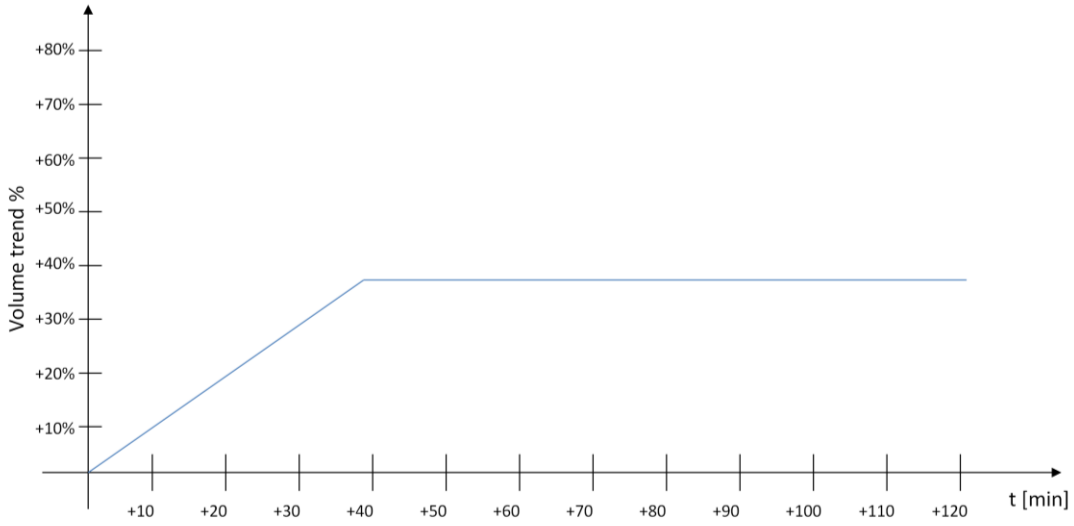

Figure 22: Modification of the volume using the observed radar rainfall field: the trend extract from the observations is distributed along the first three time steps and then assumed constant

2) The volume is modified according to the trend forecasted by the NWP model MOLOCH, presented in section 4.3. This trend is calculated on the hourly forecasted rainfall field and is then applied every ten minutes (time step of the nowcasting update) using the trend related to the hour (Figure 23): for example, at the PhaSt forecast at 18:20 of 9th October 2014 the trend that will be applied for the first hour is the trend related to the volume variation between the 18:00 forecasted rainfall field and the 19:00 forecasted rainfall field. For the forecasted rainfall fields between 19:20 and the end of the forecast the trend applied is the one calculated between the rainfall field forecasted for 19:00 and the one for 20:00.

3) Similar to the trend presented at point 2 the attempt in the modification of the volume has been performed retrieving the information derived by the forecast of the NWP model MOLOCH corrected with DA (nudging), presented in section 4.3. This approach is aiming to have a compromise between the information content of the NWP model forecast, available and reliable for longer lead time, and that one of the observations, that for shorter lead time is probably closer to the reality. The way of calculating and applying this trend is the same used for the NWP model without DA correction (Figure 23)

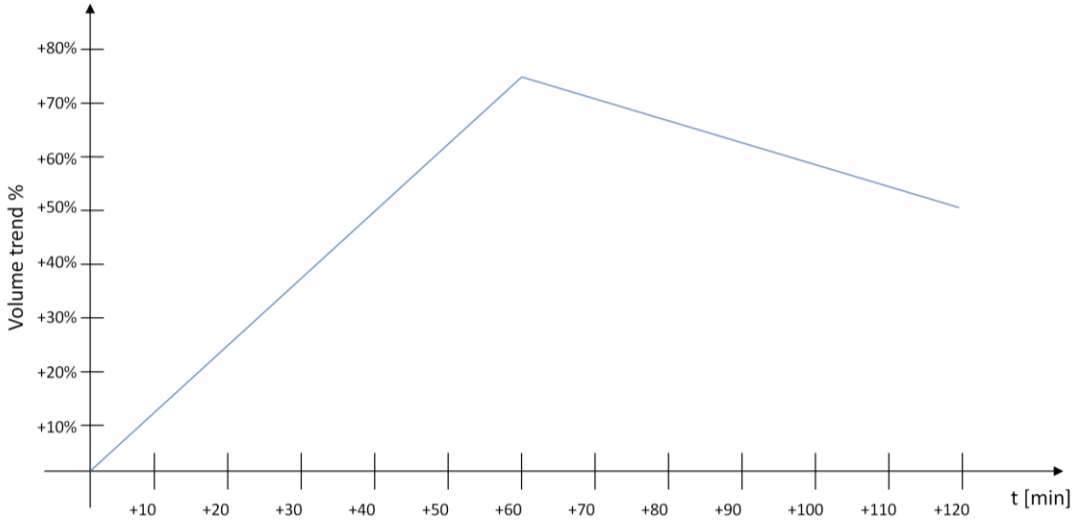

Figure 23: Modification of the volume using the information regarding the volume of the meteorological model as it is and the meteorological model corrected with DA: the trend is calculated per hour and then applied to the following two hours.

In all the alternatives of trend calculation (1,2 or 3) the rainfall field with the volume modified is calculated as follows:

$$Rainfall\ field_{Vol\ Mod}(x, y, en, T) = Rainfall\ field(x, y, en, T)_{PhaSt\ Forec} * Volume\ Trend(T) \qquad Eq.22$$

Where *x* and *y* are the coordinates in the radar rainfall field, *en* is the number of ensemble members (here 20) and *T* is the lead time of the forecast (from 10 minutes to 2 hours).

As explained in section 5.1 the results have been analyzed from the hydrological point of view. Four hydrological nowcasting chains, fed with four different input of forecasted rainfall field (the original version of PhaSt and the three version with the application of the modification of the volume of the domain), have been compared.

9th October 2014

The hydrological nowcasting chain provides as output both the forecasted hydrographs for some control sections and the distributed forecasted discharge for the computational domain of Continuum.

Hereafter are reported some examples of hydrographs built with the different rainfall input in forecast since in all the cases up to the Now the input is the radar observed rainfall field. The first ensemble of forecasted hydrograph (light blue envelope) is built then with in forecast two hours of nowcasted rainfall fields produced by PhaSt without the volume trend application. The second ensemble (green envelope) is the resulting hydrographs of two hours of forecasted rainfall field with volume variation given by the trend extrapolated by observations. The third ensemble (orange envelope) takes in input for the forecasted rainfall field two hours of nowcasted field with the application of the volume trend coming from the NWP model corrected with DA technique described in section 3.2. The last ensemble (pink envelope) is the result of the hydrological forecast with in input the nowcasted rainfall field modified according to the volume trend of the NWP model without DA assimilation correction.

The two selected run shown in Figure 24 (at 19:20 and 19:40 UTC of 9th October 2014) are representative of the behavior of the different combination of forecasted rainfall fields with the hydrological model. In addition to this these the first run in which the chain output is approaching with the forecast the real behavior of the basin in that event. Hence it is possible to have a gain in the lead time of the forecast of around three hours that, for taking real time civil protection actions, can be an essential advantage.

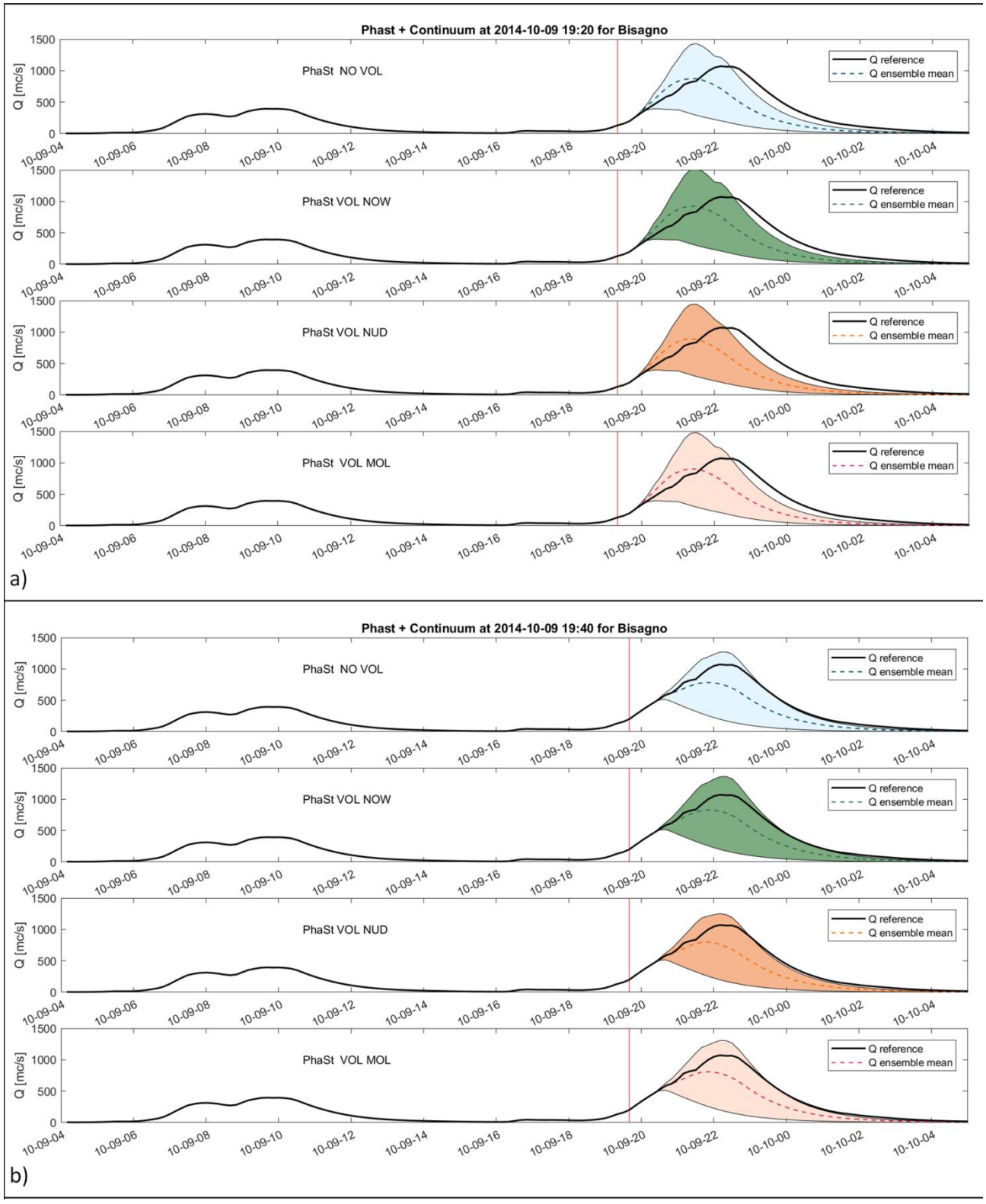

Figure 24: Run of 19:20 (a) and 19:40 (b) UTC of 9th October 2014 for Bisagno Creek at Passerella Firpo section: the different envelope forecasted are related to different input in terms of nowcasted rainfall field: the first one uses the nowcasted rainfall field without volume variation, the second one the nowcasted rainfall field with volume trend given by radar observed rainfall field, the third the nowcasted rainfall field with volume variation trend retrieved from the NWP model corrected with DA while the last one use the information of NWP model without DA correction

For what regards the differences between the four runs what it is possible to see from these figures is that the overall behavior of the hydrological forecast is mainly the same for all the forecasted rainfall input. Only looking carefully at the ensembles it is possible to notice some differences among the four versions.

In general the ensemble forecasted using the nowcasting modified with the information retrieved from the observations led to higher values of forecasted discharge with respect to the other type of forecasts. In the cases in which the volume modification is not applied (light blue envelope) and in which the volume trend is coming from the NWP model with DA (orange envelope) and NWP model (pink envelope) the ensemble of discharge is a slightly less than in the other case. These are examples of behavior along this event but calculating the score described at the beginning of the Chapter, RCRPS, for all the duration of the event (run starting at 13:00 and ending at 21:00 of 9th October) the performance are clearer.

The RCRPS allows to calculate a performance score on all the points of the domain for which a discharge is forecasted. In this work two filters have been to applied to take into account only the points that were affected by the main event. The points of the domain is considered only if:

1. The discharge forecasted for that pixel have overcome a certain discharge threshold for at least one time step in one of the 20 ensemble members; the threshold used is the index discharge, that is the discharge with return period 2.9 years;
2. The drained area of the pixel must be larger than 15 km^2.

To summarize the resulting values of the index, that often are thousands of values, a boxplot is used. The values of RCRPS are grouped in different classes representing the different way of varying (or not varying) the volume along the forecast horizon up to eight hours. The reason of the choice of this lead time is that over the two hours of forecasted rainfall field in input to the model it has been considered the response time of the catchments involved. In fact in Liguria few basins have a drained area up to 500 km^2, and then the maximum response time has been set to 6 hours.

In Figure 25 the colors used for the different bars are coherent with the colors used in the hydrographs: the first column is linked to the original version of PhaSt without volume variation, the second one to PhaSt modified with the volume information retrieved by observations, the third one to the modification according to the NWP model corrected with nudging, the last with NWP model information. In each column inside the box are contained the values between 25% and 75% quantiles, the horizontal line represents the median value, while the circle is the mean. The whiskers

extend to the most extreme data points not considered outliers, and the outliers are plotted individually with points.

For 9th October event is confirmed what has been noticed in the hydrographs analysis: there is a similar behavior among the different version of the hydrological nowcasting chain. However, a little enhancing of the predictive performances is achieved through the modification of the volume with the trend deduced by the observed radar rainfall field.

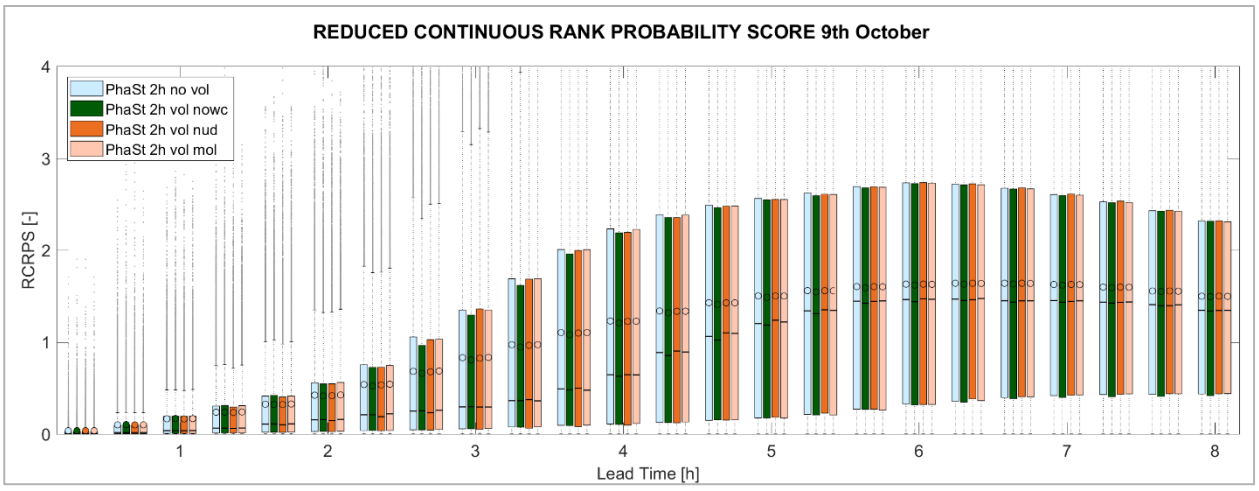

Figure 25: RCRPS for 9th October event (time window of the event between 13 UTC and 21 UTC): the boxplot groups all the values of the score distinct in the columns related to the various type of modification of the volume information expressed as a function of lead time

The reason of this behavior can be found in the fact that for this particular event the forecast of the NWP model, even corrected with the observations through nudging, were really misleading, not forecasting the main event of the evening.

10th November 2014

The hydrograph (Figure 26) selected to represent the event occurred during the evening of 10th November 2014 is related to the run at 18:40 of that day and the forecast for Entella river at Panesi section, that caused flooding in its lower part in the urban area of Chiavari.

Also in this case the ensembles show little differences between each other but there is a main difference with respect to the previous event analyzed. While during the 9th October event the modification of the volume performed applying the observed trend was improving the forecast as it was similar to the real behavior of the precipitation pattern, in this case led to an overestimation of

the volume modification. Hence in this event the use of the information contained in the NWP forecast is more useful than the recently observed rainfall trend.

The RCRPS calculated on the entire domain for the time window of the event (from 10:00 to 21:00 of 10th November 2014) is summarized in Figure 27 in the form of boxplot. Also in this analysis there are some trends to highlight: at the beginning of the forecast there is not a clear predominance in terms of better performance of a type of modification.

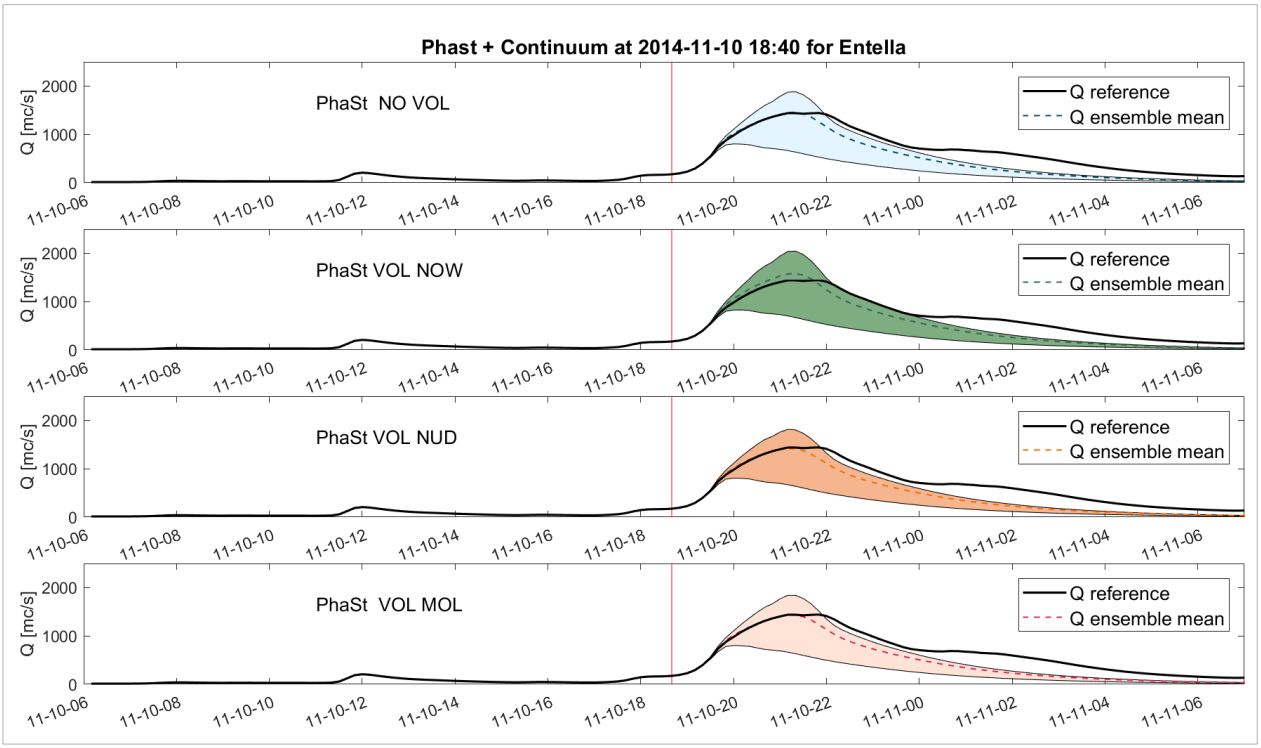

Figure 26: Run of 18:40 UTC of 10th November 2014 for Bisagno Creek at Passerella Firpo section: the different envelope forecasted are related to different input in terms of nowcasted rainfall field. Starting from the top the hydrological model is fed by the nowcasting PhaSt with the volume information not modified, then the volume modified with observations; in the last two the volume is modified with the NWP model corrected with DA and the NWP model as it is.

Starting from 4 hours ahead the modification of the volume done using the trend forecasted by the NWP model, both corrected with nudging and not, is enhancing the forecast. This can be noticed in Figure 27 since, starting from 4 hours lead time there is a reduction of the values assumed by RCRPS.

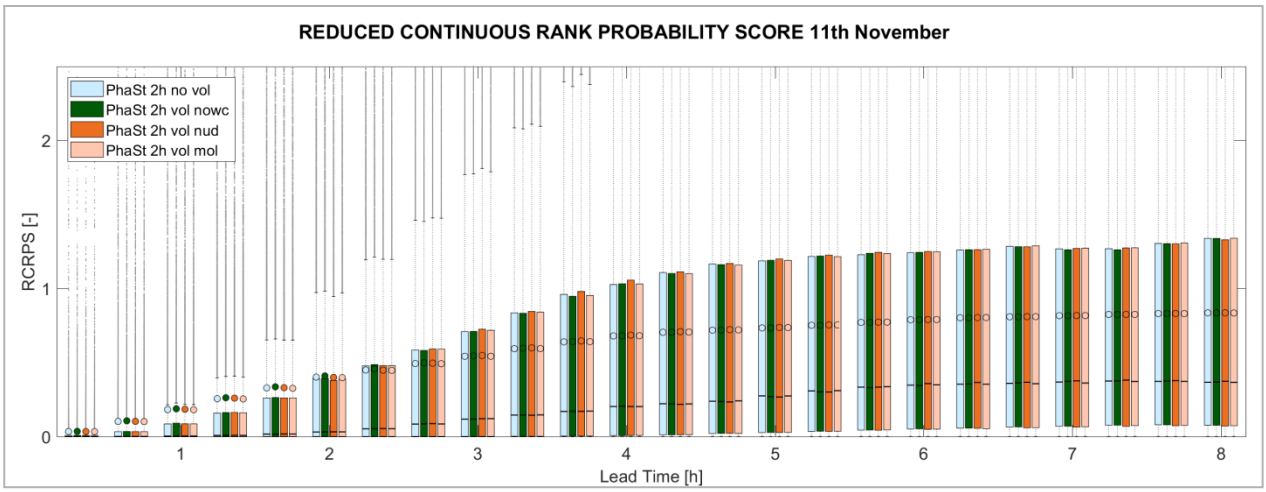

Figure 27: RCRPS for 10-11th November event: the values of the score, expressed as a function of lead time, are distinct in columns related to way of modifying the total volume on the domain.

15th November 2014

On November 15th intense and concentrated rainfall caused the raising of the level of many rivers in the western part of Liguria. One of the most affected rivers was Polcevera, whose hydrographs are reported in Figure 28 for the run of 9:00 of 15th November 2014. In this case there is a clear trend: the hydrological forecast that used in input the rainfall field modified with the information about the volume from NWP model and the NWP model corrected with DA are improving the forecast at least in some of the ensemble.

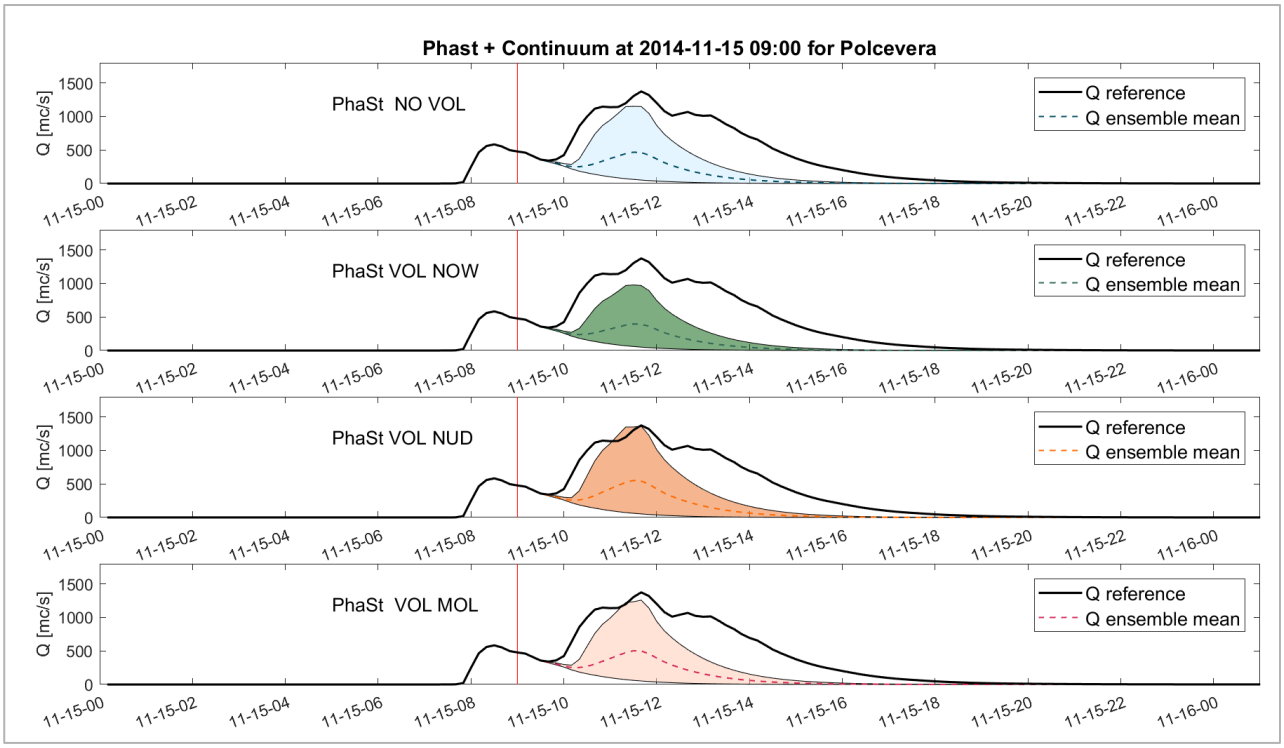

Figure 28: Run of 9:00 UTC of 15 November 2014: the hydrographs represent the hydrological model fed by different versions of nowcasting PhaSt with the volume information not modified, modified with observations, modified according to the NWP model corrected with DA and the NWP model without DA.

It is possible to notice the same trend in the boxplot related to the RCRPS calculated along the entire event (from 02:00 to 11:00 of 15th November) in Figure 29. The boxplot representing the version of PhaSt modified with the volume variation trend predicted by the NWP model corrected with nudging is the lower one, indicating better values of the score. In this case the event was well reproduced by the NWP model and the use of the observations for correcting the forecast has been improving the forecast even more.

In summary it is hard to determine within these three case studies the best way of modifying the volume along the forecast time because of the great influence of the performance of the NWP model itself. However, this analysis has been useful for a further step in the building of a hydrological nowcasting chain that tries to combine different elements for an accurate forecast of the rainfall field and a consequently accurate forecast of the discharge.

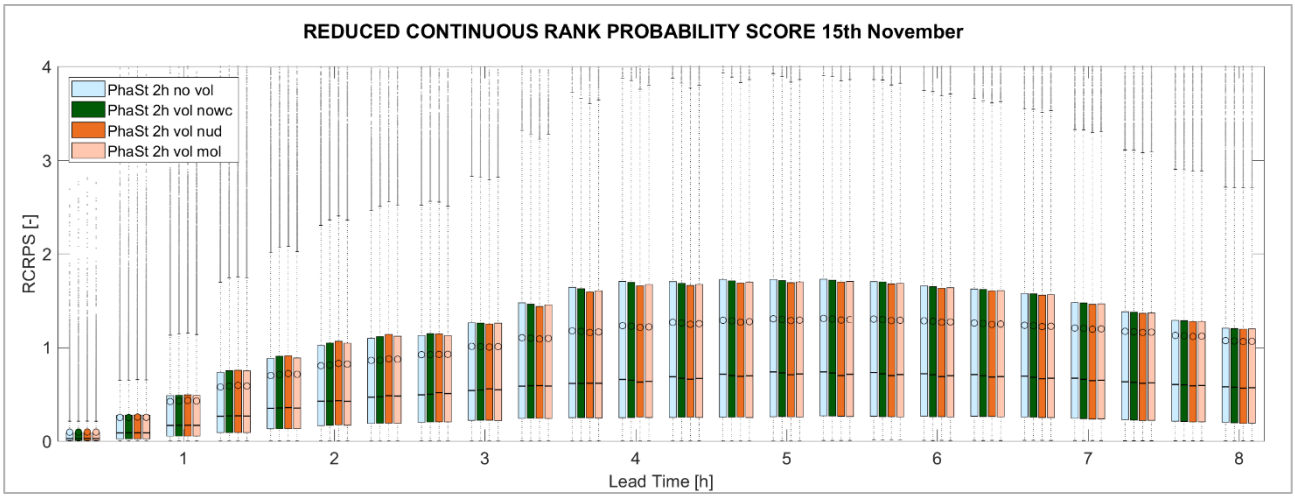

Figure 29: RCRPS values for 15th November 2014 event: the four columns are related to the different versions of PhaSt with and without volume variation feeding the hydrological model.

5.3 Effects of the blending functions on hydrological forecast

The use of the blending technique has been a natural further step for the building of an integrated hydrological nowcasting chain that tries to use the most accurate QPF in input available at the time of the forecast. As already said for very short lead time of precipitation (0–3 h), radar nowcast performs best, whereas for longer lead times, NWPS forecasts are better (Kilambi and Zawadzki, 2005; Lin et al., 2005; Kober et al., 2012; Wang et al., 2015). Hence an attempt has been done in achieving a hydrological nowcasting chain in which, after the very first hours (usually 0–3 h) of radar-based nowcasting, NWP forecasts can be merged to generate a seamless 0-6 hours prediction with higher skill. This technique, called blending, counts many studies in recent years, as already explained in section 3.3. In the majority of them the blending function, that is used to give different weight to the rainfall field forecasted by the nowcasting or the NWP model, is a function based on the performances of the forecasting models. As said in section 4.4 in this work the blending function has been retrieved starting from the state of the art of this research area. The resulting rainfall field is the linear combination of the fields forecasted by NWP model and nowcasting weighted in different way according to the lead time.

The innovative element that is introduced in this work with respect to the other studies on blending is that, beyond the blending applied on the forecast domain to the rainfall field that is mainly acting on the location of the structures, a first blending is performed exploiting the information regarding the volume variation along the lead time. So, what has been done previously using the volume trend

information to modify the nowcasted rainfall field is here applied not only for two hours of forecast but for all the forecasts in which the nowcasted rainfall field is used.

The volume of the nowcasted rainfall field is then modified according the information retrieved from the NWPS corrected through the assimilation technique (total volume on the domain). The choice of this way of modifying the total volume is linked both to the results shown in section 5.2 and to the fact that there is the need of having a trend that is applicable to all the lead times of the forecast. As for the trend calculated for the two hours of PhaSt the volume trend is calculated for the hours of the forecast using the information about the total volume of precipitation on the radar domain (Fig 3) according to Equation 22.

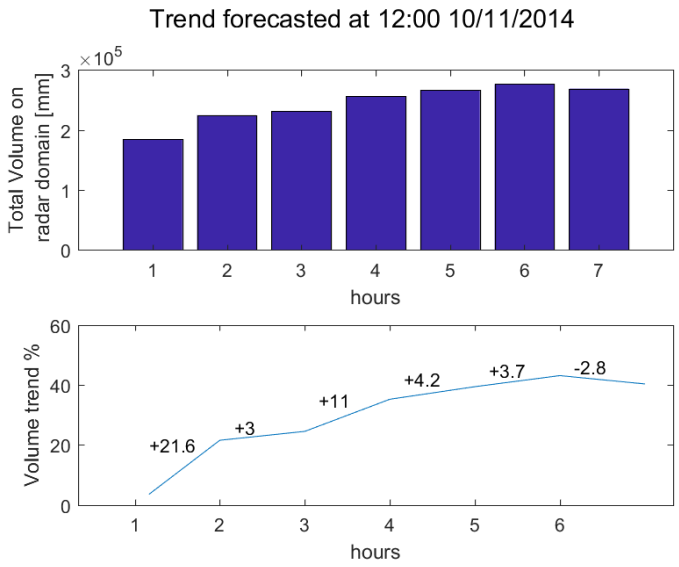

Figure 30: Volume trend for rainfall field modification (example for 10-11-2014 at 12:00 UTC). The total volume on the domain considered is summed for each time step of the NWPS forecast with DA. The trend volume is applied as multiplicative factor to the first rainfall forecasted by the nowcasting technique.

In this way the information about the potential growth and decay of the rainfall structures is given as an additional information to the nowcasted rainfall field.

The distributed analysis has been carried on exploiting the distributed maps of discharge produced by Continuum. As already said this allows to use several sampling points for the comparison even if the events analyzed are only three. In this case a first distinction has been done dividing all the interested points according to their associated drained area into three classes:

- Points with upstream drained area in the range of 15 to 50 km^2 (small catchments)
- Points with upstream drained area in the range of 50 to 150 km^2 (medium size catchments)
- Points with upstream drained area in the range of 150 to 500 km^2 (big catchments)

This distinction finds a motivation in the concentration time related to the different size of catchments: a longer influence of the forecast rain can be found for the basins with greater drained area and then bigger concentration time. Hence, analyzing the performance indexes and relating them to the lead time, a longer lead time will be considered in calculating the indexes for the bigger catchments. In particular beyond the 6 hours of lead time corresponding with the rainfall forecast a further window of forecast discharge is considered: 1 additional hour for the 1st class of catchments, 2 additional hours for the 2nd and 3 additional hours for the 3rd.

As already said, a first analysis has been performed to evaluate the performance of the complete chain with the four considered configurations of the blending function that allows to generate forecasted rainfall fields by linearly combining nowcasted rainfall field and NWPS forecast. This analysis has been done evaluating the performance in terms of forecasted discharge using the RCRPS score; the distributed approach is here considered, so the predictions in all the points of the domain are involved. The results are then distinguished into the three drainage area classes presented before.

Below (Figure 31) is reported the summary of the results considering the entire sample of data for the three events: in this boxplot each group of column represents the values of RCRPS (y axis) for the indicated lead time every 20 minutes (x axis). Each box indicates the values of the 25% and 75% quantiles, the horizontal line inside the box represents the median value, while the circle indicates the mean. The whiskers extend to the most extreme data points not considered outliers, and the outliers are plotted individually with points. The four columns represent the results related to the use of the different blending functions: the first one is related to the step blending function (red column); the second (green column) and the third (yellow column) ones are the results of the use of the intermediate functions; the last one (blue column) is related to the smoothest of the blending functions presented in Section 4.4.

The first thing that is possible to notice is that there are no large differences between the four configurations of the blending functions, but in general it seems opportune to rapidly move from nowcasting to NWP model forecast avoiding long smoothing periods. In fact another evidence: the scores for all the classes of drainage area performs indicate a worse performance (large values of RCRPS) around 4-5 hours of lead time. This result is probably due to the fact that, even if data assimilation is performed on NWPS with hourly updating, PhaSt rainfall scenarios and NWPS rainfall fields are often not seamless These discontinuities can affect the blending process,

generating, in the transition phase from the rainfall fields forecasted with the nowcasting and those generated by the NWPS, an unrealistic final rainfall scenario.

Regarding the comparison of the results related to the different blending function in general the best score is the one related to the step function. However, this behavior is a mean behavior along the three events: each event has its "local" best blending function, that will be shown in the results regarding each event.

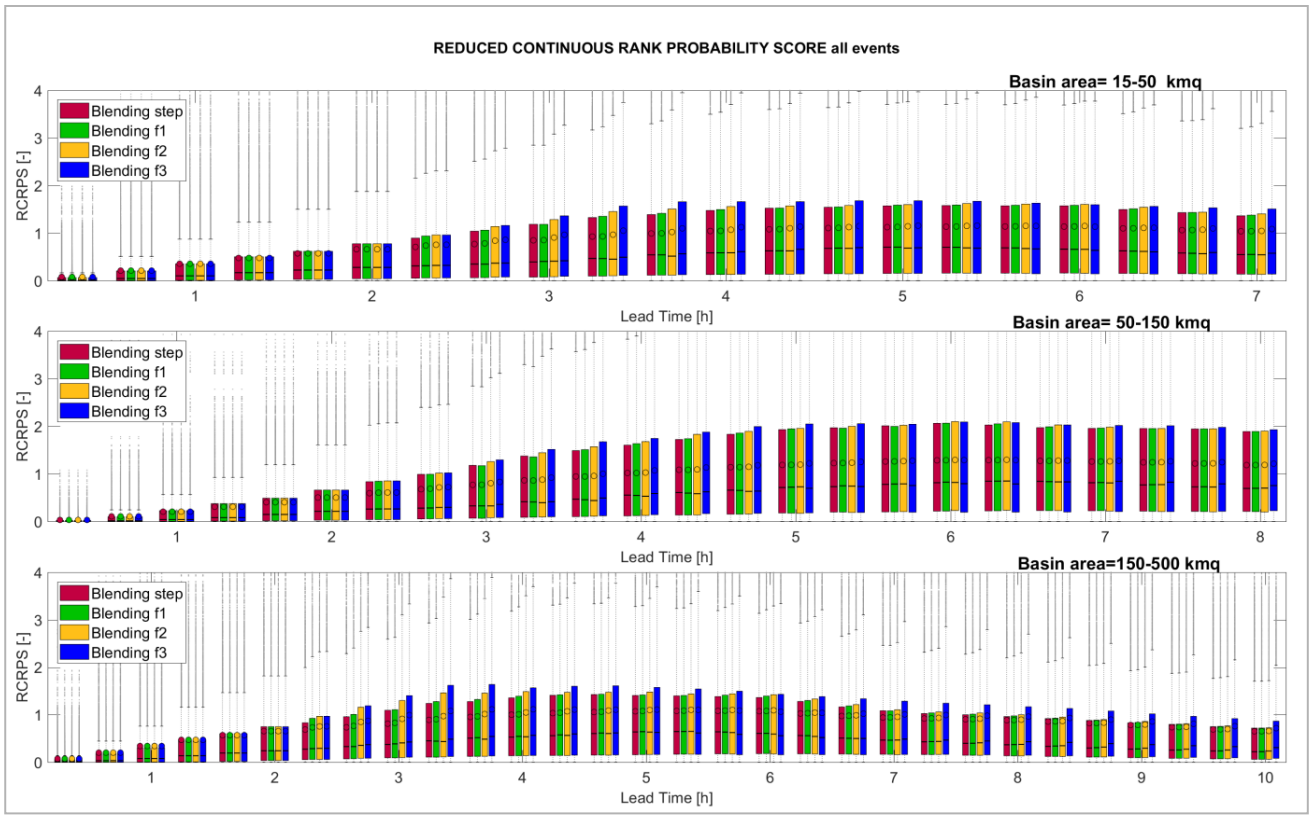

Figure 31: RCRPS for all the events: analysis of the discharge output related to the different four blending functions: the red column represents the results of applying the step function, the other three columns the effect of application of the other three growingly smoothing blending functions. The results are presented in form of boxplot distinguished in three drainage class area (15-20 kmq, 50-150 kmq and 150-500 kmq)

5.3.2 Basin scale analysis

The results regarding the discharge forecasted for the main basins stroke by the analyzed events were examined starting from a first qualitative visual comparison between the hydrographs forecasted for each configuration at every time step (every 20 minutes).

Two examples are hereafter reported (Figure 32): the first one is the forecast at 20:10 of the 9th October 2014 on Bisagno creek, that was the main responsible for the flood of the municipality of Genoa during this event. The second one is the forecast at 19:40 of 11th November 2014 for Entella, mainly interested during this event with its tributaries Graveglia and Lavagna.

The figures show the envelopes of the forecasted discharge for one time step during the considered time window of the event. The black thick line is the reference hydrograph, derived by the run of the hydrological model with the observed radar rainfall field as input, while the dashed lines represent the mean of the forecasted discharge ensemble for each lead time.

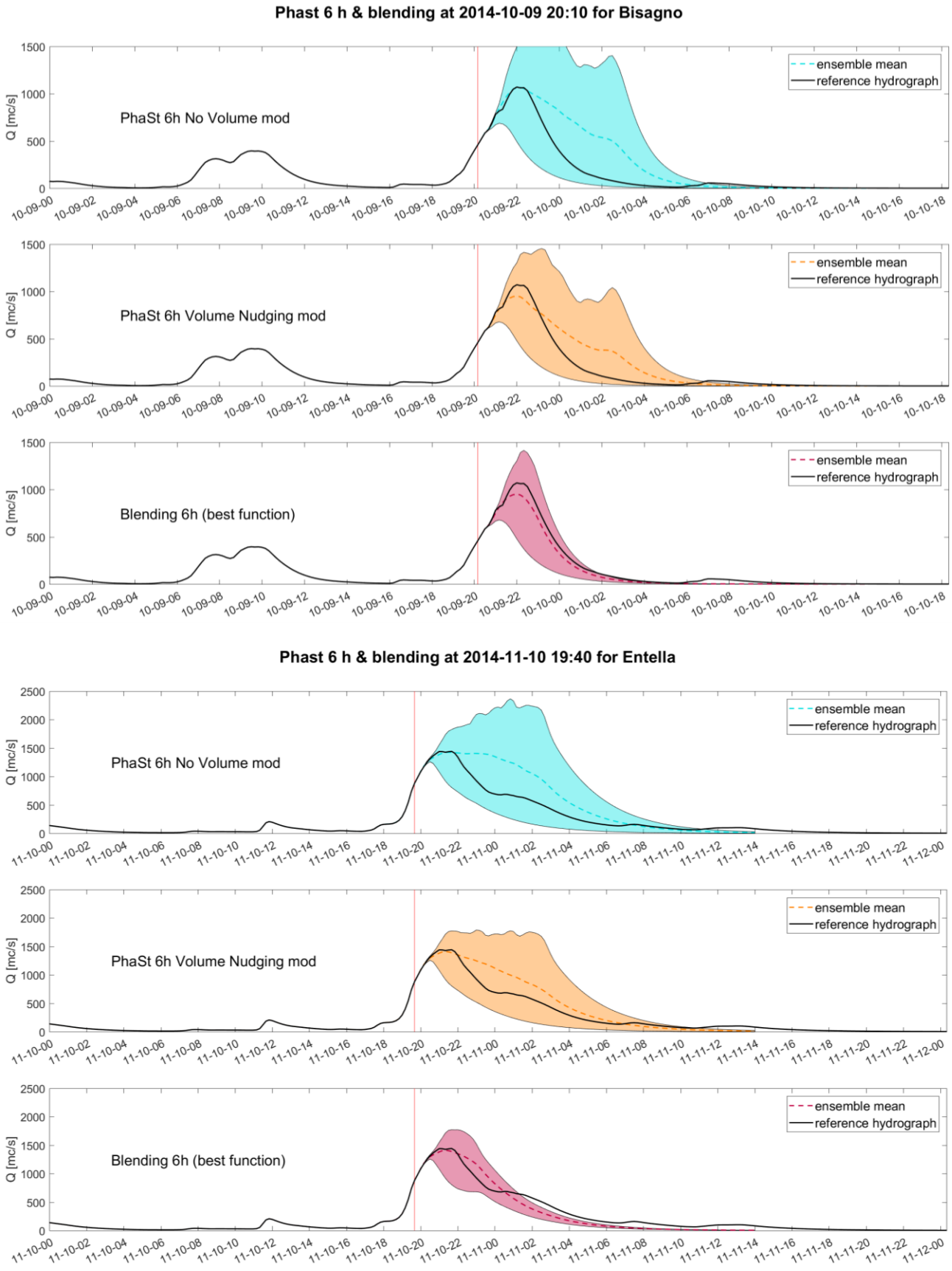

Figure 32: Example hydrographs for 9th October and 11th November event for Bisagno and Entella outlet sections. In both the figure the light blue envelope is the result of the forecast using 6 hours forecast of the nowcasting output without volume variation; the orange envelope results from the use of the nowcasting modified with the

information regarding the volume; the red envelope takes in input the rainfall fields resulting from the linear combination obtained with the blending.

The first hydrograph envelope (light blue) shows the discharge forecast obtained with 6 hours of rainfall from nowcasting, without the volume modification (Figure 33a). For the second hydrograph (orange), the 6 hours of rainfall are obtained from nowcasting but applying the modification of the volumes according to the trend forecast by NWP model with nudging (Figure 33b). For the last hydrograph (red) the input rainfall field results from the blending using the mean best function for the three events identified in the previous section 5.3.1: the blending step (Figure 33c).

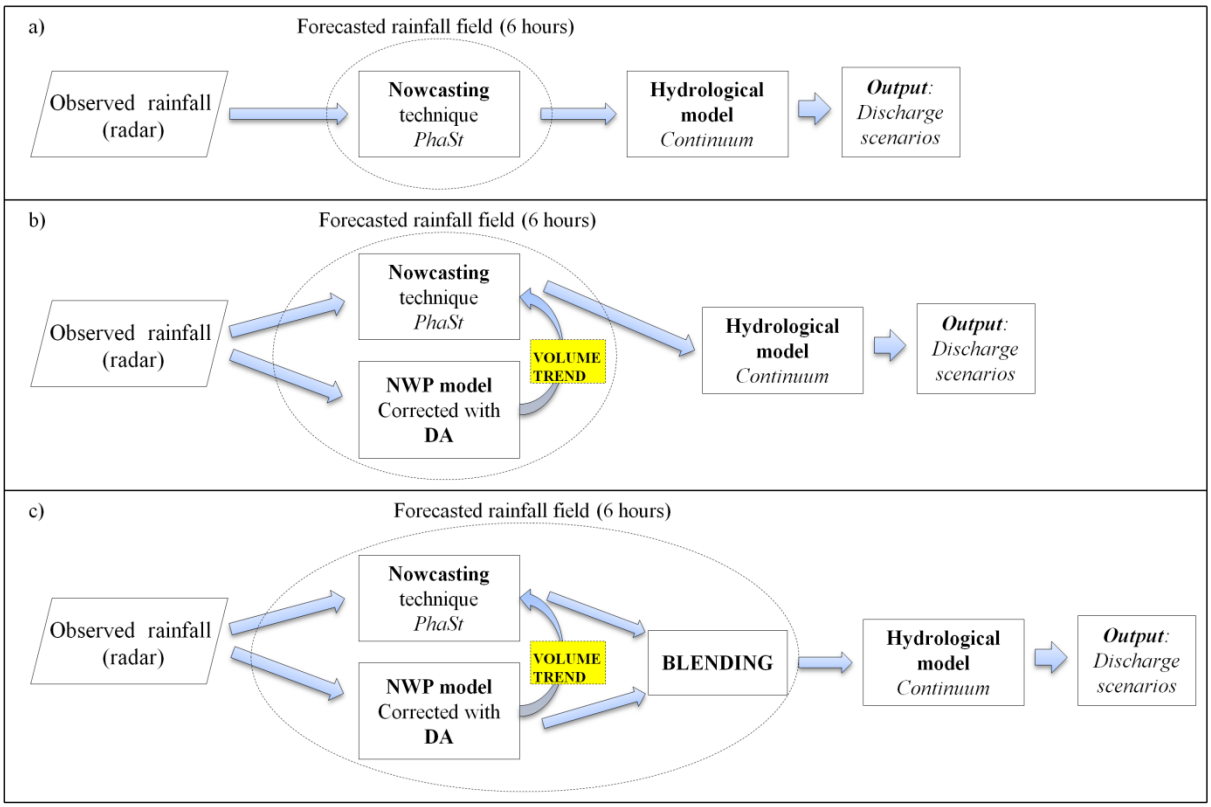

Figure 33: The hydrological nowcasting chain in its three configurations: : the first one in which is used only the nowcasted rainfall field without volume modification (a); the second one with the nowcasted rainfall field modified with the trend retrieved by the NWP model (b); in the last one the nowcasted rainfall fields with volume modification are combined through blending with the fields forecasted by NWP model corrected with DA

What it is possible to notice firstly is the difference between the forecasts performed using as input only the nowcasted rainfall field for 6 hours of forecast and the forecast with the blended rainfall field as input. The main difference that points out is that the ensemble spread of the forecasted discharge is larger for the first two configurations while it is radically reduced for forecast related to the blending.

This is possibly ascribable to the fact that while nowcasting provides a probabilistic forecast (20 ensemble) of different rainfall scenarios, blending connects a deterministic forecast from the NWP model, with nowcasting ensemble. Since each member of this ensemble is blended with the same NWP model forecast the spread of the final ensemble is smaller.

The scores summarized in Section 3.7 (Nash-Sutcliffe efficiency, Variance and Reduced Continuous Rank Probability Score) are calculated at basin scale (at the outlet section), for some representative basins (see the location of the basins in Figure 34) for each of the events studied in this work.

Figure 34: Location of the basins considered in the analysis of the punctual sections: Bisagno for 9th October event; Graveglia for 10th November event; Polcevera for 15th November event.

The use of the RCRPS in this punctual analysis allows to take into account, even in a analysis in a river section, of many sample points, that will be taken along the forecast time.

In the following figures the four configurations compared are the hydrological chain fed by the two types of nowcasting already described (with and without the volume modification) and by two type of blending obtained with the mean best blending function and the local best blending function, different for each event.

The event of 9th October is sadly known for the flood that affected the municipality of Genoa during the evening of that day. The main creek interested by the flood was Bisagno and hereafter are presented the results at the Passerella Firpo section (A≈97 km^2) in the frames a), b), c) of Figure 35.

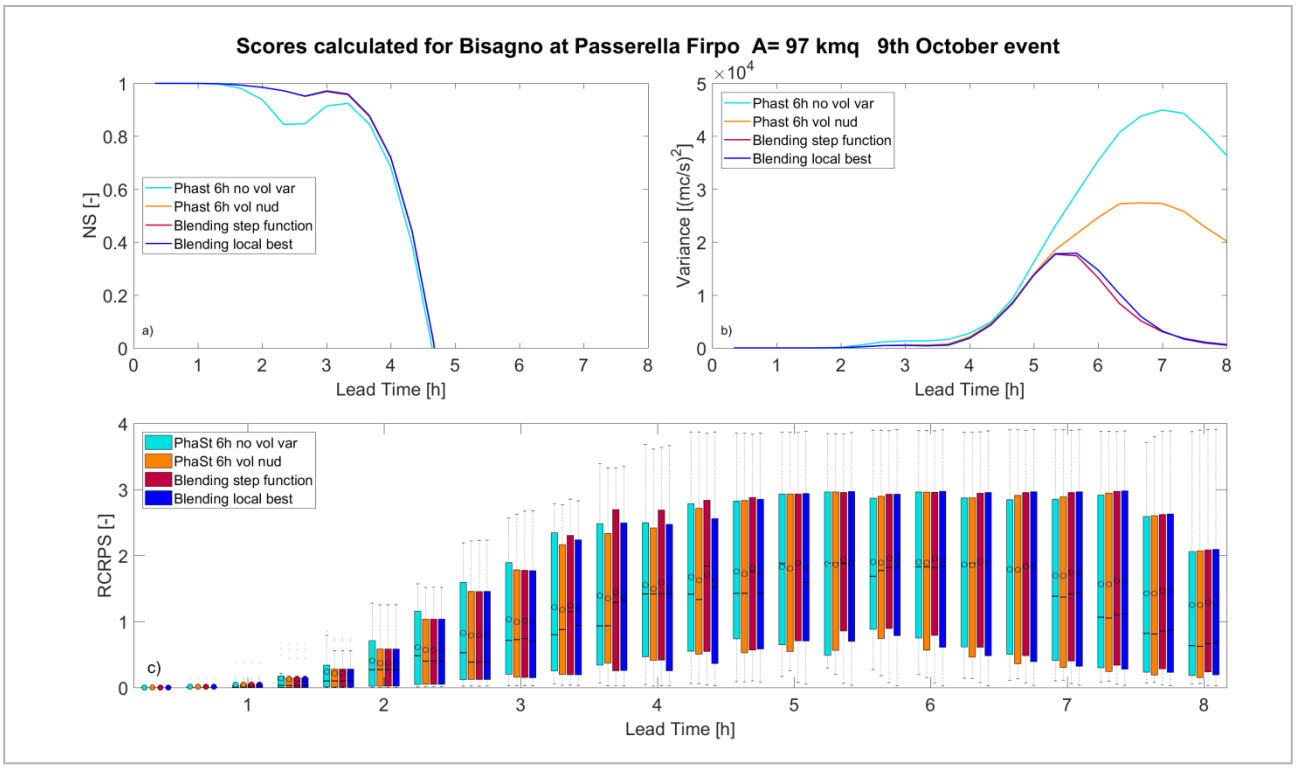

Figure 35: Scores calculated at river section (Passerella Firpo for Bisagno creek) for 9th October event (from 13:00 to 21:00 UTC of 9th October 2014). Nash Sutcliffe efficiency (a), Variance of the forecast (b), Reduced Continuous Probability Rank Score (c)

It can be noticed that, while for the NS the performances of the hydrological nowcasting chain are really similar between each other, the variance of the forecast related to the blended field in input is smaller than the other two, giving a forecast with less uncertainty than nowcasting forecast. The good performances of the two scores at the first lead times are connected to the response time of the basin, in the order of around 3 hours.

For what regard the RCRPS score the behavior is varying along the lead time: at the beginning are performing better the chains that take in input the nowcasting modified with the information regarding the volume obtained by the NWPS forecast hourly corrected; in the transition phase, when the combination of nowcasting and NWPS forecast is performed, there is no a best configuration prevailing on the others; for longer lead times seems to be better the use of the nowcasting as it is, without the correction with the meteorological model or the combination with it. In fact in this event the forecast of the meteorological model, even corrected with the observations through data assimilation, is not able to improve the rainfall forecast.

The event of 11th November affected the whole Liguria Region but the main effects at ground were caused by Entella river, that caused the flooding of the urban area of Chiavari and by its tributaries

Lavagna and Graveglia. In this case study the scores on Graveglia basin at Caminata section (A≈42 km2) are shown in the subplots a), b), c) of Figure 36.

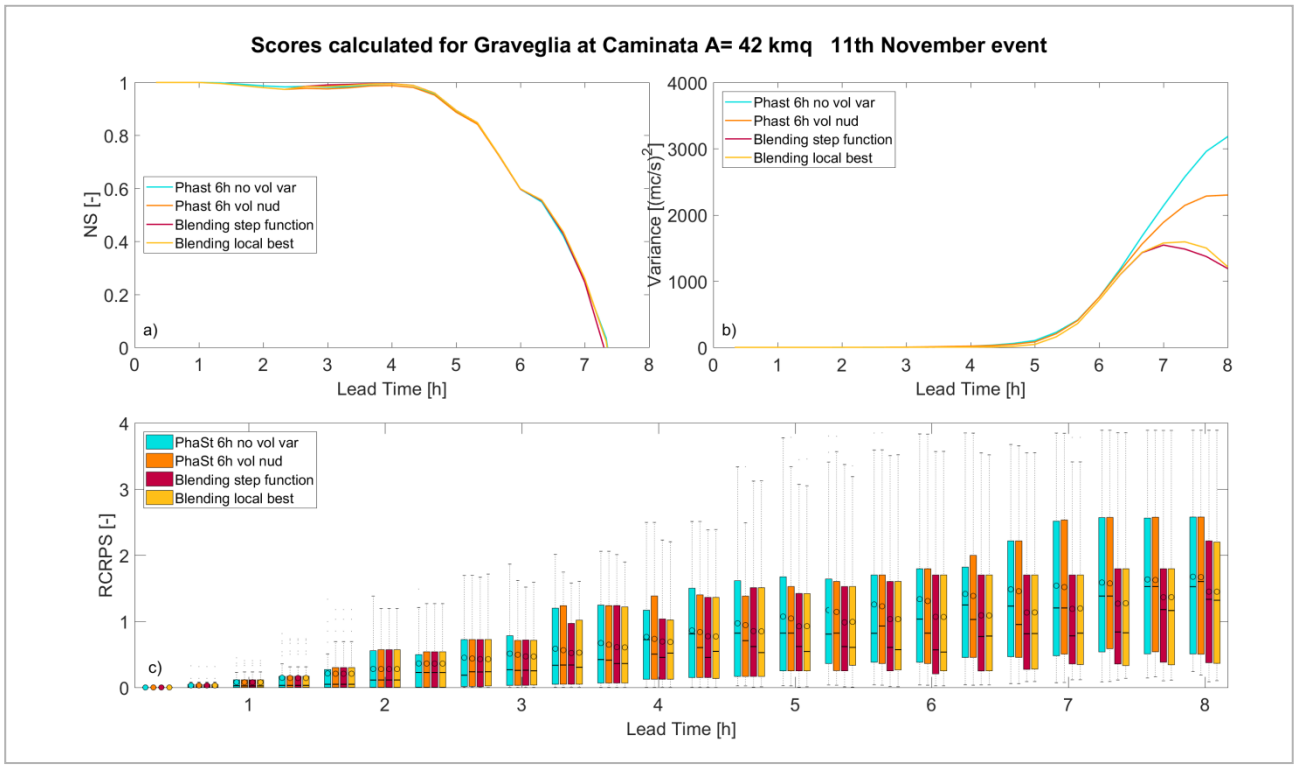

Figure 36: Scores calculated at river section Caminata for Graveglia catchment) for 11th November event (from 10:00 to 21:00 UTC of 10th November 2014). Nash Sutcliffe efficiency (a), Variance of the forecast (b), Reduced Continuous Probability Rank Score (c)

Here the different color of the fourth configuration compared (in yellow) represents the configuration in which the input are the blended rainfall fields resulting from the linear combination obtained applying the blending function that performed better for this event (f2, as it can be evinced by Figure 31).

The effects of the use of the meteorological model are clearly positive in terms of RCRPS. In this event the forecast of the rainfall field performed only with the nowcasting technique lead to an overestimation of the discharge, while the rainfall forecast obtained through the blending of the nowcasting output and the assimilated NWPS output gives an important enhancement. Besides that, also in this case the smaller variance related to the forecast performed with the blending is giving an additional value to this configuration: the forecast shows less spread, is more confident of what is predicting with respect to the nowcasting alone.

For the event of 15th November, the performance of the scores calculated for Polcevera at Rivarolo section (140 km2) are reported in the frames a), b), c) of Figure 37.

In this case the two configurations related to the blending assume the same color (red) since for this event the local best blending function coincides with mean best blending functions for all the events (the step function, see again Figure 31).

The more interesting score in this event is the RCRPS: it is relevant that, in this case, the performance of the score connected with the blending are decreasing around 4 to 6 hours lead time. As already explained this can be related to the unrealistic rainfall field produced by the blending when the nowcasting and the NWP model forecast are really different between each other.

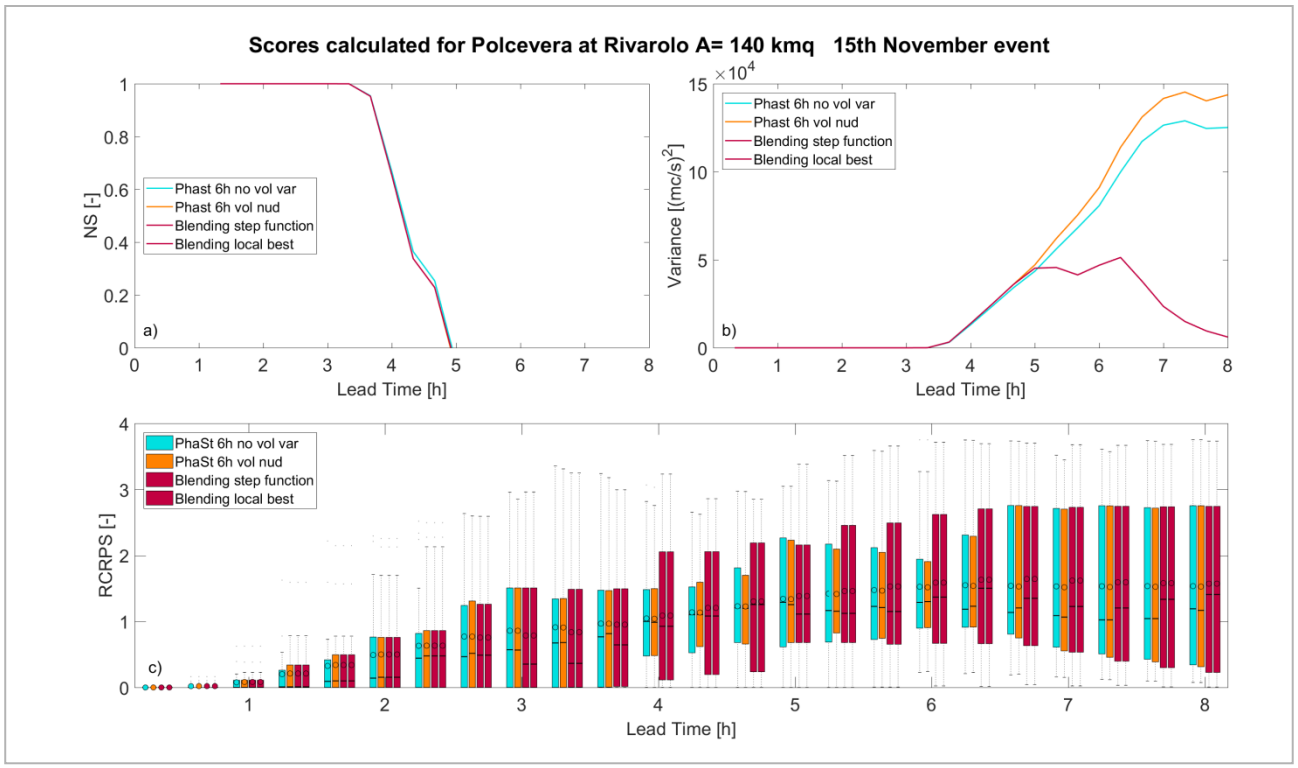

Figure 37: Scores calculated at river section (Rivarolo for Polcevera catchment) for 15th November event (from 02:00 to 11:00 UTC of 15th November 2014). Nash Sutcliffe efficiency (a), Variance of the forecast (b), Reduced Continuous Probability Rank Score (c)

5.3.3 Distributed analysis

While in the section 5.3.2 the scores where related to single punctual sections of the basins mainly involved in the analyzed events, in this section the distributed analysis is aimed to give a more general idea of the performance of the hydrological nowcasting chain fed with different rainfall

input. In fact, with the distributed analysis it is possible to compile the score, in this case the RCRPS, over all the points of the domain, for which Continuum is computing the forecasted discharge. For this analysis the comparison will be performed always between the nowcasting without the volume variation (1st column of the boxplot), nowcasting with volume modification (2nd column), Blending performed through the best blending function in average for the three events, i.e. the step function (3rd column), Blending performed through the blending function that performs better for the specific event (4th column).

9th October 2014

For this event the best blending function is the function referred in Chapter 3.4 as blending function f3 (blue column). Figure 38 shows the general behavior during the entire event: the use of the information retrieved by the meteorological model in the rain forecast is worsening the hydrological forecast. This can be due to the peculiar type of event characterized by stationary and persistent precipitation on the same portion of territory that was not forecast precisely by the meteorological model but well reproduced by the nowcasting model. However, even if the information regarding the location of the rainfall, coming from the meteorological model, is misleading for the hydrological forecast, the information about the total volume on the domain is adding a value to the nowcasting rainfall field.

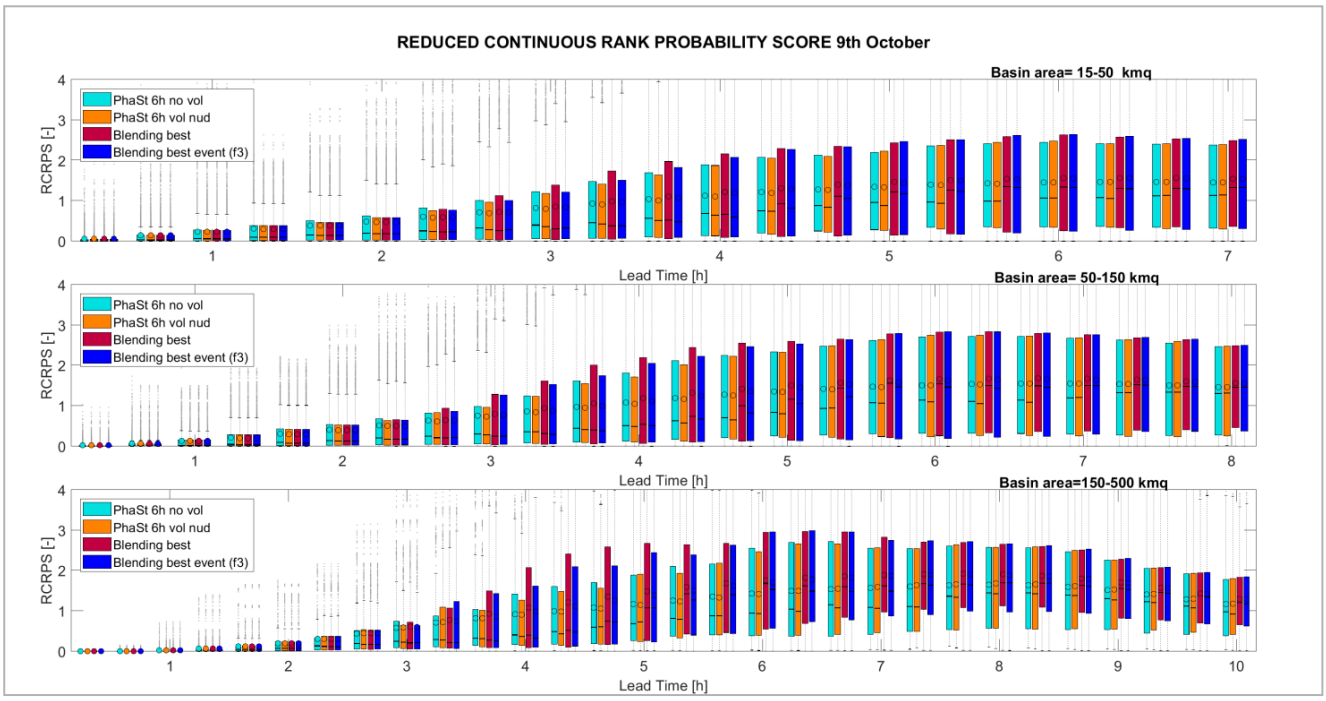

Figure 38: 9 Oct. 2014 event: RCRPS for three distinct classes of area. Each column refers to a different configuration of the forecasting system, whose rainfall is provided by: nowcasting without volume variation (light blue), nowcasting with the volume variation (orange), blending using the step blending function (red), and blending using the best local blending function (blue) which in this case is the function f3.

11th November 2014

In this event the blending function that is performing better is the one referred before as Blending function f2 (yellow column).

As already pointed out in the previous basin scale analysis, the distributed analysis (Figure 39) confirms, even more clearly that for this event the system using the blending performs markedly better. Especially for the bigger basins, due to their response time, the effects of a proper rainfall forecast provided with blending are beneficial for longer lead times, probably due to the slow response of the basins.

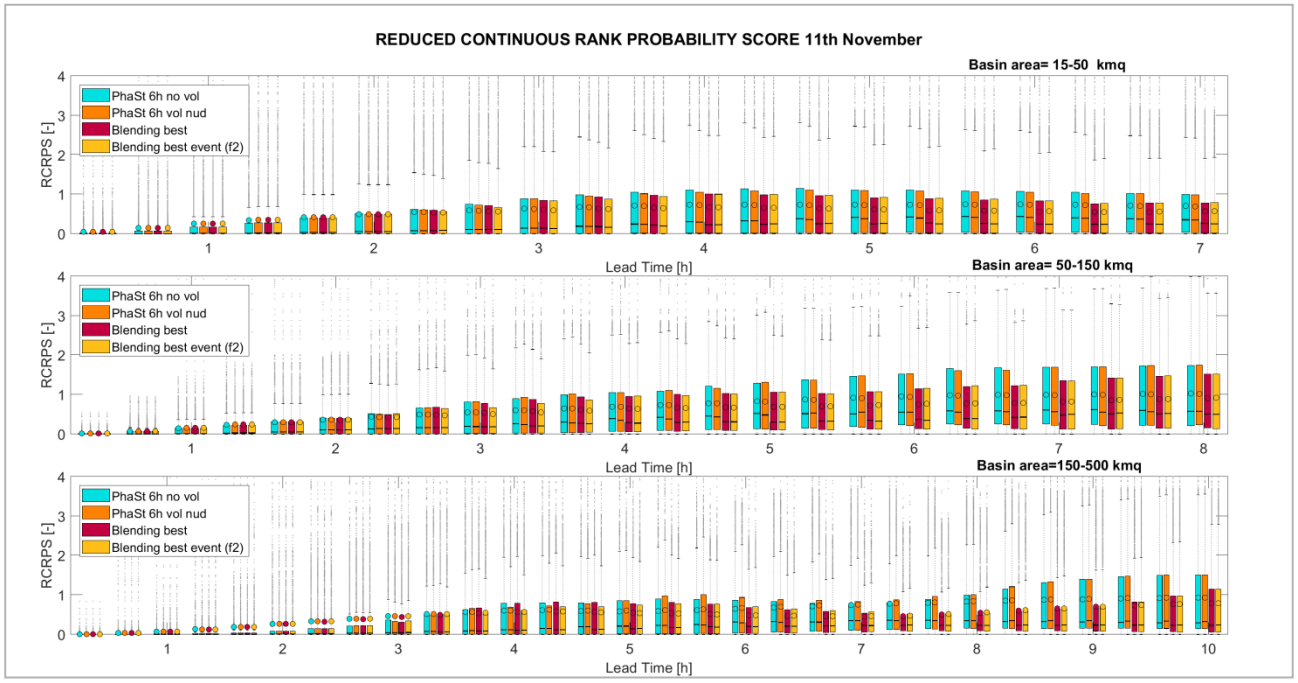

Figure 39: 11 Nov. 2014 event: RCRPS for three distinct classes of area. Each column refers to a different configuration of the forecasting system, whose rainfall is provided by: nowcasting without volume variation (light blue), nowcasting with the volume variation (orange), blending using the step blending function (red), and blending using the best local blending function (blue) which in this case is the function f2

15th November 2014

In this event the blending function that is performing better coincide with the best in average for all the three events, the step function (in red).

In this case (Figure 40) the difference among the configurations can be noticed most of all in the first two classes of area, where the use of the blending technique improves the rainfall forecast: the column related to the blending is always lower and presents less spread with respect to those related to the nowcasting. In the last class of area (larger basin) the behavior is different especially at the lead time corresponding to the transition in the blending between the rainfall field from nowcasting and from the NWP model. This transition phase is confirmed to be the most critical for the blending as it can produce unrealistic rainfall fields.

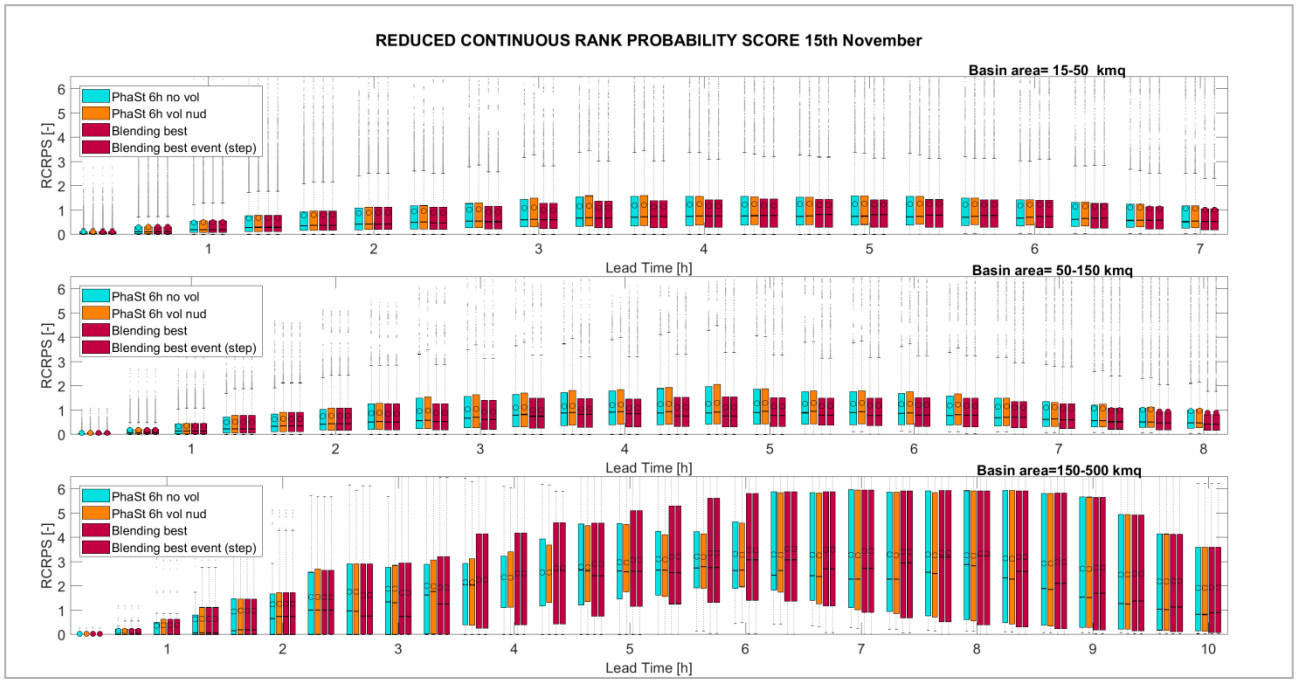

Figure 40: 15 Nov. 2014 event: RCRPS for three distinct classes of area. Each column refers to a different configuration of the forecasting system, whose rainfall is provided by: nowcasting without volume variation (light blue), nowcasting with the volume variation (orange), blending using the step blending function (red), and blending using the best local blending function (blue) which in this case is the step function.

5.4 Intercomparison between two nowcasting methods

This research activity has been developed in parallel to the main activity of the PhD during the period spent at CRAHI-UPC in Barcelona during spring 2018. CRAHI is the Centre of Applied Research of Hydrometeorology, of the Polytechnic University of Catalunya. The CRAHI focuses its activity on providing scientific and technological support in the area of hydrometeorological management and forecasting, particularly on developing models of the processes that drive the cycle of surface waters.

The main argument of this work has been the intercomparison between the nowcasting algorithm applied and improved in the PhD, PhaSt, and the nowcasting method developed at CRAHI, SBMcast (Berenguer et al., 2005; 2011). This comparison has been performed in different steps, with increasing degree of complexity: first of all starting from the analysis of the performances of the deterministic versions of the nowcasting methods in terms of rainfall forecast, then studying the features of both the techniques in their probabilistic version.

Successively, an analogue hydrological nowcasting chain connecting SBMcast and Continuum has been built similarly the one based on PhaSt. The results obtained with the two hydrological nowcasting chain in terms of discharge forecasted have been compared. Finally an analysis in terms of propagation of the error through the hydrological nowcasting chain has been performed.

SBMcast (Berenguer et al., 2005; 2011) is based on the extrapolation of radar precipitation observations according to the estimated motion. The algorithm is composed of two modules for:

- tracking-extrapolation of precipitation: the tracking algorithm estimates the motion field with a given resolution based on the analysis of 2 or 3 consecutive radar maps, based on a modified version of COTREC (Li et al., 1995).
- simulation of the evolution of the rainfall field in Lagrangian coordinates assuming the hypotheses of the String of Beads model (Pegram and Clothier, 2001).

This second module is used to perform the probabilistic forecast: starting from the real radar reflectivity fields as the first time steps of each time series of the ensemble, it forecasts IMF (t), the Image Mean Flux and WAR (t), Wet Area Ratio, constrained with observed values, and the motion of the field.

In this study the deterministic version uses the first module only: TREC (Tracking Radar Echoes by Correlation, Rinehart and Garvey,1978) Starting from the last three observed radar images up to 20 minutes before the "now" the velocity field of the rainfall filed is obtained and kept constant in the advection of the future rainfall fields.

The deterministic version of PhaSt is obtained switching off the noise component in the equation that describes the phases evolution. For the complete equations upon which the model is based see Equation 6 in Chapter 4.2.

Setting the noise equal to zero and according to the hypothesis that after the correlation time the tendency velocity is also equal to zero, in a first deterministic version of PhaSt the structures tend to stop after few time steps, making it similar to an Eulerian persistence. For this reason, a second version of deterministic PhaSt has been explored, relaxing the hypothesis of the tendency velocity equal to the estimated initial velocity. A fourth type of nowcasted rainfall field is compared with these ones: the Eulerian persistence, that is keeping the most recent observation frozen for the following two hours of forecast.

The analysis of the four nowcasting chains has been performed starting from a simpler comparison between the two deterministic nowcasting techniques and then of the deterministic output of the hydrological nowcasting chain.

Regarding the scores used hereafter some new score have been used beyond the scores described at the beginning of this chapter. For the analysis of the forecasted rainfall fields:

- Root Mean Square Error: square root of the average of the squared differences between forecasts and observations.

$$RMSE = \sqrt{\overline{(rain_{for} - rain_{obs})^2}} \qquad Eq.23$$

- Bias: the difference between the mean of the forecasts and the mean of the observations.

$$BIAS = rain_{for} - \overline{rain}_{obs} \qquad Eq.24$$

- Ensemble spread of the forecast for the probabilistic analysis: the average difference between the individual ensemble forecasts (F_{ie}) of a quantity and the ensemble mean forecast ($\overline{F_i}$) of the quantity.

$$spread = \frac{1}{N}\sum_{i=1}^{N}\sqrt{\frac{1}{E-1}\sum_{e=1}^{E}(F_{ie} - \overline{F_i})^2} \qquad Eq.25$$

For discharge analysis has been used the already mentioned NS efficiency (Nash and Sutcliffe 1970) and an analysis performed through rank histogram or Talagrand diagram (Talagrand et al., 1997). To build the diagram a rank of a verification (e.g., the observed runoff) is identified sorting the values from an ensemble from lowest to highest. As forecast data are used to create the bins (class intervals), for an ensemble with 20 members there are 20 bins and then observed (new) data are used to fill those bins.

5.4.1 Deterministic comparison

9 October 2014

The scores for the rainfall analysis are calculated at basin scale for the main catchments involved. In the 9th October event the main catchments considered are Bisagno, Scrivia and Sturla (Figure 6).

In the following figures it is possible to see the scores calculated for the rain at basin scale: the score is computed pixel by pixel and then a mean value at the basin scale considered is calculated. The first thing to observe is the behaviour of rainfall on the considered catchments. Looking at the rainfall cumulative map for the time window of the event considered (from 00 UTC of 9th Oct to 6 UTC of 10th Oct) it is possible to see that in Bisagno and Scrivia the most intense observed rainfall structure has been stationary for about 6 hours (Figure 41), while in Sturla basin the rain has been less persistent. This pattern strongly influences the rainfall and discharge scores performance.

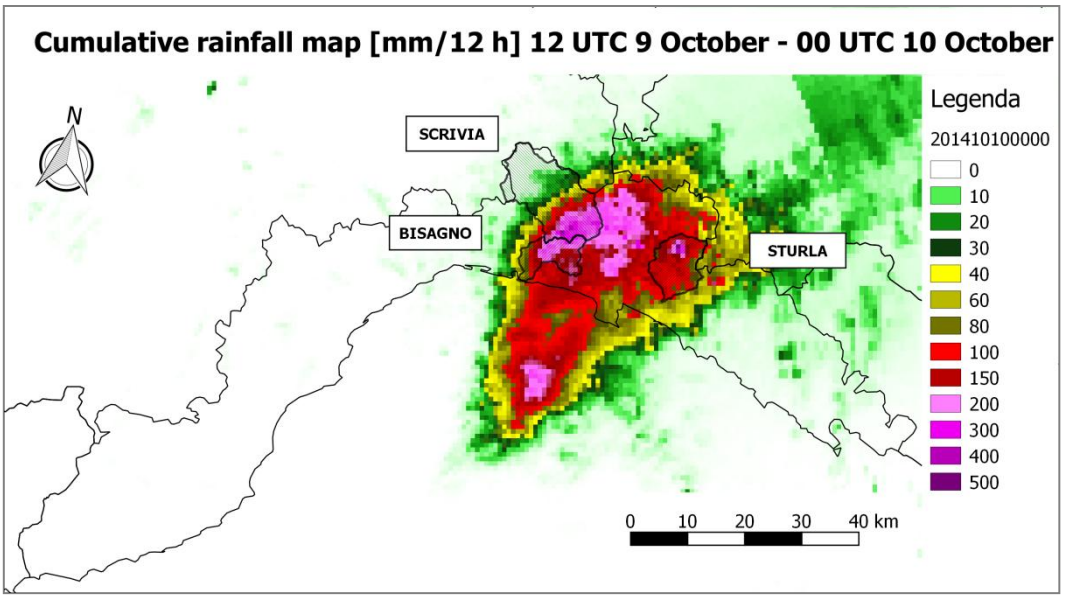

Figure 41: Cumulative rainfall map between 12 UTC of 9 October and 00 UTC of 10 October 2014 on the main basins involved in the event: Bisagno, Sturla and Scirvia

In the following figures the performances of the four nowcasting techniques are compared in terms of rainfall prediction accuracy: the black line represents the Eulerian persistence, the blue line the deterministic version of PhaSt with tendency velocity equal to 0, hereafter referred as phast det0, the green line the deterministic version of PhaSt with tendency velocity equal to the initial velocity, hereafter referred as phast det0, and the red line the deterministic version of SBMcast.

Firstly, what can be noticed is the similar behaviour of the persistence forecast and the deterministic version of PhaSt det0. This is due to the fact that in this version of the deterministic PhaSt the lack of the noise component results into the transformation of the nowcasted field into an Eulerian persistence after the first two or three time steps of forecast.

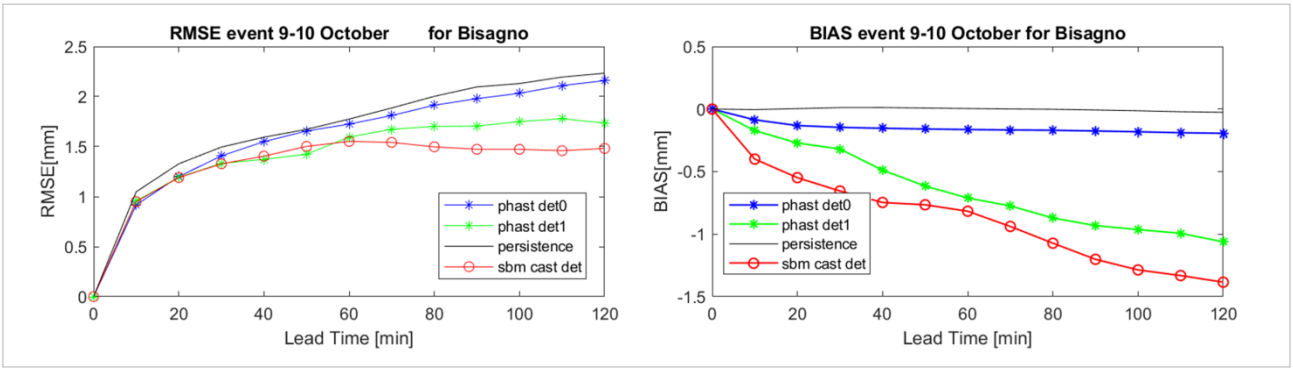

Figure 42: RMSE and BIAS calculated for rainfall aggregated at basin scale for Bisagno varying along the forecast time up to 2 hours lead time

Besides that also the other two nowcasting methods Phast det1 and SBMcast deterministic have similar results between each other. The persistence in this case perform better in term of BIAS as its closer to zero while for the other two there's a tendency to underestimate the rainfall on the basin, moving it too rapidly with respect to what really happened. This behaviour is registered both for the rainfall aggregated at basin scale of Bisagno (Figure 42) and of Scrivia (Figure 43).

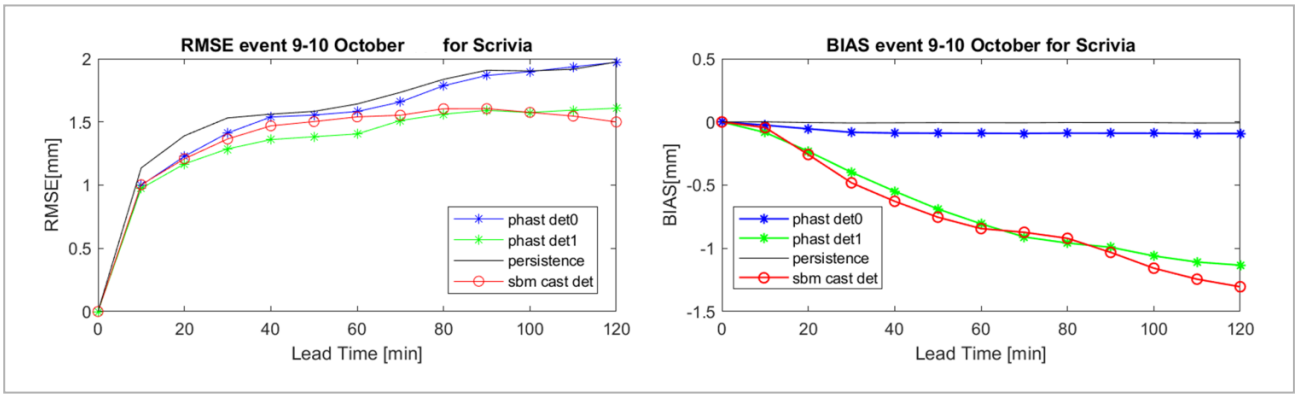

Figure 43: RMSE and BIAS calculated for rainfall aggregated at basin scale for Scrivia varying along the forecast time up to 2 hours lead time

On the other hand, during the same event on Sturla basin (Figure 44) the rainfall pattern was less stationary and the score for RMSE is comparable for each nowcasting technique. Also the BIAS is performing better, even if is varying along the forecast time for SBMcast and Phast det1 there is no clear underestimation or overestimation of the rainfall fields.

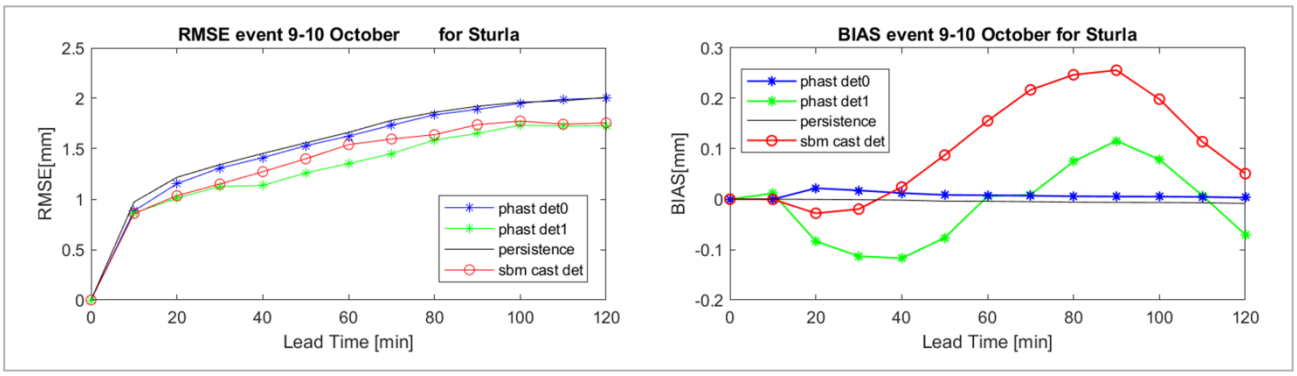

Figure 44: RMSE and BIAS calculated for rainfall aggregated at basin scale for Sturla varying along the forecast time up to 2 hours lead time

The results in terms of hydrological forecast are strongly related to those obtained by the rainfall analysis. The score shown in Figure 45, the Nash Sutcliffe efficiency, is obtained comparing the forecasted hydrograph to the reference hydrograph. In these graphs the results of the hydrological model fed with the different nowcasting methods are compared also with the result of a "no rain"

forecast, that mean that the hydrological model takes in input only the observed rainfall field without adding nowcasted rainfall field, indicated with the light blue line. The second light blue line interrupted by triangles represents the score that would be the result of a prefect rainfall input: this is performed using in input as forecasted rain the observed rainfall filed for the next two hours.

As said before the performances of the hydrological forecast are strongly correlated to those of the rainfall forecast. In fact, looking at the NS related to Bisagno and Scrivia catchments (Figure 45 a) and b)), on which for the rainfall analysis the model performing better where those connected to the persistence, the eulerian persistence and phast det0, an enhancement in the predictive capability can be seen most of all for greater lead time. On the other hand, for what regard the Sturla catchment (Figure 45 c)), the hydrological forecast is more accurate for SBMcast and PhaSt det1, for which the rainfall forecast scores were performing better.

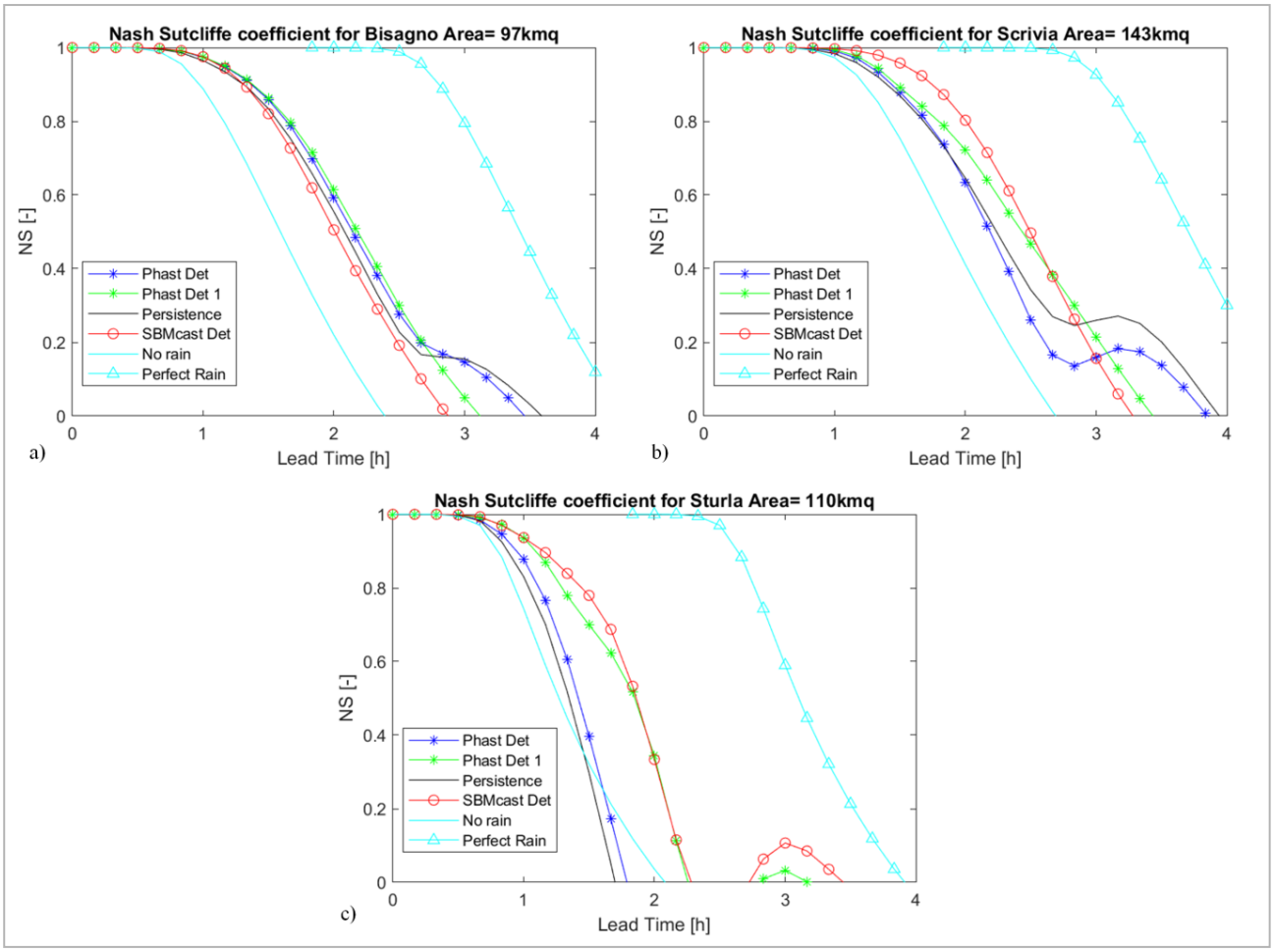

Figure 45: NS efficiency calculated for discharge forecasted through the different deterministic nowcasting (the Eulerian persistence, the two deterministic versions of PhaSt and SBMcast deterministic), the "perfect rainfall" and the "no rain" forecast in input to the hydrological model. For 9th October 2014 event the basins analyzed are Bisagno (a), Scrivia (b), Sturla (c)

Anyway, what can be observed is that there is almost in all the cases a gain of lead time from 30 minutes to 1 hour and half, that is an important benefit in real time management operations especially for these small catchments. The analysis of this event allowed also to notice firstly the strong impact of the rainfall pattern on the resulting forecast of the hydrological nowcasting chain.

10-11 November 2014

The event that occurred during the evening of 11th November is characterized by a rainfall pattern similar to the one for the event of October. The main rainfall structure that stroke the Entella basin (see location in Figure 7) lead to its flooding in various sections close to the city of Chiavari.

The scores have been calculated for the time window of the event from 12 UTC of 10th November 2014 to 02 UTC of 11th November. Looking at the rainfall scores (Figure 46) also for this event is possible to notice the correspondence of behaviour between the eulerian persistence and phast det0 and between SBMcast and phast det1.

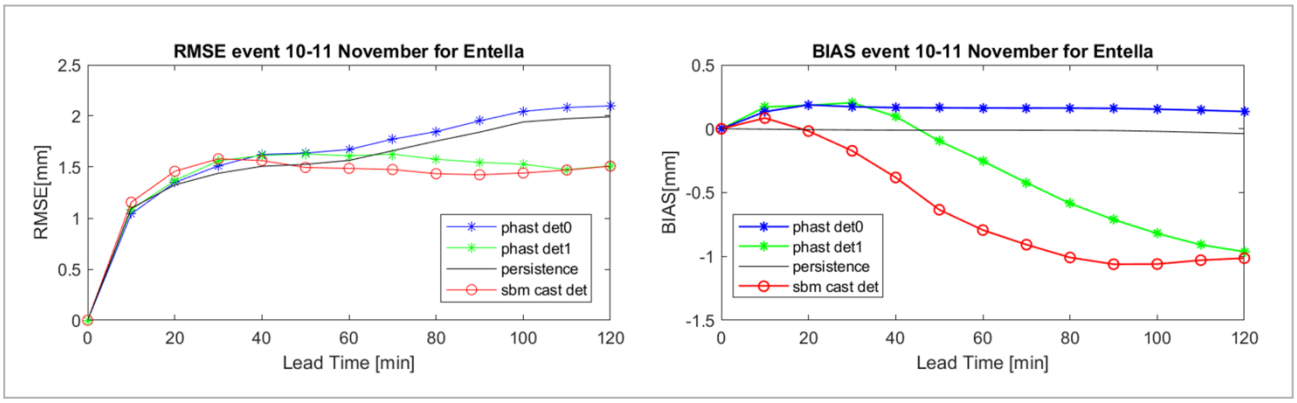

Figure 46: RMSE and BIAS calculated for rainfall aggregated at basin scale for Entella varying along the forecast time up to 2 hours lead time

RMSE shows better performances for the SBMcast and phast det1 forecast while BIAS performs better in the cases related to the persistence forecast. Looking at the score of the hydrological forecast (Figure 47) even in the event of 11th November the rainfall pattern played an important role: even if the NS is very similar for all the different configuration of hydrological nowcasting, for longer lead time the best performances are achieved by the Eulerian persistence forecast.

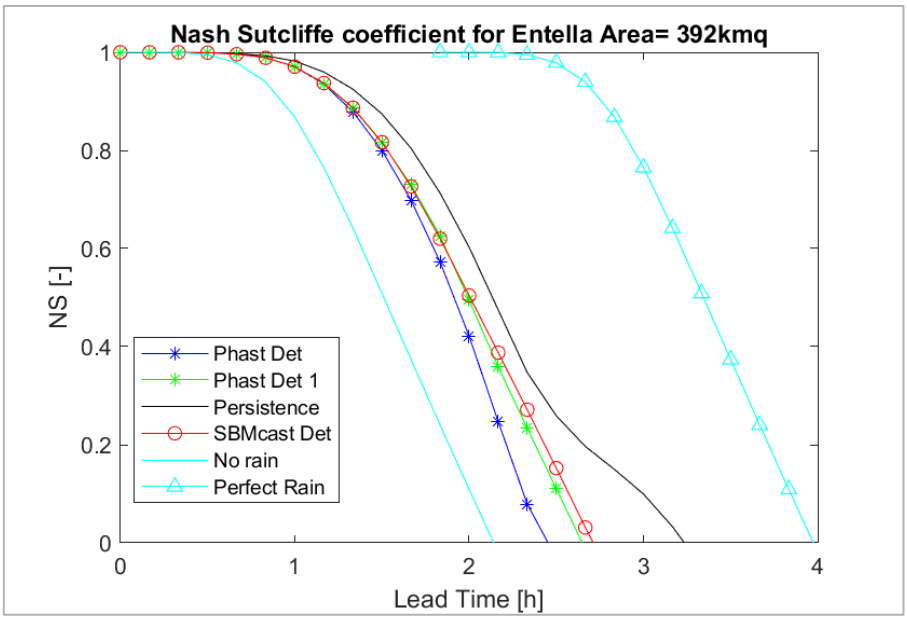

Figure 47: NS efficiency for Entella calculated for discharge forecasted through the different deterministic nowcasting (the Eulerian persistence, the two deterministic versions of PhaSt and SBMcast deterministic), the "perfect rainfall" and the "no rain" forecast in input to the hydrological model.

15 November 2014

For this event it is possible to do some considerations about the performances of the nowcasting models related to the size of the catchments as the size of the catchments considered is really different: Cerusa has a drained area of 25 km^2 while Polcevera of almost 150 km2 (see Figure 8). The time window of the event analyzed goes from 00 to 16 UTC of 15th November 2014 .

The performances of the rainfall forecasts in terms of RMSE are really similar in the two basins (Figure 48 and Figure 49) even if it can be noticed a slightly better behaviour for Polcevera with the forecast done with phast det1.

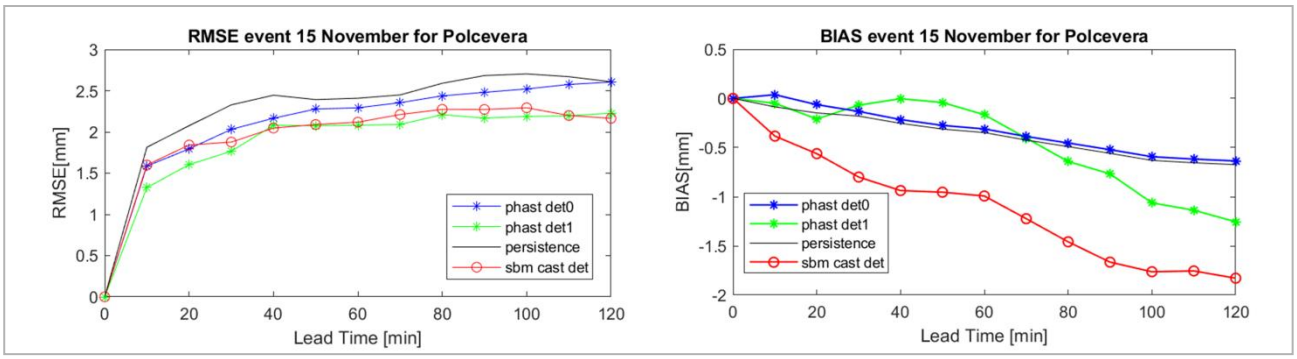

Figure 48: RMSE and BIAS calculated for rainfall aggregated at basin scale for Polcevera varying along the forecast time up to 2 hours lead time

For BIAS on Polcevera basin there is the same trend at the beginning of the forecast while for longer lead times it become better the forecast related to persistence; for Cerusa is harder to find a unique best nowcasting technique because their performances are sensitive to the lead time of the forecast.

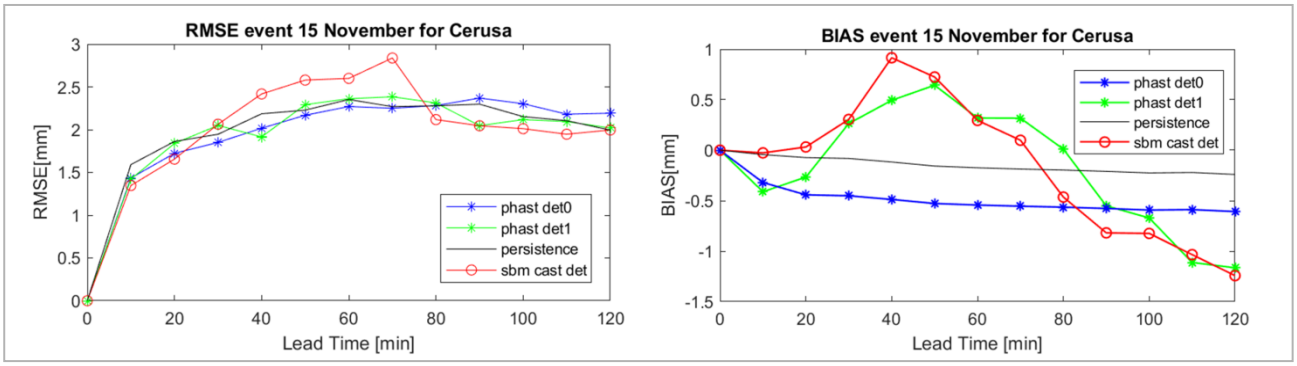

Figure 49: RMSE and BIAS calculated for rainfall aggregated at basin scale for Cerusa varying along the forecast time up to 2 hours lead time

Looking at the scores of the hydrological forecast (Figure 50), the better performance noticed for phast det1 are confirmed by the better behaviour of the corresponding NS: at equal NS there is a gain of almost 2 hours of lead time in the forecast performed through the nowcasting phast det1. Focusing on this aspect of performance of the forecast, the gain in term of lead time, a pronounced difference is undeniable between the two basins analysed. For Polcevera (around 145 km^2) the use of two hours of nowcasted rainfall allows to gain from 30 minutes to 2 hours with respect to the forecast without rain while in the smaller Cerusa, that is only 25 km^2, this gain is not achieved.

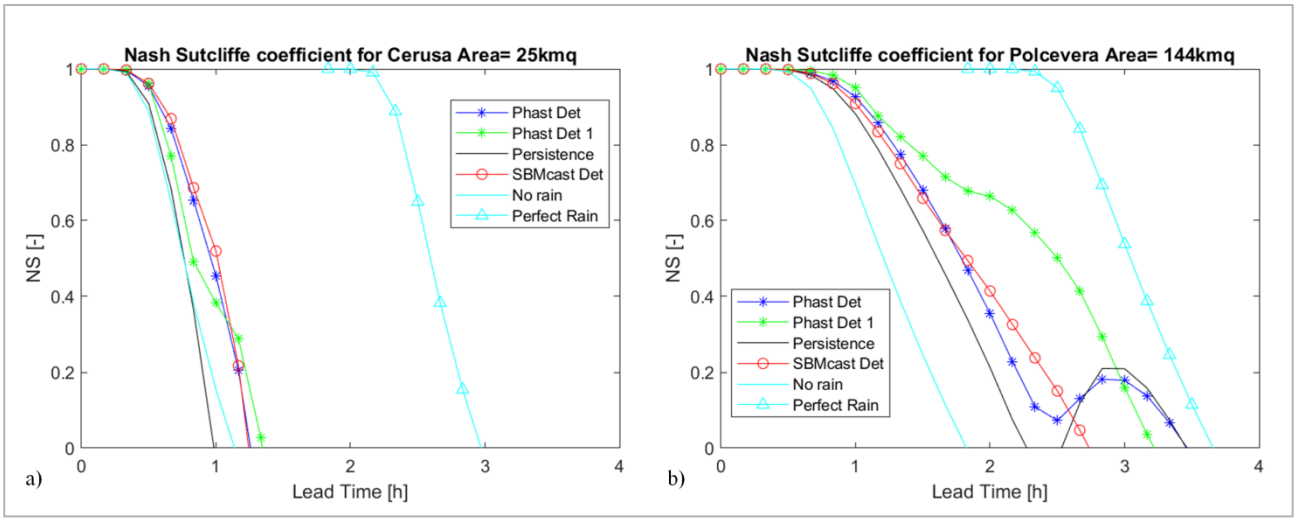

Figure 50: NS efficiency calculated for discharge forecasted through the different deterministic nowcasting (the Eulerian persistence, the two deterministic versions of PhaSt and SBMcast deterministic), the "perfect rainfall" and the "no rain" forecast in input to the hydrological model. For 15th November 2014 event the basins analyzed are Cerusa (a) and Polecevera (b) catchments.

The reason of this discrepancy can be found in the different response time of the two basins: the very fast response of Cerusa, connected to its geomorphologic characteristics, makes really difficult to exploit the forecasts of the nowcasting to enhance the hydrological model output.

5.4.2 Probabilistic comparison

In the probabilistic comparison the nowcasting models compared are PhaSt in its probabilistic version as it is described in Section 4.2 and SBMcast as it is presented at the beginning of the section 5.4. The case event is the 9th October 2014 and the basin of analysis is Bisagno.

The comparison of two probabilistic nowcasting techniques and of the related output of the hydrological nowcasting chain is a challenging problem. In fact many factors have to be taken into account: the uncertainty of the probabilistic forecast, the errors in terms of rainfall forecast but also the propagation of the errors in the hydrological nowcasting chain. Trying to understand this process a first effort has been done starting from an analysis carried on in (Foresti et al., 2016).

Firstly, referring to the rainfall forecast all over the domain, the dispersion of the forecast has been analyzed comparing the RMSE of the ensemble mean with the ensemble spread of the forecast. Since the spread of the forecast should represent the uncertainty of the forecast a good representation of the latter is obtained when the ensemble spread is as closer as possible to the

average variability of the observations around the ensemble mean, represented by the RMSE of the ensemble mean.

The result is shown in Figure 51, in which, for the two probabilistic nowcasting techniques (PhaSt a) and SMBcast b)), three lines are represented: the values of RMSE (line with stars) and the ensemble spread (line with circles) refers to the left axis, having the same unity of measure. The third line (solid line), representing the ratio between spread and RMSE, refers to the right axis, being expressed in terms of percentage. The RMSE and the spread have been calculated pixel by pixel on the entire radar domain and then the mean is represented in function of the lead time.

The fact that the ensemble spread is lower than the error for all the lead times means that the ensemble forecasts are under dispersive, in other words, the nowcasting model is under estimating the forecast uncertainty. What can be observed is that this under-dispersion is emphasized for SBMcast, for which the ratio between the spread of the ensemble and the RMSE is for every lead time lower than 40%. Then, a different behavior of the two techniques can be noticed looking at the ratio: the different trend outlines that for PhaSt this underestimation of the uncertainty grows initially very quickly and is flattened for the remaining lead time, while for SBMcast it gradually increases with the lead time.

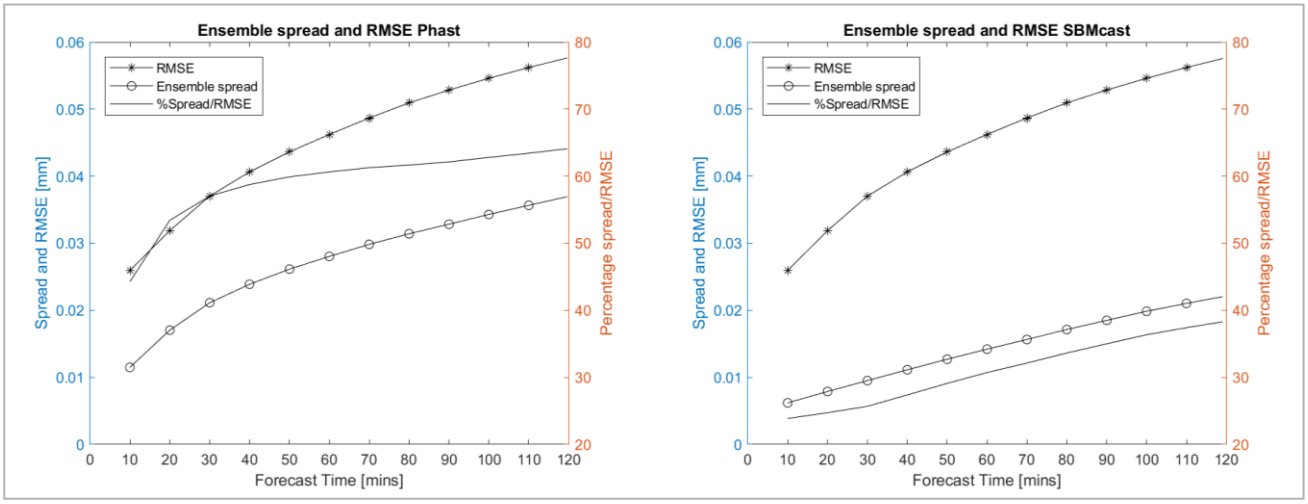

Figure 51: Ensemble spread (solid line with circles) and RMSE (solid line with stars) calculated for the rainfall field nowcasted with PhaSt (a) and SBMcast (b). The third solid line represents the ratio between the ensemble spread and the RMSE

To analyze the capability of the nowcasting techniques to represent the uncertainty of the forecast trough the spread of the forecasted discharge another way of analysis has been used: the rank histograms (also known as Talagrand diagram). To build it the discharge values forecasted are

ranked in increasing order to create bins; then the bins are then filled with the observed discharge. Among the 20 bins, in the first bin are contained the values of observed discharge lower than the minimum forecasted, while in the last one there are the values higher than the maximum value forecasted. A good ensemble forecasting shows a flat histogram because each ensemble member is an equi-probable realization of the future. If the histogram takes the shapes of a U or of an L with over-population of the extreme bins this means that the values of the observations fall often below or above the highest value of the ranked ensemble. Hence the forecast is under-dispersive, that is not dispersive enough to capture the extremes.

Performing this analysis for the forecasted discharge for Bisagno at different lead times the following behavior can be noticed: at the first time step the histogram is flat, indicating that the forecast is representative of the spread (Figure 52)

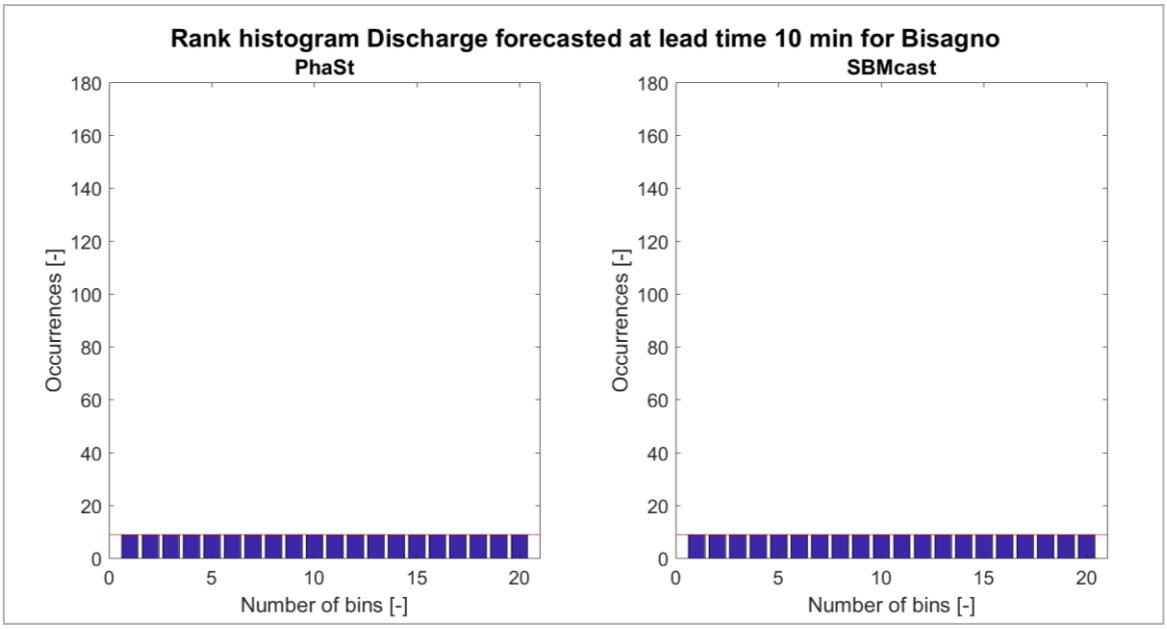

Figure 52: Rank histogram calculated for forecasted discharge at lead time 10 minutes result of the probabilistic hydrological nowcasting chain fed with PhaSt and SBMcast

Going on with forecast time (Figure 53 and Figure 54) in the histograms there is a marked over-population of the extreme bins, creating an intermediate shape between the U and the L.

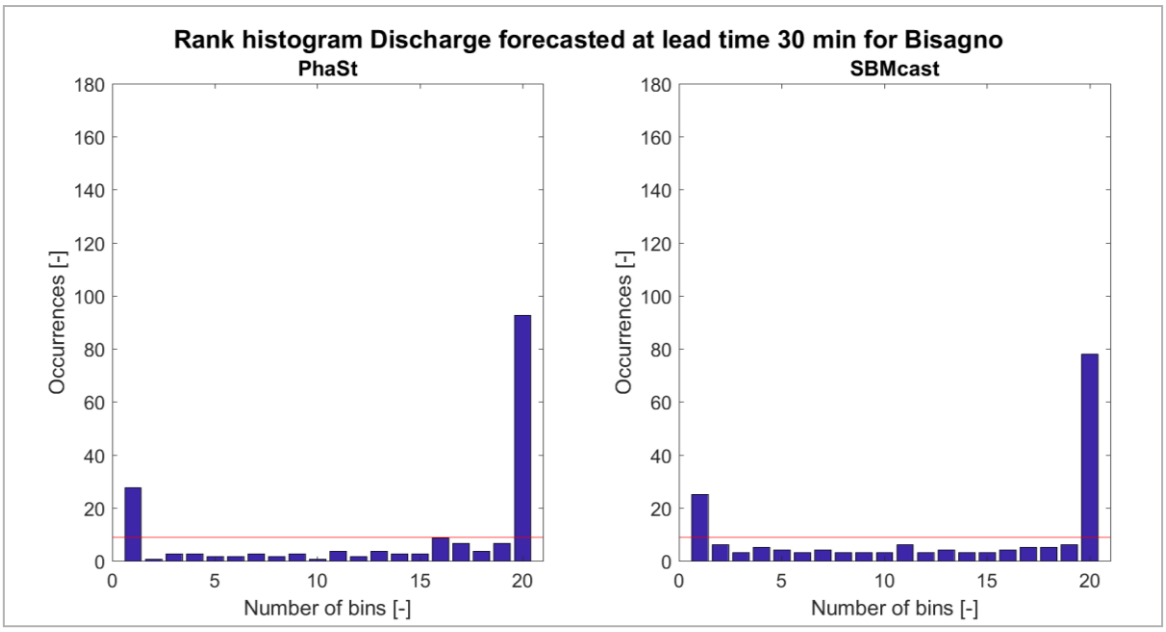

Figure 53: Rank histogram calculated for forecasted discharge at lead time 30 minutes result of the probabilistic hydrological nowcasting chain fed with PhaSt and SBMcast

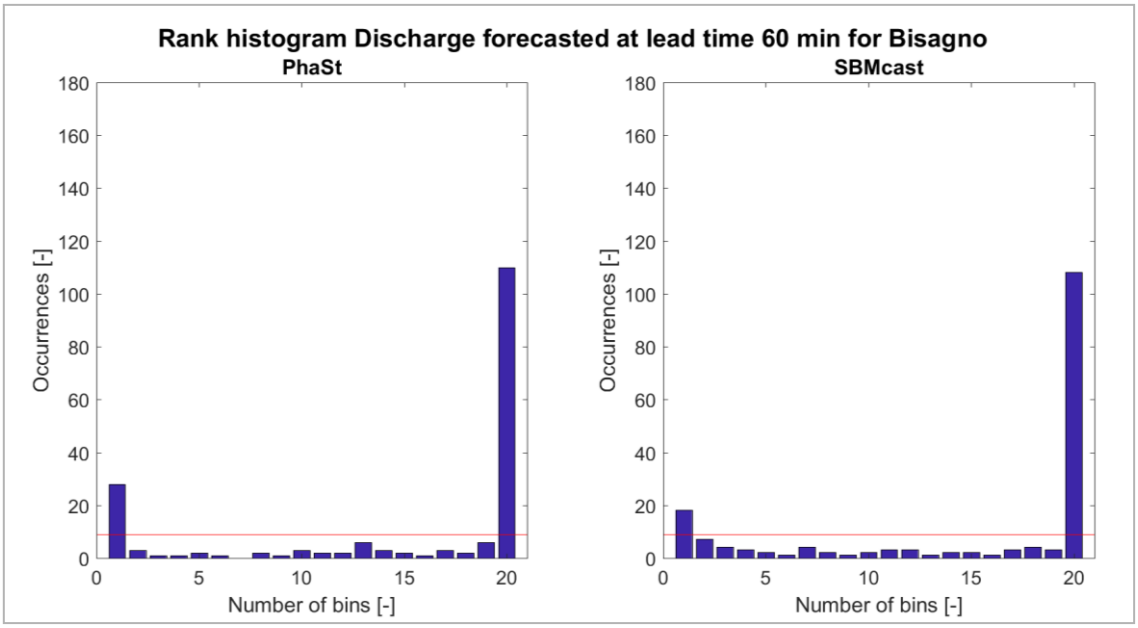

Figure 54: Rank histogram calculated for forecasted discharge at lead time 1 hour result of the probabilistic hydrological nowcasting chain fed with PhaSt and SBMcast

From the forecast at 2 hours lead time (Figure 55) the over-population regards mainly the last bin and for higher lead time, as it can be seen in Figure 56 for the forecast at 4 hours lead time, the L shape becomes emphasized, with higher over population of the last bin. This means that both the hydrological forecasts are under-dispersive, not representing adequately the spread. This is

connected with the observation on the under-dispersion of the nowcasting techniques that has been highlighted for the rainfall probabilistic comparison.

This work has been useful to explore the different instruments available for the comparison and the analysis of the performances of two nowcasting technique, both from the deterministic and the probabilistic point of view. Moreover, the coupling of the nowcasted rainfall field with the hydrological model has been exploited to analyze the propagation of the error inside the hydrological nowcasting chain and also for this analysis new approaches have been investigated.

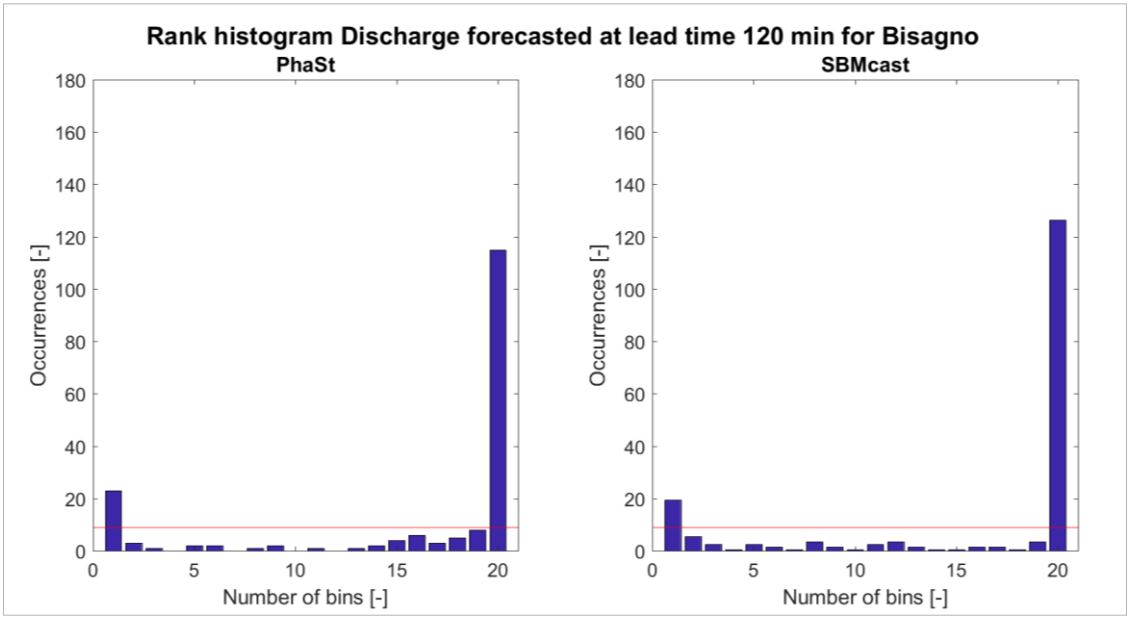

Figure 55: Rank histogram calculated for forecasted discharge at lead time 2 hours result of the probabilistic hydrological nowcasting chain fed with PhaSt and SBMcast

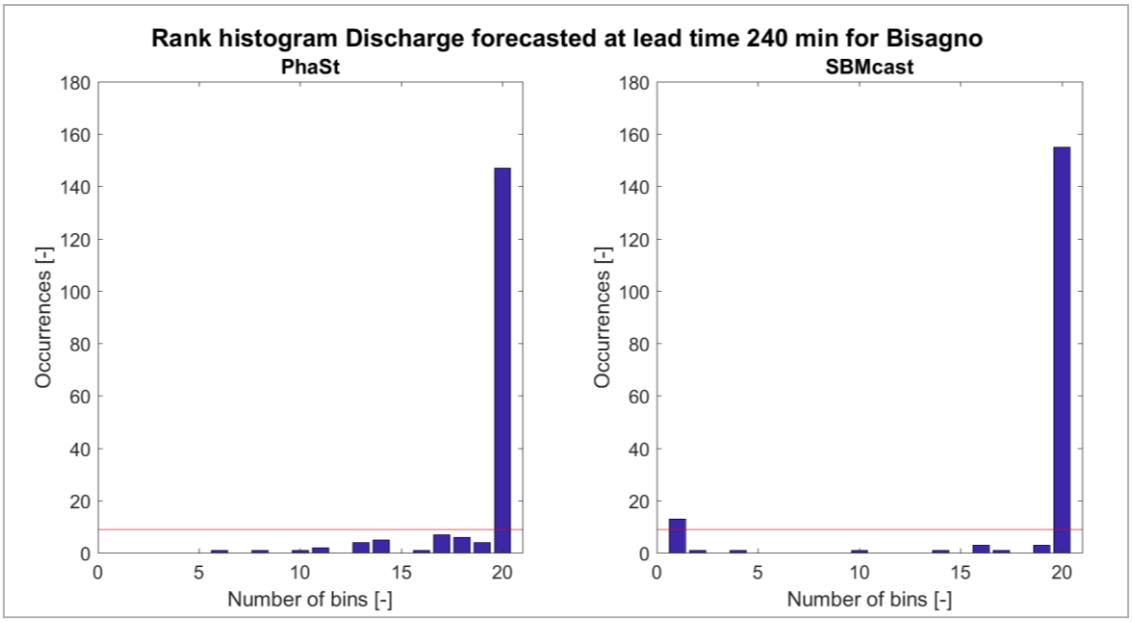

Figure 56: Rank histogram calculated for forecasted discharge at lead time 4 hours result of the probabilistic hydrological nowcasting chain fed with PhaSt and SBMcast

5.5 Visualization of the results

A crucial part of the work from an operational perspective, is making the output of the models useful in order to support civil protection decisions and actions is the communication of the final results. Risk communication in flood management can be improved through developing tools for communicating risk between scientists and emergency management professionals.

In order to answer to the operational requirements a possible way to visualize PhaSt output have been studied.

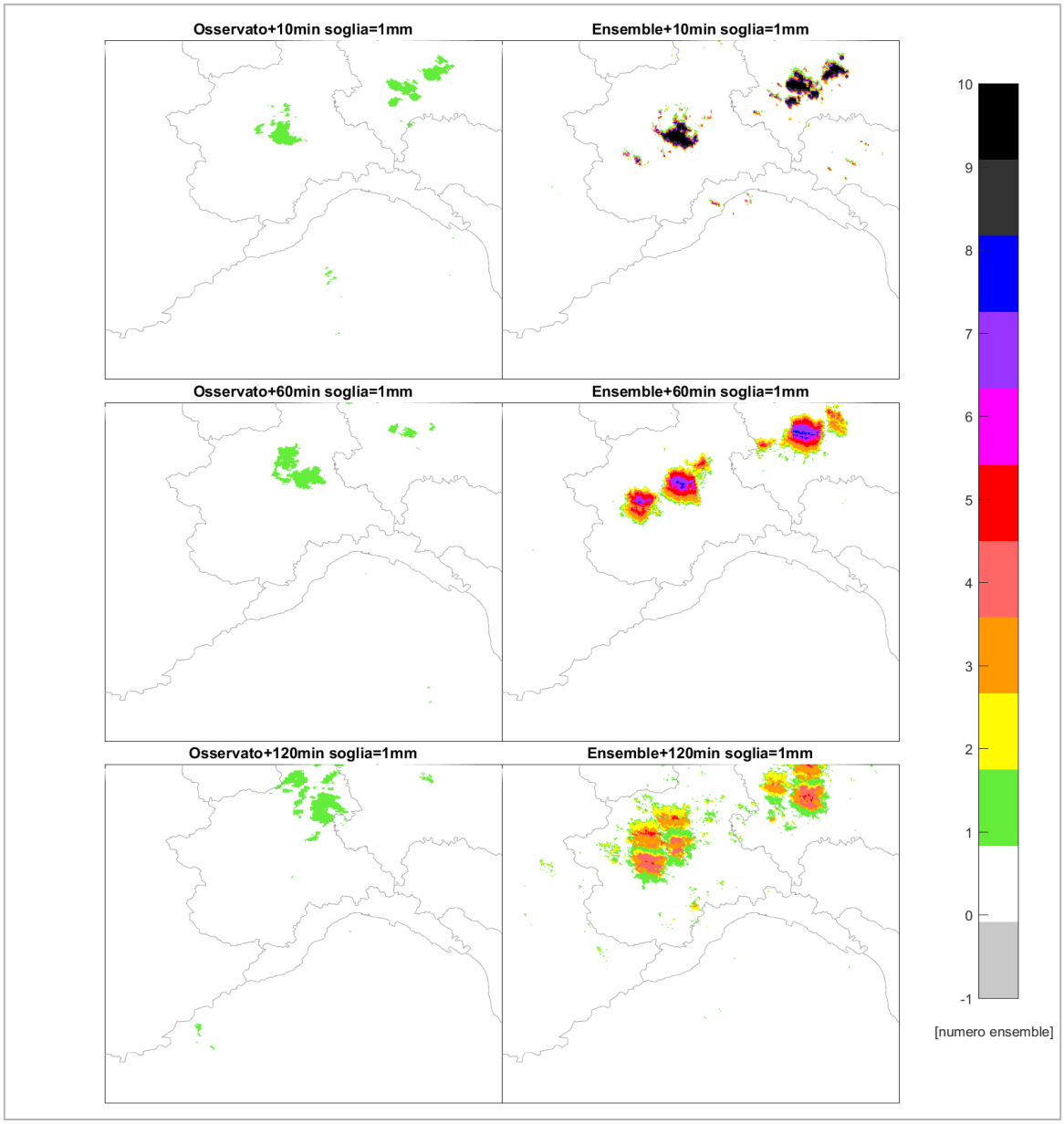

Figure 57: Comparison between observed rain field and PhaSt forecast for run at 23:00 of 1-08-2014

The visualization of the 10 ensemble members in the same figure can be useful to have an idea on the uncertainty of the forecast along the forecast horizon.

In Figure 57 the agreement of the different ensemble is represented through the colour used. Darker colours are used to represent the fact that many scenarios are forecasting the same rainfall pattern. In fact for short lead time, for which the uncertainty is very little, there is almost a total agreement between the different scenarios. Then, going on with the lead time, the uncertainty grows and consequently the spread of the forecast: at the end of the forecast the rainfall pattern is wider, covering a larger area. What can be noticed is the overlapping of the rainfall fields in the first time steps and then the relaxation of this overlap for the following steps: at 2 hours the rain field distribution covers a bigger area and less scenarios agree on the location of the structures.

The threshold used here is connected to the location of the rainfall field: the threshold of 1 mm/10 min means the simple presence of a precipitation structure. If the objective is to identify the location of the most intense rainfall structures the idea is to use the same visualization tool applying higher thresholds.

Regarding the representation of the output of the hydrological model, the discharge, an important step forward has been the use of the distributed output of the hydrological model. In fact the hydrological model Continuum allows to compute the hydrological forecast over the domain of Liguria Region. As said before a suitable visualization of the results is advisable in order to communicate the information in the most effective way. In this framework the flood forecast is difficult to interpret without a specific knowledge of the catchments involved.

Looking at Figure 58, in which the maps of forecasted discharge (maximum and minimum values) are represented for 1, 2 and 3 hours ahead at 19:40 UTC of 9th October 2014; for a lot grid points of the stream-network a high value of discharge is forecasted, but it is difficult to interpret whether this value is overcoming a critical threshold of flowing discharge. In fact what can be a critical value for a small catchment can correspond to ordinary values of discharge flowing in medium or big size catchments as a consequence, visualize results in terms of discharge, is not the optimal and most efficient solution.

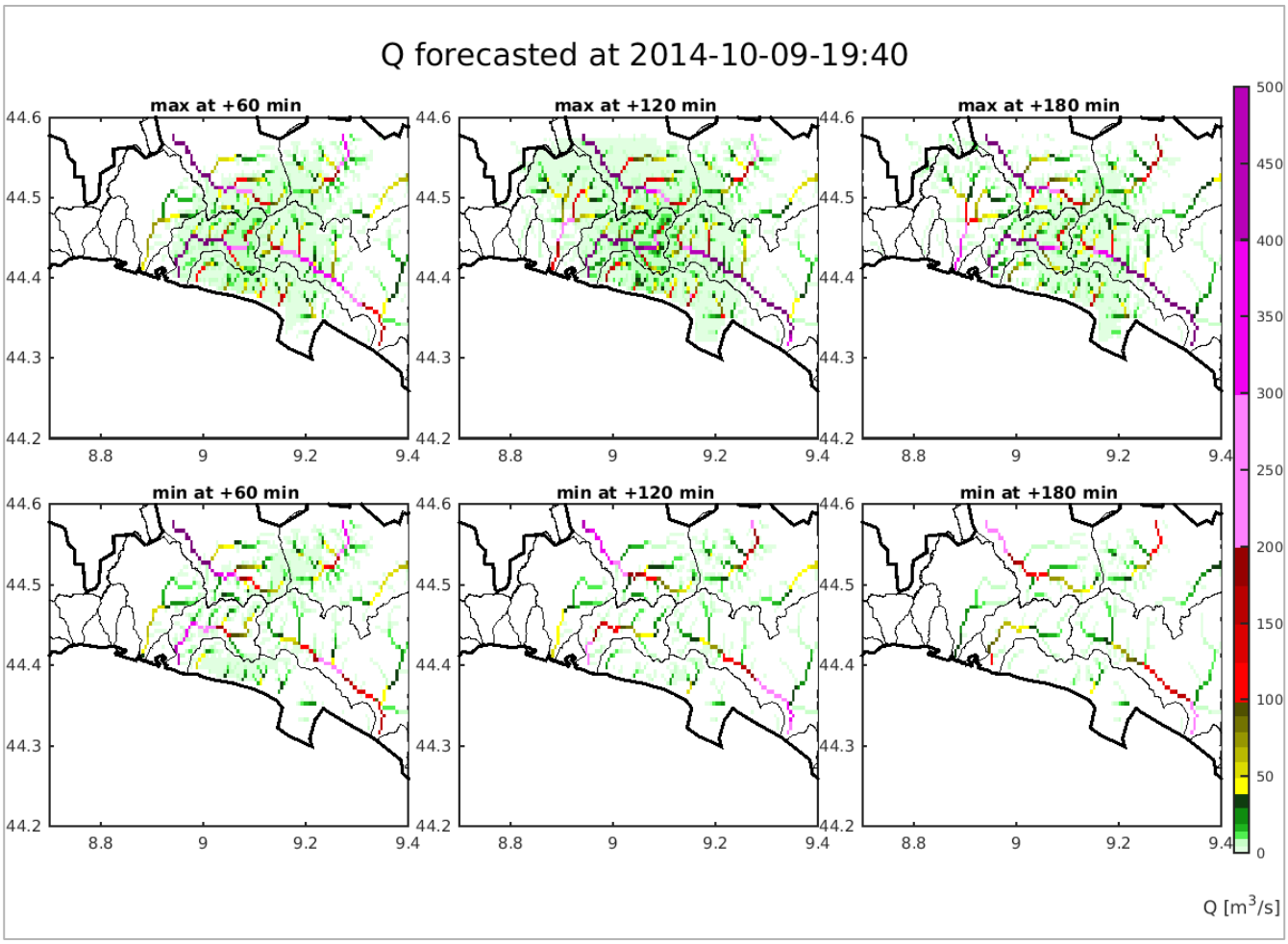

Figure 58: Map of discharge forecasted at 19:40 of 9th October 2014: distinct into two series of maps, maximum and minimum discharge forecasted at 1, 2 and 3 hours of lead time. It is hard to determine which are the basins really involved in the event that are causing at soil effects because the value of the critical discharge is really sensitive to the characteristics of the basin such as the area and the

In order to visualize the information of discharge in a distributed way independently on the basin scale, the flood forecast is converted in terms of return period T.

This conversion is possible applying the regionalization approach valid for Liguria Region (Boni et al., 1999), according to which quantiles of discharge (Q_T) are calculated using the flood index (with a return period of 2.9 years) and the known flood frequency factor (K_T):

$$Q_T = K_T \cdot Q_{2.9} \qquad Eq.26$$

The flood index, depending on geomorphological and climatological characteristics of the basin, can be calculated according to the following formula:

$$Q_{2.9} = 0.3 \cdot A \cdot C_F \cdot a_{2.9}^{4/3} \cdot t_b^{-0.48} \qquad Eq.27$$

Where:

- A is the area of the basin;
- C_F is a dimensionless parameter calculated from the Curve Number (Mishra and Sing, 2013), function of the type of soil of the basin:

$$C_F = \frac{3}{4}\left(4 \cdot 25.4 \cdot \frac{1000 - 10CN}{CN}\right)^{-1/3} \qquad \textit{Eq.28}$$

- a is a parameter related to the rain index $E[H_1]$ that is varying with longitude:

$$a = 1.06 \cdot E[H_1] \qquad \textit{Eq.29}$$

Longitude		**$E[H_1]$**	**Longitude**		**$E[H_1]$**	**Longitude**		**$E[H_1]$**
degree	minutes	mm	degree	minutes	mm	degree	minutes	mm
7	30	30.3	8	25	39.2	9	20	39.9
7	32.5	30.7	8	27.5	39.6	9	22.5	39.7
7	35	31.1	8	30	39.9	9	25	39.7
7	37.5	31.5	8	32.5	40.0	9	27.5	39.5
…	…	…	…	…	…	…	…	…

Table 1: example of table of the values assumed by the rain index $E[H_1]$, varying as a function of Longitude: for the intermediate values of Longitude it is possible to calculate the value of $E[H_1]$ trough interpolation

- t_b is the concentration time of the basin, that is the response time of the catchment and within this study is calculated as function of only the area of the basin according to the following empirical formulation:

$$t_b = 0.25 + 0.27 \cdot A^{1/2} \qquad \textit{Eq.30}$$

Then, known the discharge index (Q2.9), it is possible to calculate the discharge for every return period using the corresponding value of the discharge frequency factor K_T.

Some values of the K_T index have been calculated for Liguria Region (Table 2) for return period equal to 5, 10, 30, 50, 100, 200, 500 years, significant values of return period.

T [years]	5	10	30	50	100	200	500
K_T	1.29	1.79	2.90	3.47	4.25	5.02	6.04

Table 2: Values of the coefficient K_T for some meaningful values of return period T[years]

However, it is possible to build a regression curve to calculate the other intermediate values of this factor (Figure 59).

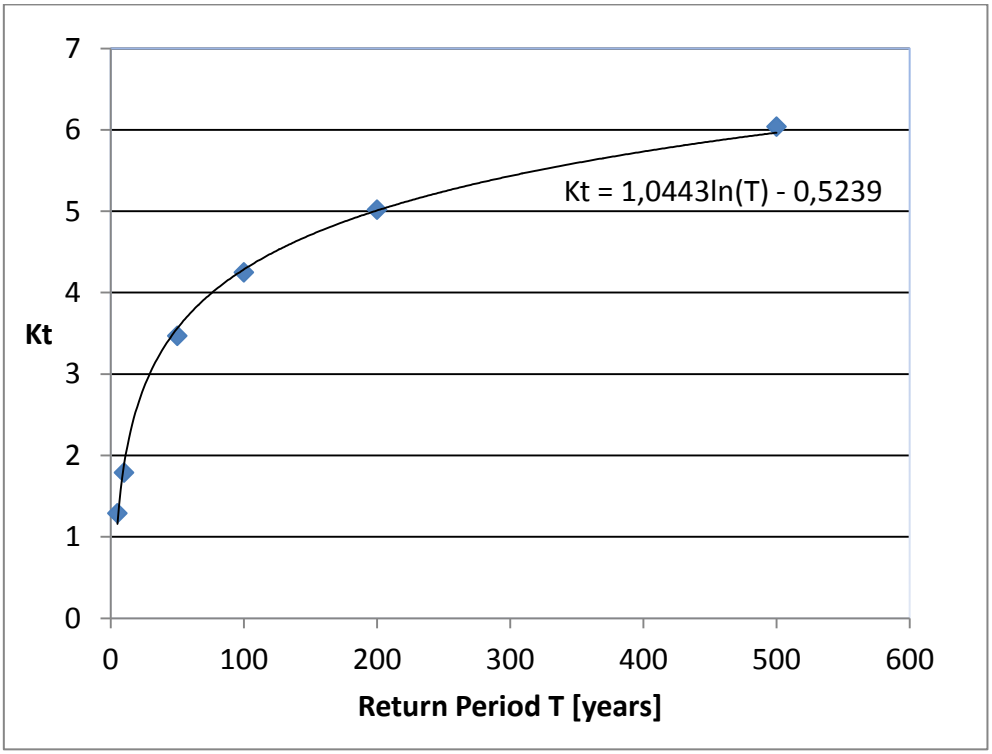

Figure 59: Regression curve for Return Period - K_T values: starting from some known points of correspondence between K_T and T it is possible to build the curve interpolating them to obtain also the intermediate values of K_T

From the regression curve in this way calculated is possible to extract the corresponding equation of the trend line, reported in Figure 59. From this equation and from the definition of the discharge index it is possible to express the value of the return period as a function of the observed/forecasted discharge an of the discharge index:

$$T = e^{\frac{(Q_{2.9} \cdot 0.5239) + Q}{Q_{2.9} \cdot 1.0433}} \qquad Eq.31$$

In this way the information visualized does not depend on the size of the basin involved and is more uniform. Information of drainage area and hydro-climatology in each single grid point, are implicitly accounted by the methodology of estimation of the Return Period.

In Figure 60, in which the same time step of Figure 58 is shown, it is possible to see the maps of maximum and minimum forecasted return period for 1, 2 and 3 hours calculated through the regionalization method explained above. It can be clearly noticed that the use of the return period to communicate which is the area most affected by the event is efficient. As an example, in this case the Bisagno creek that indeed was the most affected basin during 9th October event shows very high values of T. For the forecast at 2 hours of lead time the basin shows high values of return period corresponding to those observed during the event.

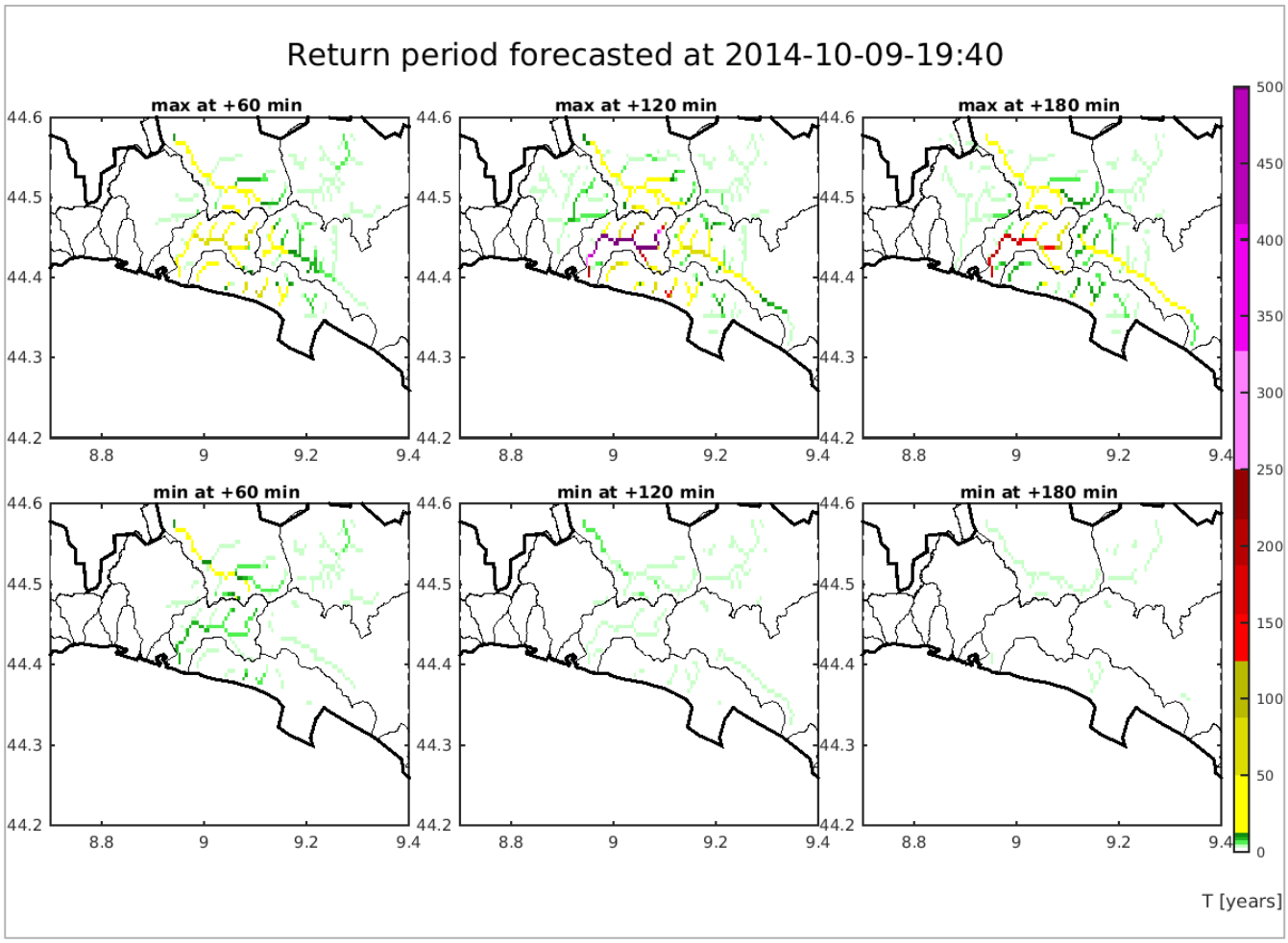

Figure 60: Maps of the return period forecasted at 19:40 of 9th October 2014: in the upper part the maximum values of return period forecasted and in the lower part the minimum values. The maps are calculated following the regionalization method for 1, 2 and 3 hours of lead time.

The information of the return period is therefore useful to communicate in terms of possible forecasted hazard magnitudo an information that is distributed and easily interpretable even without a deep knowledge of the river network.

Chapter 6: Conclusions

Along this PhD thesis different works have been developed, linked with the same final goal, the building of an integrated hydrological nowcasting chain for the forecast of floods and flash floods. The application of this chain would be useful especially for small basins of the Mediterranean area, for which, due to their fast response time, the forecast with a sufficient lead time is essential for civil protection management actions.

The use of a reliable QPF in input to hydrological model is essential to extend the lead time of the hydrological forecast. To deal with this fact the first aspect analyzed in work has been the analysis of the nowcasting spectral based technique PhaSt: starting from an analysis of the model characteristics a calibration of some of the parameters in input has been performed (section 4.2).

To extend the validity of the forecast is important to take into account the processes such as increase and decrease of the volume of precipitation structures that have increasing importance with increasing lead times. Then, to extend the validity of the forecasts produced by PhaSt a first step has been the relaxation of the constraint regarding the volume of rainfall on the map (section 5.2). In the original version this constraint kept the volume constant along the forecast horizon. Some attempts have been done to introduce this information in the nowcasting model. The modification of the volume on the domain has then been performed according to the information retrieved in three different way: trend estimated by the last available observations, trend forecasted by the NWP model MOLOCH, trend forecasted by the NWP model MOLOCH corrected with DA (nudging). The case studies on which the chain has been tested are 3 events of autumn 2014 that hit Liguria Region involving different catchments and urban areas: 9th October event, 11th November event, 15th November event. However, the study did not identify a specific better way of modifying the volume along the forecast horizon as the resulting performances are comparable between the different versions. Despite of that it has been useful for a further step in the building of a hydrological nowcasting chain that attempts to combine different elements for an accurate forecast of the rainfall field and a consequently accurate forecast of the discharge.

A natural following step has been consequently a step forward in the creation of an integrated forecasting chain that is exploiting all the instruments available at the time of the forecast to provide the most accurate input to the hydrological model (section 5.3). The elements involved in the chain are the high resolution NWP model MOLOCH, the nowcasting model PhaSt and the hydrological distributed model Continuum. Also along this work an intermediate goal has been the improvement of the single elements of the chain.

To enhance the NWP forecasts, the model is frequently (every hour) corrected with data assimilation of rainfall estimates derived from both radar and raingauges. Then the forecasted rainfall fields produced by PhaSt are modified along the forecast horizon according to the information related to the variation of rainfall volume derived from the NWP model corrected with DA. The combination of the resulting rainfall field has been performed through the use of a technique, called blending, used to combine the rainfall fields according to an estimated blending function that is giving different weight to the QPF according to the lead time.

The probabilistic QPF obtained (20 rainfall ensembles for 6 hours of forecast) is the input of the distributed hydrological model Continuum that produce a probabilistic discharge forecast in a frequent updated Flood Forecasting System (every 20 minutes). The events on which the chain has been tested are always the same three main floods occurred during the autumn of 2014 that affected in different areas Liguria Region. Even if the number of events analysed is restricted the resulting distributed maps produced by Continuum allow to verify the performance of the chain on a large data sample.

A first analysis has been done comparing the results of the application of various blending functions to combine the forecasted fields, highlighting the presence of a best function for the three events considered together and a best local function for each single event. Then a comparison has been performed between the configurations of the hydrological nowcasting chain fed only with nowcasting, with and without volume modification, and with the rainfall blended fields.

The scores used for the analysis showed that various cases the use of the rainfall fields resulting from the blending process lead to an improvement of the performances of the whole chain with respect to the use on the nowcasting alone. In other cases the benefit gained using the complete configuration with the blending is not so evident and the performances result similar to the use of the nowcasting for all the lead time. However, a worsening of the performance is rarely observed and occurs in the time window of transition between the nowcasted and the NWP rainfall field. In summary there’s an adding value in the use of the blending between nowcasting and NWP model as it’s producing better ore equal scores than the use of the nowcasting alone.

Besides this work a research activity has been carried on at the Centre of Applied Research in Hydrometeorology performing a study of inter-comparison between PhaSt and the nowcasting method developed at CRAHI, SBMcast (section 5.4). In this work has been developed an analysis of their performances in terms of rainfall forecast but also in terms of representativeness of the probabilistic forecast. Exploiting the coupling of the nowcasted rainfall fields with the hydrological

model, another aspect analysed has been the propagation of the error inside the hydrological forecasting chain.

A concluding element of this work has been the study related to the communication of the information coming from the instruments used in this study, the nowcasting model and the hydrological nowcasting chain. This is an essential element in the chain to make the information available useful to support those that are using it to take decisions and actions in flood management actions.

Future works and improvement to the chain presented in this work can be explored always in terms of enhancing of the elements that are composing it.

Other ways for the modification of the volume can be investigated to modify the volume of the nowcasting technique along the forecast time such as the information coming from satellite observations regarding the precipitable water content of the atmosphere.

Other technique of DA with increasing degree of complexity can be used to assimilate in the NWP model not only the observed precipitation field as it done with the nudging but also other variables. Among these techniques the first one that will be approached is the 3DVAR technique applied to WRF (Weather Research and Forecasting) model.

Finally, following recent works (Atencia et al., 2010) further research can be done exploring different kind of blending. First of all some attempts will be done trying to perform the so called spatial blending, that introduces, besides the dependence on the lead time, a spatial dependence of the weights as distance function to rainfall structures.

References

Acquaotta, F., Faccini, F., Fratianni, S., Paliaga, G., Sacchini, A. (2018). Rainfall intensity in the Genoa Metropolitan Area: secular variations and consequences. Weather, Vol. 73, 11, 356-362.

Arduino, G., Reggiani, P., & Todini, E. (2005). Recent advances in flood forecasting and flood risk assessment. *Hydrology and Earth System Sciences Discussions*, *9*(4), 280-284.

Atencia, A., Rigo, T., Sairouni, A., Moré, J., Bech, J., Vilaclara, E., ... & Garrote, L. (2010). Improving QPF by blending techniques at the Meteorological Service of Catalonia. Natural Hazards and Earth System Sciences, 2010, Vol. 10, p. 1443-1455.

Austin, G. L., & Bellon, A. (1974). The use of digital weather radar records for short-term precipitation forecasting. *Quarterly Journal of the Royal Meteorological Society*, *100*(426), 658-664.

Baldauf, M., Seifert, A., Förstner, J., Majewski, D., Raschendorfer, M., & Reinhardt, T. (2011). Operational convective-scale numerical weather prediction with the COSMO model: Description and sensitivities. *Monthly Weather Review*, *139*(12), 3887-3905.

Benjamin, S. G., Dévényi, D., Weygandt, S. S., Brundage, K. J., Brown, J. M., Grell, G. A., ... & Manikin, G. S. (2004). An hourly assimilation–forecast cycle: The RUC. *Monthly Weather Review*, *132*(2), 495-518.

Berenguer, M., Corral, C., Sánchez-Diezma, R., & Sempere-Torres, D. (2005). Hydrological validation of a radar-based nowcasting technique. *Journal of Hydrometeorology*, *6*(4), 532-549.

Berenguer, M., Sempere-Torres, D., & Pegram, G. G. (2011). SBMcast–An ensemble nowcasting technique to assess the uncertainty in rainfall forecasts by Lagrangian extrapolation. *Journal of Hydrology*, *404*(3-4), 226-240.

Berenguer, M. Surcel, I. Zawadzki, M. Xue, and F. Kong, 2012: The diurnal cycle of precipitation from continental radar mosaics and numerical weather prediction models. Part II: Intercomparison among numerical models and with nowcasting. Mon. Wea. Rev., 140, 2689–2705, doi:10.1175/ MWR-D-11-00181.1

Berthet, L., Andréassian, V., Perrin, C., & Javelle, P. (2009). How crucial is it to account for the antecedent moisture conditions in flood forecasting? Comparison of event-based and continuous approaches on 178 catchments. *Hydrology and Earth System Sciences*, *13*(6), 819-831.

Bick, T., Simmer, C., Trömel, S., Wapler, K., Hendricks Franssen, H. J., Stephan, K., ... & Potthast, R. (2016). Assimilation of 3D radar reflectivities with an ensemble Kalman filter on the convective scale. *Quarterly Journal of the Royal Meteorological Society*, *142*(696), 1490-1504.

Boni, G. (1999, October). A physically based regional rainfall frequency analysis: application to a coastal region in Northern Italy. In *Proc. of EGS Plinius Conference on Mediterranean Storms, Maratea, Italy* (pp. 365-376).

Borga, M. (2002). Accuracy of radar rainfall estimates for streamflow simulation. *Journal of Hydrology*, *267*(1-2), 26-39.

Bourgin, F., Payrastre, O., Lebouc, L., Le Bihan, G., & Gaume, E. (2017, July). The October 2015 flash-floods in south eastern France: hydrological analyses, inundation mapping and impact estimations. In 10th HyMeX Workshop (p. 15p).

Bowler, N. E., Pierce, C. E., & Seed, A. W. (2006). STEPS: A probabilistic precipitation forecasting scheme which merges an extrapolation nowcast with downscaled NWP. Quarterly Journal of the Royal Meteorological Society, 132(620), 2127-2155.

Brandolini, P., Cevasco, A., Firpo, M., Robbiano, A., & Sacchini, A. (2012). Geo-hydrological risk management for civil protection purposes in the urban area of Genoa (Liguria, NW Italy). *Natural Hazards and Earth System Sciences*, *12*(4), 943.

Brown, T. A., (1974): Admissible scoring systems for continuous distributions. Manuscript P-5235, The Rand Corporation, Santa Monica, CA, 22 pp. [Available from The Rand Corporation, 1700 Main St., Santa Monica, CA 90407-2138.

Browning, K. A., & Monk, G. A. (1982). A simple model for the synoptic analysis of cold fronts. *Quarterly Journal of the Royal Meteorological Society*, *108*(456), 435-452.

Buizza, R., Milleer, M., & Palmer, T. N. (1999). Stochastic representation of model uncertainties in the ECMWF ensemble prediction system. *Quarterly Journal of the Royal Meteorological Society*, *125*(560), 2887-2908.

Buzzi, A., Davolio, S., D'Isidoro, M., & Malguzzi, P. (2004). The impact of resolution and of MAP reanalysis on the simulations of heavy precipitation during MAP cases. *Meteorologische Zeitschrift*, *13*(2), 91-97.

Buzzi, A., & Davolio, S. (2007). Rainfall Assimilation into Limited Area Models. In *Measuring Precipitation From Space* (pp. 459-470). Springer, Dordrecht.

Buzzi, A., S. Davolio, P. Malguzzi, O. Drofa, and D. Mastrangelo, (2014): Heavy rainfall episodes over Liguria of autumn 2011: Numerical forecasting experiments

Caparrini, F., Castelli, F., & Entekhabi, D. (2003). Mapping of land-atmosphere heat fluxes and surface parameters with remote sensing data. *Boundary-Layer Meteorology*, *107*(3), 605-633.

Caparrini, F., Castelli, F., & Entekhabi, D. (2004). Variational estimation of soil and vegetation turbulent transfer and heat flux parameters from sequences of multisensor imagery. *Water Resources Research*, *40*(12).

Carpenter Jr, R. L., Bassett, G. M., Brewster, K. A., Weber, D., Wang, Y., Brotzge, J. A., ... & Jahn, D. (2004). 14.3 A Globally Relocatable Numerical Weather Prediction System Based on WRF and ADAS. paper presented at 20th Conference on Weather Analysis and forecasting and 16th Conference on Numerical Weather Prediction, Am. Meteorol. Soc., Seattle, Wash.

Cenci L., Laiolo P., Gabellani S., Campo L., Silvestro F., Delogu F., Boni G., and Rudari R., (Dec. 2016) Assimilation of H-SAF Soil Moisture Products for Flash Flood Early Warning Systems. Case Study: Mediterranean Catchments. IEEE Journal of Selected Topics in Applied Earth Observations and Remote Sensing, vol. 9, no. 12, pp. 5634-5646,. DOI: 10.1109/JSTARS.2016.2598475

Cevasco, A., Brandolini, P., Scopesi, C., & Rellini, I. (2013). Relationships between geo-hydrological processes induced by heavy rainfall and land-use: the case of 25 October 2011 in the Vernazza catchment (Cinque Terre, NW Italy). Journal of Maps, 9(2), 289-298.

Cioni, G., Cerrai, D., Ricchi, A., Anagnostou, E., Nikolopoulos, E., Carniel, S., ... & Borga, M. (2018, April). A numerical study of the Livorno 9-10 September 2017 flash flood. In EGU General Assembly Conference Abstracts (Vol. 20, p. 19253).

Codo, M., & Rico-Ramirez, M. (2018). Ensemble Radar-Based Rainfall Forecasts for Urban Hydrological Applications. *Geosciences*, *8*(8), 297.

Collier, C. G. (1981, June). Objective rainfall forecasting using data from the United Kingdom weather radar network. In Nowcasting: Mesoscale Observations and Short-Range Prediction (Vol. 165, p. 201).

Corral, C., Sempere-Torres, D., Berenguer, M., & Escaler, I. (2001). A distributed rainfall runoff model integrated in an operational hydrometeorological forecasting system in Catalunya based in weather radar. In 5th Int. Symp. on Hydrol. Appl. of Weather Radar (pp. 407-412).

Côté, J., Gravel, S., Méthot, A., Patoine, A., Roch, M., & Staniforth, A. (1998). The operational CMC–MRB global environmental multiscale (GEM) model. Part I: Design considerations and formulation. *Monthly Weather Review*, *126*(6), 1373-1395.

Craig, G. C., Keil, C., & Leuenberger, D. (2012). Constraints on the impact of radar rainfall data assimilation on forecasts of cumulus convection. *Quarterly Journal of the Royal Meteorological Society*, *138*(663), 340-352.

Cuevas Tascón, G., Pascual Berghaenel, R., Callado, A., & Compte, M. (2018). Analysis of the 12 October 2016 flash floods in Maresme, Catalonia. *Física del caos en la predicción meteorológica*. Madrid: Agencia Estatal de Meteorología, p. 751-760

Cuo, L., Pagano, T. C., & Wang, Q. J. (2011). A review of quantitative precipitation forecasts and their use in short-to medium-range streamflow forecasting. *Journal of hydrometeorology*, *12*(5), 713-728.

Davolio, S., Silvestro, F., & Malguzzi, P. (2015). Effects of increasing horizontal resolution in a convection-permitting model on flood forecasting: The 2011 dramatic events in Liguria, Italy. *Journal of Hydrometeorology*, 16(4), 1843-1856.

Davolio, S., Silvestro, F., & Gastaldo, T. (2017a). Impact of Rainfall Assimilation on High-Resolution Hydrometeorological Forecasts over Liguria, Italy. *Journal of Hydrometeorology*, 18(10), 2659-2680.

Davolio, S., R. Henin, P. Stocchi, and A. Buzzi, (2017b): Bora wind and heavy persistent precipitation: Atmospheric water balance and role of air–sea fluxes over the Adriatic Sea. *Quarterly Journal of the Royal Meteorological Society, 143(703), 1165-1177.* doi:10.1002/qj.3002.

Delrieu, G., Nicol, J., Yates, E., Kirstetter, P. E., Creutin, J. D., Anquetin, S., et al. (2005). The catastrophic flash-flood event of 8–9 September 2002 in the Gard Region, France: a first case study for the Cévennes–Vivarais Mediterranean Hydrometeorological Observatory. *Journal of Hydrometeorology*, *6*(1), 34-52.

Dickinson, R. E. (1988). The force–restore model for surface temperatures and its generalizations. *Journal of Climate*, *1*(11), 1086-1097.

Dingman, S. L. (2002). Water in soils: infiltration and redistribution. *Physical hydrology*, 575, Waveland Press.

Diskin, M. H., & Nazimov, N. (1995). Linear reservoir with feedback regulated inlet as a model for the infiltration process. Journal of Hydrology, 172(1-4), 313-330.

Dixon, M., & Wiener, G. (1993). TITAN: Thunderstorm identification, tracking, analysis, and nowcasting—A radar-based methodology. *Journal of atmospheric and oceanic technology*, 10(6), 785-797.

Dow, G., & Macpherson, B. (2013). Benefit of convective-scale data assimilation and observing systems in the UK models. *Forecasting Research Technical Report 585*.

Drobinski, P., Ducrocq, V., Alpert, P., Anagnostou, E., Béranger, K., Borga, M., ... & Estournel, C. (2014). HyMeX: A 10-year multidisciplinary program on the Mediterranean water cycle. *Bulletin of the American Meteorological Society*, *95*(7), 1063-1082.

Droegemeier, K. K., Smith, J. D., Businger, S., & Doswell III, C. (2000). Hydrological aspects of weather prediction and flood warnings: Report of the Ninth Prospectus Development Team of the US Weather Research Program.*Bulletin of the American Meteorological Society*, *81*(11), 2665.

Ducrocq, V., Nuissier, O., Ricard, D., Lebeaupin, C., & Thouvenin, T. (2008). A numerical study of three catastrophic precipitating events over southern France. II: Mesoscale triggering and stationarity factors. *Quarterly journal of the royal meteorological society*, *134*(630), 131-145.

Ercolani, G. and Castelli, F. (2017). Variational assimilation of streamflow data in distributed flood forecasting. Water Resources Research, 53(1), 158-183.

Evensen, G. (2003). The ensemble Kalman filter: Theoretical formulation and practical implementation. Ocean dynamics 53.4, 343-367.

Faccini, F., Piccazzo, M., & Robbiano, A. (2009). Natural hazards in San Fruttuoso of Camogli (Portofino Park, Italy): a case study of a debris flow in a coastal environment. Bollettino della Società Geologica Italiana, 128(3), 641-654.

Faccini, F., Robbiano, A., & Sacchini, A. (2012). Geomorphic hazards and intense rainfall: the case study of the Recco Stream catchment (Eastern Liguria, Italy). Natural Hazards and Earth System Science, 12(4), 893-903.

Faccini, F., Luino, F., Sacchini, A., & Turconi, L. (2015a). Flash flood events and urban development in Genoa (Italy): lost in translation. In Engineering Geology for Society and Territory-Volume 5 (pp. 797-801). Springer, Cham.

Faccini, F., Luino, F., Sacchini, A., & Turconi, L. (2015b). The 4th October 2010 flash flood event in Genoa Sestri Ponente (Liguria, Italy). Disaster Adv, 8(8), 1-14.

Faccini, F., Giostrella, P., Lazzeri, R., Melillo, M., Raso, E., & Roccati, A. (2015c). The 10th November 2014 flash-flood event in Chiavari city (Eastern Liguria, Italy). *RENDICONTI ONLINE SOCIETA GEOLOGICA ITALIANA*, *35*, 124-127.

Ferraris, L., Rudari, R., & Siccardi, F. (2002). The uncertainty in the prediction of flash floods in the northern Mediterranean environment. *Journal of hydrometeorology*, *3*(6), 714-727.

Ferretti, R., Panegrossi, G., Rotunno, R., Pichelli, E., Marzano, F. S., Dietrich, S., ... & Vulpiani, G. (2013, April). An analysis of three disastrous rain events occurred in Italy: Rome, Cinque Terre and Genoa. In *EGU General Assembly Conference Abstracts* (Vol. 15).

Fiori, E., Comellas, A., Molini, L., Rebora, N., Siccardi, F., Gochis, D. J., ... & Parodi, A. (2014). Analysis and hindcast simulations of an extreme rainfall event in the Mediterranean area: The Genoa 2011 case. Atmospheric Research, 138, 13-29.

Foresti, L., Reyniers, M., Seed, A., & Delobbe, L. (2016). Development and verification of a real-time stochastic precipitation nowcasting system for urban hydrology in Belgium. *Hydrology and Earth System Sciences*, *20*(1), 505.

Foresti, L., Sideris, I. V., Panziera, L., Nerini, D., & Germann, U. (2018). A 10-year radar-based analysis of orographic precipitation growth and decay patterns over the Swiss Alpine region. *Quarterly Journal of the Royal Meteorological Society*, *144*(716), 2277-2301.

Gabellani, S., Silvestro, F., Rudari, R., Boni, G., (2008), General calibration methodology for a combined Horton-SCS infiltration scheme in flash flood modeling, Nat. Hazards Earth Science., 8, 1317 - 1327.

Garrote, L., & Bras, R. L. (1995). A distributed model for real-time flood forecasting using digital elevation models. *Journal of Hydrology*, *167*(1), 279-306.

Gaume, E., Bain, V., Bernardara, P., Newinger, O., Barbuc, M., Bateman, A., ... & Daliakopoulos, I. (2009). A compilation of data on European flash floods. Journal of Hydrology, 367(1-2), 70-78.

Gaume, E., Borga, M., Llassat, M. C., Maouche, S., Lang, M., & Diakakis, M. (2016). Mediterranean extreme floods and flash floods.

Germann, U., & Zawadzki, I. (2002). Scale-dependence of the predictability of precipitation from continental radar images. Part I: Description of the methodology. Monthly Weather Review, 130(12), 2859-2873.

Germann, U., & Zawadzki, I. (2004). Scale dependence of the predictability of precipitation from continental radar images. Part II: Probability forecasts. *Journal of Applied Meteorology*, *43*(1), 74-89.

Germann, U., Zawadzki, I., & Turner, B. (2006). Predictability of precipitation from continental radar images. Part IV: Limits to prediction. Journal of the Atmospheric Sciences, 63(8), 2092-2108.

Germann, U., Berenguer, M., Sempere-Torres, D., & Zappa, M. (2009). REAL—Ensemble radar precipitation estimation for hydrology in a mountainous region. *Quarterly Journal of the Royal Meteorological Society: A journal of the atmospheric sciences, applied meteorology and physical oceanography*, *135*(639), 445-456.

Giannoni, F., Roth., G., Rudari, R., (2000), A Semi – Distributed Rainfall – Runoff Model Based on a Geomorphologic Approach, Physics and Chemistry of the Earth, 25/7-8, 665-671.

Giannoni, F., Roth, G., & Rudari, R. (2003). Can the behaviour of different basins be described by the same model's parameter set? A geomorphologic framework. *Physics and Chemistry of the Earth, Parts A/B/C*, *28*(6-7), 289-295.

Giannoni, F., Roth., G., Rudari, R., (2005), A procedure for drainage network identification from geomorphology and its application to the prediction of the hydrologic response, Advances in Water Resources, 28, 6, 567-581.

Golding, B. W. (1998). Nimrod: A system for generating automated very short range forecasts. Meteorological Applications, 5(1), 1-16.

Gourley, J. J., Giangrande, S. E., Hong, Y., Flamig, Z. L., Schuur, T., & Vrugt, J. A. (2010). Impacts of polarimetric radar observations on hydrologic simulation. *Journal of Hydrometeorology*, *11*(3), 781-796.

Haiden, T., Kann, A., Wittmann, C., Pistotnik, G., Bica, B., & Gruber, C. (2011). The Integrated Nowcasting through Comprehensive Analysis (INCA) system and its validation over the Eastern Alpine region. *Weather and Forecasting*, *26*(2), 166-183.

Hersbach, H., (2000): Decomposition of the continuous ranked probability score for ensemble prediction systems. Wea. Forecasting, 15, 559–570.

Holm E. (2003). Lecture notes on assimilation algorithms. Technical report, European Centre for Medium-Range Weather Forecasts (ECMWF), Meteorological/Training Course Lecture Series.

Huet, P., Martin, X., Prime, J. L., Foin, P., Laurain, C., & Cannard, P. (2003). Retour d'expérience des crues de septembre 2002 dans les départements du Gard, de l'Hérault, du Vaucluse, des Bouches-du-Rhône, de l'Ardèche et de la Drôme. Rapport de l'Inspection Générale de l'Environnement, Ministere de l'écologie et du développement durable, 15.

Ide, K., Courtier, P., Ghil, M., & Lorenc, A. C. (1997). Unified Notation for Data Assimilation: Operational, Sequential and Variational (gtSpecial IssueltData Assimilation in Meteology and Oceanography: Theory and Practice). *Journal of the Meteorological Society of Japan. Ser. II*, *75*(1B), 181-189.

Ivanov, V. Y., Vivoni, E. R., Bras, R. L., & Entekhabi, D. (2004a). Catchment hydrologic response with a fully distributed triangulated irregular network model. *Water Resources Research*, *40*(11).

Ivanov, V. Y., Vivoni, E. R., Bras, R. L., & Entekhabi, D. (2004b). Preserving high-resolution surface and rainfall data in operational-scale basin hydrology: a fully-distributed physically-based approach. *Journal of Hydrology*, *298*(1), 80-111.

Javelle, P., Organde, D., Demargne, J., Saint-Martin, C., de Saint-Aubin, C., Garandeau, L., & Janet, B. (2016, October). Setting up a French national flash flood warning system for ungauged catchments based on the AIGA method. In *3rd European Conference on Flood Risk Management FLOODrisk 2016* (Vol. 7, pp. 11-p).

Kain, J. S., (2004): The Kain–Fritsch convective parameterization: An up- date, J. Appl. Meteorol., 43, 170–181.

Kain, J. S., S. J. Weiss, J. J. Levit, M. E. Baldwin, D. R. Bright (2006). Examination of convection-allowing configurations of the WRF model for the prediction of severe convective weather: The SPC/NSSL Spring Program 2004. Wea. Forecasting, 21, 167-181.

Kalman, R. E. (1960). A new approach to linear filtering and prediction problems. Journal of basic Engineering, 82(1), 35-45.

Kilambi, A., & Zawadzki, I. (2005, October). An evaluation of ensembles based upon MAPLE precipitation nowcasts and NWP precipitation forecasts. In Preprints, 32nd Conf. on Radar Meteorology, Albuquerque, NM, Amer. Meteor. Soc., P3R (Vol. 4).

Klinker, E., Rabier, F., Kelly, G., & Mahfouf, J. F. (2000). The ECMWF operational implementation of four-dimensional variational assimilation. III: Experimental results and diagnostics with operational configuration. *Quarterly Journal of the Royal Meteorological Society*, *126*(564), 1191-1215.

Kober, K., & Tafferner, A. (2009). Tracking and nowcasting of convective cells using remote sensing data from radar and satellite. *Meteorologische Zeitschrift*, *18*(1), 75-84.

Kober, K., Craig, G. C., Keil, C., & Dörnbrack, A. (2012). Blending a probabilistic nowcasting method with a high-resolution numerical weather prediction ensemble for convective precipitation forecasts. Quarterly Journal of the Royal Meteorological Society, 138(664), 755-768.

Kozak, J. A., Ahuja, L. R., Green, T. R., & Ma, L. (2007). Modelling crop canopy and residue rainfall interception effects on soil hydrological components for semi-arid agriculture. *Hydrological Processes: An International Journal*, *21*(2), 229-241.

Krzysztofowicz, R. (2001). The case for probabilistic forecasting in hydrology. *Journal of hydrology*, *249*(1-4), 2-9.

Kyznarova, H., Salek, M., & Novak, P. (2012). Preliminary results of use of INCA system in the Czech Hydrometeorological Institute. ERAD2012 proceedings (this issue).

Kyznarova, H., Novak, P., Brezkova, L., Janal, P., & Salek, M. (2013, April). Precipitation output of INCA system: evaluation and use. In EGU General Assembly Conference Abstracts (Vol. 15).

Lee, H., Seo, D. J., Liu, Y., Koren, V., McKee, P., & Corby, R. (2012). Variational assimilation of streamflow into operational distributed hydrologic models: effect of spatiotemporal scale of adjustment. Hydrology and Earth System Sciences, 16(7), 2233.

Leuenberger, D., & Rossa, A. (2007). Revisiting the latent heat nudging scheme for the rainfall assimilation of a simulated convective storm. *Meteorology and atmospheric physics*, *98*(3-4), 195-215.

Llasat, M. C., Marcos, R., Turco, M., Gilabert, J., & Llasat-Botija, M. (2016). Trends in flash flood events versus convective precipitation in the Mediterranean region: The case of Catalonia. Journal of Hydrology, 541, 24-37.

Li, L., Schmid, W., & Joss, J. (1995). Nowcasting of motion and growth of precipitation with radar over a complex orography. *Journal of applied meteorology*, *34*(6), 1286-1300.

Liechti, K., Panziera, L., Germann, U., & Zappa, M. (2013). The potential of radar-based ensemble forecasts for flash-flood early warning in the southern Swiss Alps. *Hydrology and Earth System Sciences*, *17*(10), 3853-3869.

Liechti, K., & Zappa, M. (2016). Verification of Short-Range Hydrological Forecasts. *Handbook of Hydrometeorological Ensemble Forecasting*, 1-24.

Lin, C., Vasić, S., Kilambi, A., Turner, B., & Zawadzki, I. (2005). Precipitation forecast skill of numerical weather prediction models and radar nowcasts. *Geophysical research letters*, *32*(14).

Macpherson, B. (2001). Operational experience with assimilation of rainfall datain the Met Office Mesoscale model. *Meteorology and Atmospheric Physics*, *76*(1-2), 3-8.

Mahfouf, J. F., & Rabier, F. (2000). The ECMWF operational implementation of four-dimensional variational assimilation. II: Experimental results with improved physics. *Quarterly Journal of the Royal Meteorological Society*, *126*(564), 1171-1190.

Malguzzi, P., G. Grossi, A. Buzzi, R. Ranzi, and R. Buizza, 2006: The 1966 ‘‘century’’ flood in Italy: A meteorological and hydrological revisitation. J. Geophys. Res., 111, D24106, doi:10.1029/2006JD007111.

Martina, F., Silvestro, F., Giannoni, F., & Poletti, M. L. (2018, April). Flood nowcasting procedure for small and very small basins. In *EGU General Assembly Conference Abstracts* (Vol. 20, p. 17288).

Matheson, J. E., and Winkler R. L., (1976): Scoring rules for continuous probability distributions. Manage. Sci., 22, 1087–109

Metta, S., von Hardenberg, J., Ferraris, L., Rebora, N., & Provenzale, A. (2009). Precipitation nowcasting by a spectral-based nonlinear stochastic model. Journal of Hydrometeorology, 10(5), 1285-1297.

Mishra, S. K., & Singh, V. P. (2013). *Soil conservation service curve number (SCS-CN) methodology* (Vol. 42). Springer Science & Business Media.

Montaldo, N., & Albertson, J. D. (2001). On the use of the force–restore SVAT model formulation for stratified soils. *Journal of Hydrometeorology*, *2*(6), 571-578.

Monteith, J., & Unsworth, M. (2013). *Principles of environmental physics: plants, animals, and the atmosphere*. Academic Press.

Mueller, C., Saxen, T., Roberts, R., Wilson, J., Betancourt, T., Dettling, S., ... & Yee, J. (2003). NCAR auto-nowcast system. Weather and Forecasting, 18(4), 545-561.

Nash, J. E., & Sutcliffe, J. V. (1970). River flow forecasting through conceptual models part I—A discussion of principles. Journal of hydrology, 10(3), 282-290.

Nerini, D., Germann, U., & Foresti, L. (2018, April). A Bayesian framework based on the ensemble Kalman filter for flow-dependent integration of weather radar extrapolation nowcasts and NWP precipitation fields. In EGU General Assembly Conference Abstracts (Vol. 20, p. 4865).

O'Callaghan, J. F., & Mark, D. M. (1984). The extraction of drainage networks from digital elevation data. Computer vision, graphics, and image processing, 28(3), 323-344.

Panziera, L., Germann, U., Gabella, M., & Mandapaka, P. V. (2011). NORA–Nowcasting of Orographic Rainfall by means of Analogues. *Quarterly Journal of the Royal Meteorological Society*, *137*(661), 2106-2123.

Pappenberger, F., Thielen, J., & Del Medico, M. (2011). The impact of weather forecast improvements on large scale hydrology: analysing a decade of forecasts of the European Flood Alert System. *Hydrological Processes, 25*(7), 1091-1113.

Pappenberger, F., Stephens, E., Thielen, J., Salamon, P., Demeritt, D., Andel, S. J., ... & Alfieri, L. (2013). Visualizing probabilistic flood forecast information: expert preferences and perceptions of best practice in uncertainty communication. *Hydrological Processes, 27*(1), 132-146.

Parodi, A., Boni, G., Ferraris, L., Siccardi, F., Pagliara, P., Trovatore, E., & Kranzlmueller, D. (2012). The "perfect storm": From across the Atlantic to the hills of Genoa. Eos, Transactions American Geophysical Union, 93(24), 225-226.

Payrastre, O., Lebouc, L., Ayral, P. A., Brunet, P., Delrieu, G., Douvinet, J., ... & Adnes, C. (2016, April). The October 2015 flash-floods in south eastern France: first discharge estimations and comparison with other flash-floods documented in the framework of the Hymex project. In EGU General Assembly Conference Abstracts (Vol. 18, p. 13912).

Payrastre, O., Bourgin, F., Lebouc, L., Le Bihan, G., & Gaume, E. (2017, April). The October 2015 flash-floods in south eastern France: hydrological analyses, inundation mapping and impact estimations. In EGU General Assembly Conference Abstracts (Vol. 19, p. 12014).

Pegram, G. G. S., & Clothier, A. N. (2001). High resolution space–time modelling of rainfall: the "String of Beads" model. Journal of Hydrology, 241(1-2), 26-41.

Pierce, C. E., & Cooper, A. M. (2000). Comparison of the performance of 2 km resolution Object-Oriented Model and Nimrod advection precipitation nowcast schemes. *Met ffice echnical § eports*, (350).

Rabier, F., & Courtier, P. (1992). Four-dimensional assimilation in the presence of baroclinic instability. *Quarterly Journal of the Royal Meteorological Society*, *118*(506), 649-672.

Rabier, F., Järvinen, H., Klinker, E., Mahfouf, J. F., & Simmons, A. (2000). The ECMWF operational implementation of four-dimensional variational assimilation. I: Experimental results with simplified physics. *Quarterly Journal of the Royal Meteorological Society*, *126*(564), 1143-1170.

Ramos, M. H., van Andel, S. J., Pappenberger, F., (2013). Do probabilistic forecasts lead to better decisions? Hydrol. Earth Syst. Sci., 17, 2219-2232. DOI: 10.5194/hess-17-2219-2232, 2013.

Rebora, N., Molini, L., Casella, E., Comellas, A., Fiori, E., Pignone, F., ... & Parodi, A. (2013). Extreme rainfall in the Mediterranean: What can we learn from observations?. Journal of Hydrometeorology, 14(3), 906-922.

Rebora, N., Fiorini, M., Gabellani, S., Parodi, A., Pignone, F., Rudari, R., & Silvestro, F. (2015, April). Genoa 2014 flash flood event: from precipitation observations to flood mapping. In EGU General Assembly Conference Abstracts (Vol. 17).

Reed, S., Koren, V., Smith, M., Zhang, Z., Moreda, F., Seo, D. J., & Participants, D. M. I. P. (2004). Overall distributed model intercomparison project results. *Journal of Hydrology*, *298*(1), 27-60.

Ricciardelli, E., Di Paola, F., Gentile, S., Cersosimo, A., Cimini, D., Gallucci, D., ... & Romano, F. (2018). Analysis of Livorno Heavy Rainfall Event: Examples of Satellite-Based Observation Techniques in Support of Numerical Weather Prediction. Remote Sensing, 10(10), 1549.

Rinehart, R. E., & Garvey, E. T. (1978). Three-dimensional storm motion detection by conventional weather radar. Nature, 273(5660), 287.

Risse, L. M., Liu, B. Y., & Nearing, M. A. (1995). USING CURVE NUMBERS TO DETERMINE BASELINE VALUES OF GREEN-AMPT EFFECTIVE HYDRAULIC CONDUCTIVITIES 1. *JAWRA Journal of the American Water Resources Association*, *31*(1), 147-159.

Rossa, A. M., Del Guerra, F. L., Borga, M., Zanon, F., Settin, T., & Leuenberger, D. (2010). Radar-driven high-resolution hydro-meteorological forecasts of the 26 September 2007 Venice flash flood. *Journal of hydrology*, *394*(1-2), 230-244.

Seed, A. W. (2003). A dynamic and spatial scaling approach to advection forecasting. Journal of Applied Meteorology, 42(3), 381-388.

Siccardi, F., Boni, G., Ferraris, L., & Rudari, R. (2005). A hydrometeorological approach for probabilistic flood forecast. *Journal of Geophysical Research: Atmospheres*, *110*(D5).

Silvestro, F., Rebora, N., & Ferraris, L. (2009). An algorithm for real-time rainfall rate estimation by using polarimetric radar: RIME. *Journal of Hydrometeorology*, *10*(1), 227-240.

Silvestro, F., Gabellani, S., Giannoni, F., Parodi, A., Rebora, N., Rudari, R., & Siccardi, F. (2012a). A hydrological analysis of the 4 November 2011 event in Genoa. Natural Hazards and Earth System Sciences, 12(9), 2743-2752.

Silvestro, F. and Rebora, N. (2012b) Operational verification of a framework for the probabilistic nowcasting of river discharge in small and medium size basins. Nat. Hazards Earth Syst. Sci., 12, 763–776.

Silvestro, F., Gabellani, S., Delogu, F., Rudari, R., Boni, G., (2013), Exploiting remote sensing land surface temperature in distributed hydrological modelling: the example of the Continuum model. Hydrol. Earth Syst. Sci., 17, 39-62, doi:10.5194/hess-17-39-2013.

Silvestro, F., N. Rebora, G. Cummings, and L. Ferraris, (2015a): Experiences of dealing with flash floods using an ensemble hydrological nowcasting chain: implications of communication, accessibility and distribution of the results. J. Flood Risk Manage., doi:10.1111/jfr3.12161.

Silvestro, F., S. Gabellani, F. Delogu, R. Rudari, P. Laiolo, and G. Boni, (2015b): Uncertainty reduction and parameter estimation of a distributed hydrological model with ground and remote-sensing data. Hydrol. Earth Syst. Sci., 19, 1727-1751.

Silvestro, F., N. Rebora, F. Giannoni, A. Cavallo, and L. Ferraris, (2016): The flash flood of the Bisagno Creek on 9th October 2014: An "unfortunate" combination of spatial and temporal scales, J. Hydrol., 541, 50-62.

Sinclair, S., & Pegram, G. (2005). Combining radar and rain gauge rainfall estimates using conditional merging. *Atmospheric Science Letters*, *6*(1), 19-22.

Sokol, Z. (2009). Effects of an assimilation of radar and satellite data on a very-short range forecast of heavy convective rainfalls. *Atmospheric research*, *93*(1-3), 188-206.

Sokol, Z., & Zacharov, P. (2012). Nowcasting of precipitation by an NWP model using assimilation of extrapolated radar reflectivity. *Quarterly Journal of the Royal Meteorological Society*, *138*(665), 1072-1082.

Smith, K. T., & Austin, G. L. (2000). Nowcasting precipitation—a proposal for a way forward. *Journal of Hydrology*, *239*(1), 34-45.

Stanki, H. R., L. J. Wilson, and W. R. Burrows, (1989): Survey of common verification methods in meteorology. WMO/TD 358, 114 pp.

Stauffer, D. R. and Seaman, N. L. (1990). Use of four-dimensional data assimilation in a limited-area mesoscale model. Part I: Experiments with synoptic-scale data. Monthly Weather Review, 118(6), 1250-1277.

Stephan, K., Klink, S., & Schraff, C. (2008). Assimilation of radar-derived rain rates into the convective-scale model COSMO-DE at DWD. *Quarterly Journal of the Royal Meteorological Society: A journal of the atmospheric sciences, applied meteorology and physical oceanography*, *134*(634), 1315-1326.

Sun, J., M. Xue, J. W. Wilson, I. Zawadzki, S. P. Ballard, J. Onvlee-Hooimeyer, P. Joe, D. M. Barker, P.-W. Li, B. Golding, M. Xu, J. Pinto (2014). Use of NWP for nowcasting convective precipitation. Recent progress and challenges. Bull. Am. Meteorol. Soc., Vol. 95, 3, 409-426.

Talagrand, O., Vautard, R., and Strauss. B., (1997): Evaluation of probabilistic prediction systems. Proceedings, ECMWF Workshop on Predictability, ECMWF, 1–25.

Thielen, J., Bartholmes, J., Ramos, M. H., & Roo, A. D. (2009). The European flood alert system–part 1: concept and development. *Hydrology and Earth System Sciences*, *13*(2), 125-140.

Thorndahl, S., Einfalt, T., Willems, P., Ellerbæk Nielsen, J., ten Veldhuis, M. C., Arnbjerg-Nielsen, K., ... & Molnar, P. (2017). Weather radar rainfall data in urban hydrology. *Hydrology and Earth System Sciences*, *21*(3), 1359-1380.

Trinh, B. N., J. Thielen-del Pozo, and G. Thirel, (2013): The reduction continuous rank probability score for evaluating discharge forecasts from hydrological ensemble prediction systems. Atmos. Sci. Lett., 14, 61–65,

Turner, B. J., Zawadzki, I., & Germann, U. (2004). Predictability of precipitation from continental radar images. Part III: Operational nowcasting implementation (MAPLE). *Journal of Applied Meteorology*, *43*(2), 231-248.

Uhlenbeck, G. E., & Ornstein, L. S. (1930). On the theory of the Brownian motion. *Physical review*, *36*(5), 823.

Unger, D. A., (1985): A method to estimate the continuous ranked probability score. Preprints, Ninth Conf. on Probability and Statistics in Atmospheric Sciences, Virginia Beach, VA, Amer. Meteor. Soc., 206–213

Vieux, B. E., & Bedient, P. B. (2004). Assessing urban hydrologic prediction accuracy through event reconstruction. *Journal of Hydrology*, *299*(3-4), 217-236.

Vivoni, E. R., Entekhabi, D., Bras, R. L., Ivanov, V. Y., Van Horne, M. P., Grassotti, C., & Hoffman, R. N. (2006). Extending the predictability of hydrometeorological flood events using radar rainfall nowcasting. *Journal of Hydrometeorology*, *7*(4), 660-677.

Vivoni, E. R., Entekhabi, D., & Hoffman, R. N. (2007). Error propagation of radar rainfall nowcasting fields through a fully distributed flood forecasting model. *Journal of Applied Meteorology and Climatology*, *46*(6), 932-940.

Wang, G., Wong, W. K., Hong, Y., Liu, L., Dong, J., & Xue, M. (2015). Improvement of forecast skill for severe weather by merging radar-based extrapolation and storm-scale NWP corrected forecast. *Atmospheric Research*, *154*, 14-24.

Weisman, M. L., Davies, C., Wang, W., Manning, K. W., and Klemp, J. B., (2008): Experiences with 0-36-h explicit convective fore- casts with the WRF-ARW model, Weather Forecast., 23, 407– 437.

Wilson, J. W., Crook, N. A., Mueller, C. K., Sun, J., & Dixon, M. (1998). Nowcasting thunderstorms: A status report. Bulletin of the American Meteorological Society, 79(10), 2079.

Wilson, J. W., Ebert, E. E., Saxen, T. R., Roberts, R. D., Mueller, C. K., Sleigh, M., ... & Seed, A. (2004). Sydney 2000 forecast demonstration project: convective storm nowcasting. *Weather and forecasting*, *19*(1), 131-150.

Wilson, J. W., & Roberts, R. D. (2006). Summary of convective storm initiation and evolution during IHOP: Observational and modeling perspective. *Monthly weather review*, *134*(1), 23-47.

Xiao, Q., & Sun, J. (2007). Multiple-radar data assimilation and short-range quantitative precipitation forecasting of a squall line observed during IHOP_2002. *Monthly Weather Review*, *135*(10), 3381-3404.

Xu, G., & Chandrasekar, V. (2005). Operational feasibility of neural-network-based radar rainfall estimation. IEEE Geoscience and Remote Sensing Letters, 2(1), 13-17.

Zawadzki, I. I. (1973). Statistical properties of precipitation patterns. *Journal of Applied Meteorology*, *12*(3), 459-472.

Appendix 1- Publications

- ✓ Publication of the paper, with the title "*Severe hydro-meteorological events in Liguria Region: calibration and validation of a meteorological indices based forecasting operational tool*" (Poletti, M.L, Turato, B., Parodi, A.; 2017) above the results obtained in the Master thesis, on the journal Meteorological Applications (DOI 10.1002/met.1653).

- ✓ Publication of the paper: "*Comparison of two systems for regional flash flood hazard assessment*" to the Journal of Hydrology (C. Corral, M. Berenguer, D. Sempere Torres, L. Poletti, F. Silvestro, N. Rebora; 2019) regarding the results of the comparison between the flood warning system operating at the Regional Environmental Protection Agency of Liguria Region and the rainfall based flood warning system operational in the Spanish Regional Water Agency of Catalonia.

- ✓ Submission of the paper: "*Using nowcasting technique and data assimilation in a meteorological model to improve very short range hydrological forecasts*" (Poletti, M. L., Silvestro, F., Davolio S., Pignone, F., & Rebora, N.) above the results of the PhD thesis on Hydrology and Earth System Science.

- ✓ Conference Abstract EGU General Assembly 2017 (Vol. 19, p. 14367). Poletti, M. L., Pignone, F., Rebora, N., & Silvestro, F. (2017, April). "*Probabilistic hydrological nowcasting using radar based nowcasting techniques and distributed hydrological models: application in the Mediterranean area*". Presented in poster session.

- ✓ Conference Abstract EGU General Assembly 2018 (Vol. 20, p. 17022). Poletti, M. L., Silvestro, F., Rebora, N., & Pignone, F. (2018, April). "*Predicting flash-floods in small Mediterranean catchments: application and results of a probabilistic hydrological nowcasting technique*". Presented in PICO session.

- ✓ Conference Abstract EGU General Assembly 2018 (Vol. 20, p. 17288). Martina, F., Silvestro, F., Giannoni, F., & Poletti, M. L. (2018, April). "*Flood nowcasting procedure for small and very small basins*". Presented in PICO session.

- ✓ Conference Abstract EGU General Assembly 2019 (Vol. 21, 8197). Poletti, M. L., Silvestro, F., Davolio, S., Pignone, F., & Rebora, N. (2019, April). "*Using nowcasting technique and data assimilation in a meteorological model to improve very short range hydrological forecasts*". Presented in PICO session.

Appendix 2- Participation to conferences and workshops

- ✓ **15th Plinius Conference on Mediterranean Risks, Giardini Naxos, Italy, 8-11 June 2016**

  The objective of the 2016 edition of the conference is to provide special emphasis to discuss both the current state of knowledge, as well as advancements in multidisciplinary researches and applications, related to Mediterranean risks and hydro-related hazards, such as floods, landslides, coastal flooding and coastal erosion, and their expected impacts on people, society, the environment, and the economy, also with respect to predicted climate changes. Presentation of two posters related to the topic "Floods, flash floods and related hydrological processes: modeling, forecasting, global and climate change effects". One of the poster, with the title "Probabilistic hydrological nowcasting using radar based nowcasting techniques and distributed hydrological models" presents the first results of the PhD work. The other one, entitled "The role of spatial and temporal scales in defining the magnitude of flash flood events: analysis of the 9th October 2014 event in Genoa" shows the results of the study on the 9th October 2014 flood event.

- ✓ **Anywhere Workshop, Genova, Italy, 5-8 September 2016**

  The Anywhere (EnhANcing emergencY management and response to extreme WeatHER and climate Events) project, has the ultimate objective to empower exposed responder institutions and citizens to enhance their anticipation and pro-active capacity of response to face extreme and high-impact weather and climate events. ANYWHERE proposes to implement a Pan-European multi-hazard platform providing a better identification of the expected weather-induced impacts and their location in time and space before they occur. This platform will support a faster analysis and anticipation of risks

prior the event occurrence, an improved coordination of emergency reactions in the field and help to raise the self-preparedness of the population at risk.

- ✓ **European Geoscience Union (EGU) General Assembly 2017, Wien, 23–28 April 2017**

  The EGU General Assembly brings together geoscientists from all over the world to one meeting covering all disciplines of the Earth, planetary and space sciences. The EGU aims to provide a forum where scientists, especially early career researchers, can present their work and discuss their ideas with experts in all fields of geoscience. Poster presentation for the work related to the PhD thesis theme with the title "Probabilistic hydrological nowcasting using radar based nowcasting techniques and distributed hydrological models: application in the Mediterranean area"

- ✓ **Giornate dell'Idrologia 2017, Favignana, Italy, 21-24 June 2017**

  Meeting with the aim of establishing opportunity of discussion between the world of Hydrological Research and the Public Administration of technical professions in order to work synergistically for a proper prevention and mitigation of natural hazards (floods, droughts and landslides) in a context of global change. In particular, the Days intended to provide a synthesis of the state of the art on issues of extreme events for the prevention and mitigation of natural hazards and adaptation to global change. Poster presentation on the work related to the PhD thesis theme and on Flood PROOFS Italy project.

- ✓ **ICUD, International Conference on Urban Drainage 2017, Prague, 10-15 September 2017**

  The ICUD conference aims to present the latest advances and innovative approaches in fundamental and applied research on urban drainage, taking into account meteorological, hydrological, hydraulic, water quality and socio-economic aspects worldwide. Oral presentation on the work related to the PhD thesis theme with the title "Probabilistic hydrological nowcasting using radar based nowcasting techniques and distributed hydrological models: application in urban small basins"

- ✓ **Anywhere Workshop, Helsinki, 19-22 September 2017**

  Second workshop on the progress of the project Anywhere. Scope of the workshop is to consolidate the collaboration between European civil protection actors and present new tools for them for monitoring of weather and climate–related hazards and impacts. The Project

Meeting aimed to monitor, interact and make further detailed plans of the ongoing and future progress among the Anywhere project Partners, as well as perform constructive interaction with the Advisory Board.

- ✓ **European Geoscience Union (EGU) General Assembly 2018, Wien, 9–13 April 2018**

  In EGU 2018 PICO presentations (first oral presentation to the audience of the essence of the work in 2 minutes and then interactive presentation to the screens) of the work related to the PhD thesis ("Predicting flash-floods in small Mediterranean catchments: application and results of a probabilistic hydrological nowcasting technique") and of a work done in collaboration with CFMI-PC ARPAL ("Flood nowcasting procedure for small and very small basins").

- ✓ **11th HyMeX Workshop, Lecce, 29 May-2 June 2018**

  Organized by the Institute of Atmospheric Sciences and Climate of the Italian National Research Council (ISAC-CNR) in collaboration with the University of Salento and the Euro-Mediterranean Center on Climate Change (CMCC). Contribution to the oral presentation of Silvio Davolio entitled "Rainfall data assimilation in a convection permitting model for improving meteo-hydrological forecasts over Liguria".

- ✓ **European Radar Conference (ERAD) 2018, Ede-Wageningen, 1-6 July 2018**

  ERAD is held to promote the exchange of knowledge between students, research scientists, radar engineers and operators, and end users of weather radar. ERAD provides a platform to transfer knowledge from research into operational use (and vice versa) of weather radar. Poster presentation "Operational hydrological nowcasting: chain comparison applied on mediterranean small catchments" on the results of the collaboration with CRAHI-UPC obtained in the months passed in Barcelona to this Centre of Research.

- ✓ **1st AISAM National Congress, Bologna, 10-13 September 2018**

  The first National Congress of the Italian Association of Atmospheric Sciences and Meteorology aimed to be a meeting of the Italian scientific community involved in the atmospheric sciences, meteorology and climatology. Contribution to the oral presentation by Silvio Davolio of the work done in collaboration with ISAC-CNR with the title "Meteo-hydrological forecast of intense events in Liguria: rainfall assimilation in a high resolution meteorological model".

- ✓ **16th Plinius Conference on Mediterranean Risks, Montpellier, France, 9-12 October 2018**

  The objective of the 2018 conference is to provide an interdisciplinary forum for discussions on our current state of knowledge of Mediterranean risks. Poster presentation on the collaboration with ISAC-CNR for the use of Meteorological data assimilated data in the hydrological nowcasting chain ("Nowcasting hydrological chain: how to extend the forecast horizon?") and oral presentation about the results in the work with CRAHI-UPC about the comparison of the nowcasting techniques used ("Hydrological nowcasting: application and comparison of two probabilistic nowcasting technique").

- ✓ **European Geoscience Union (EGU) General Assembly 2019, Wien, 8–12 April 2019**

  In EGU 2019 PICO presentations of the last results of the PhD ("Using nowcasting technique and data assimilation in a meteorological model to improve very short range hydrological forecasts ").